Numerical investigation of thermal comfort in an isolated family house under natural cross-ventilation

THESIS SUBMITTED FOR THE DEGREE OF

DOCTOR OF PHILOSOPHY

AT THE UNIVERSITY OF LEICESTER

BY

SHERZAD HAWENDI

ENGINEERING DEPARTMENT

UNIVERSITY OF LEICESTER

JUNE 2018

Abstract

Numerical investigation of thermal comfort in an isolated family house under natural cross-ventilation

Sherzad Hawendi

This study uses Computational Fluid Dynamics (CFD) to predict the thermal comfort and the flow field in an average family house in Iraq under natural cross-ventilation in a hot climate. The study is performed on the effects of different building parameters, such as the inlet openings position, external boundary wall, wind speed and outdoor temperature, furniture and heat loads on the human thermal comfort indices and the flow field. Although the study showed that the flow rate through openings located near the centre of the building is higher and steadier than the flow rate of openings located near the sides of the building, these positions of the openings have only slight effects on the thermal comfort indices at both the seated and the standing levels. It was also observed that the external boundary wall created well-distributed indoor airflow and improved the indoor environment regarding the mean velocity inside the building. Also, increasing the height of the wall by 20% did not offer a noticeable improvement on the mean velocity distribution. This study has also predicted the range of wind temperatures that would allow for all rooms in the building to be of acceptable thermal comfort. The results of the study suggest that acceptable thermal conditions can be maintained with the external wind speeds ranging from 2 to 5 m/s at the temperature of 25°C. In addition, the results showed that the heat dissipated from electrical appliances found in daily life only have a small effect on the thermal comfort indices at both the seated and the standing levels because they use only relatively small amounts of energy, whereas these indices are increased remarkably at these two levels when an additional heat source was operated in conjunction with these appliances. Lastly, no significant differences between the empty building and the furniture-filled building were observed at the two levels when comparing the air velocity, temperature, and thermal comfort indices.

Acknowledgements

I would first thank the God Almighty for the strength, wisdom, knowledge, and health. Then, I would like to extend my sincere thanks to my thesis supervisor, Dr. Shian Gao, for his guidance, assistance, encouragement, and patience, without his advice and support, I couldn't complete my study. Also, I would like to thank my second supervisor, Dr. Aldo Rona for his useful feedback and valuable suggestions.

My deep thanks to my wife Feryal, my son and my daughters for their love, encouragement, and patience, which was always given to me to help complete this long and difficult journey despite of her complex illness. Also, my deep appreciation to my mom and my brothers, sisters, for being a source of unparalleled support. Daddy, you are gone but your belief in me has made this journey possible.

Many thanks to all my friends, especially in the engineering department for their help support. Also, I would also like to acknowledge of the previous and current members of Engineering Department, especially, Computational Engineering & Control Research Group for creating a stimulating, welcoming, and positive atmosphere. Finally, the financial support from the Ministry of Higher Education and Scientific Research of Iraq is acknowledged with thanks.

Sherzad Hawendi

Contents

Abstract .... **I**

Acknowledgements .... **II**

Contents .... **III**

List of Figures .... **VII**

List of Tables .... **XI**

Nomenclatures .... **XII**

1 Chapter 1 Introduction **1**

1.1 Background 1

1.2 Natural ventilation 2

1.3 Thermal comfort 4

1.4 Computational Fluid Dynamics (CFD) for indoor air simulation 6

1.5 Characteristics of region study 7

1.6 Description of average family house 8

1.7 Aims and objective 9

1.8 Thesis outline 10

2 Chapter 2 Literature Review **12**

2.1 Introduction 12

2.2 The role of openings position in natural ventilation 12

2.3 Impact of an external boundary wall on natural cross-ventilation 18

2.4 Thermal comfort evaluation under a naturally ventilated environment 20

3 Chapter 3 Numerical Methods **26**

3.1 Introduction 26

3.2 Governing equations 26

3.3 Turbulence models 28

3.3.1 Reynolds-Averaged Navier-Stoked model 28

3.3.2 Large Eddy Simulation 31
3.4 CFD model validation 32
3.4.1 Wind tunnel experiments 32
3.4.2 CFD setting and parameters 33
3.4.3 CFD model validation results and discussion 35
3.4.4 Validation case versus case study 37
4 Chapter 4 Impact of windward inlet opening positions on fluctuation characteristics of wind-driven natural cross-ventilation 40
4.1 Introduction 40
4.2 Case description 40
4.3 CFD cases study: setting and parameters 42
4.3.1 Computational geometry, domain and grid 42
4.3.2 Grid independence 43
4.4 Boundary condition and solver settings 44
4.5 Results and discussion 47
4.5.1 Mean flow and streamlines around the building 47
4.5.2 Mean flow pattern inside the building 50
4.5.3 Streamlines inside the building 50
4.5.4 Instantaneous wind flow pattern 55
4.5.5 Fluctuating ventilation rate 55
4.5.6 Turbulent kinetic energy 61
4.5.7 Comparison with previous work 63
4.6 Conclusion 63
5 Chapter 5 Impact of an external boundary wall on indoor flow field and natural cross-ventilation 65
5.1 Introduction 65
5.2 Case description 65
5.3 CFD case study: computational domain and grid 67

5.4 Boundary condition and solver settings 67
5.5 Results and discussion 69
5.5.1 Mean flow and streamlines around the building 69
5.5.2 Mean flow patterns inside the building 70
5.5.3 Streamlines inside the building 75
5.5.4 Fluctuating ventilation rate 77
5.5.5 Turbulent kinetic energy 79
5.6 Conclusion 82
6 Chapter 6 Thermal comfort evaluation under a naturally ventilated environment in a hot climate 83
6.1 Introduction 83
6.2 Case description 83
6.3 Computational domain and grid 85
6.4 Boundary conditions and solver settings 85
6.5 Thermal comfort indices 86
6.6 Results and discussion 88
6.6.1 Impact of opening location 88
6.6.2 Impact of wind speed 97
6.6.3 Impact of ambient temperature 105
6.7 Conclusion 108
7 Chapter 7 Effect of heat loads and furniture on thermal comfort under a naturally ventilated environment 109
7.1 Introduction 109
7.2 Case description 109
7.3 CFD case study: setting and parameters 111
7.3.1 Computational domain and grid 111
7.3.2 Boundary conditions and solver settings 113
7.4 Results and discussion 113

7.4.1 The effect of furniture on the thermal comfort 114

7.4.2 The Effect of heat loads on the thermal comfort 119

7.5 Conclusion 132

8 Chapter 8 Conclusion and Future Work 133

8.1 Conclusion 133

8.1.1 Impact of windward inlet opening positions on fluctuation characteristics of wind-driven natural cross-ventilation 133

8.1.2 Impact of an external boundary wall on indoor flow field and natural cross-ventilation 134

8.1.3 Thermal comfort evaluation under a naturally ventilated environment 134

8.1.4 Effect of heat loads and furniture on thermal comfort under a naturally ventilated environment 135

8.2 Future work 136

Appendices 137

Appendix 1 Publication List 137

References 138

List of Figures

Figure 1-1: The principle of natural ventilation [9]. 4
Figure 1-2: The geometry of the building model 8
Figure 2-1: Basic openings configurations of Karava's study [35]. 13
Figure 2-2: A schematic view of the building model [46-48]. 14
Figure 2-3: Schematic diagram of resistances in a building with internal obstacles [51]. 15
Figure 2-4: Scale model of windbreak studied by Ikeguchi et al. [103]. 19
Figure 2-5: Model layout of the buildings studied by Tuan et al. [52]. 19
Figure 2-6: Test model studied by Hassana et al. [126]. 23
Figure 2-7: (a) Experimental chamber and (b) geometrical details [38]. 23
Figure 2-8: (a) Experimental model made of Plexiglas, (b) Open channel in the Laboratory of Hydraulics [129]. 24
Figure 2-9: Building prototype render [132]. 25
Figure 3-1: The geometry of the reduced-scale building model with dimensions (in meters) as studied by Ohba et al.[148]. 33
Figure 3-2: The building inside the defined duct. 34
Figure 3-3: The mesh layout of the building. 34
Figure 3-4: Comparison of dimensionless mean velocity and turbulent kinetic energy profiles of the approaching wind with experimental results of [148] at the inlet of the duct. 35
Figure 3-5: Pressure coefficient comparison between CFD and experimental results of [148] on the centrelines of the building external walls. 36
Figure 3-6: Comparison of experimental and CFD results for the stream-wise velocity ratio $U(x)/U_{ref}$ along the horizontal centreline of the openings. 37
Figure 3-7: Comparison of the velocity vector field of measurements and the CFD simulations on the mid-plane of the building. 39
Figure 4-1: The layout of the building models (dimension in meters). 41
Figure 4-2: The geometry of the building models; (a) Perspective view and (b) Front view (dimension in meters). 41
Figure 4-3: The building inside the defined duct. 42

Figure 4-4: Computational domain and the mesh layout of grid (a) Side view and (b) Top view. 43
Figure 4-5: Profiles of LES_IQ for Grid A and Grid B in the vertical lines for the Case-I. 44
Figure 4-6: Power spectral density of the turbulent kinetic energy. 46
Figure 4-7: Contours of dimensionless mean velocity magnitude ($|V|/U_{ref}$) and streamlines around the building in the vertical plane at the middle of the building. 48
Figure 4-8: Contours of dimensionless mean velocity magnitude ($|V|/U_{ref}$) and streamlines around the building (y/H = 0.5). 48
Figure 4-9: Contours of mean pressure coefficient C_p around the building (horizontal plane y/H = 0.56). 49
Figure 4-10: Contours of dimensionless mean velocity magnitude ($|V|/U_{ref}$) inside the building in the horizontal plane (y/H = 0.56). 52
Figure 4-11: Mean streamlines velocity in the horizontal plane (y/H = 0.56). 53
Figure 4-12: Mean streamlines velocity in the X-Y section in (a) Plane-A and (b) Plane-B. 54
Figure 4-13: Contours of mean pressure coefficient C_p inside the building (horizontal plane y/H = 0.56). 55
Figure 4-14: Instantaneous wind streamlines for Case-I in the horizontal plane (y/H = 0.56). 57
Figure 4-15: Instantaneous wind streamlines for Case-II in the horizontal plane (y/H = 0.56). 58
Figure 4-16: Time history of velocity, x-velocity, at the monitoring points near the building. 59
Figure 4-17: Variation of the dimensionless ventilation rate over time steps. 59
Figure 4-18: Turbulence intensity in the centreline of openings. 60
Figure 4-19: Comparison of dimensionless ventilation rates. 60
Figure 4-20: Contours of dimensionless turbulent kinetic energy (k/ U^2_{ref}) in the horizontal plane (y/H = 0.56). 62
Figure 5-1: Schema of the case used in the study. 66
Figure 5-2: The front view of the building with opening sizes and dimensions (m). 66
Figure 5-3: The building inside the defined duct. 68
Figure 5-4: Mean velocity (m/s) and streamlines inside and around the building in the vertical plane and passing middle of opening-2. 71

Figure 5-5: Mean streamlines around the building in the horizontal plane (y/H=0.56). 72
Figure 5-6: Mean pressure contours in front of the building in the vertical plane and passing middle of opening-2. 73
Figure 5-7: Mean velocity contours (m/s) inside the building in the horizontal plane (y/H=0.56). 74
Figure 5-8: Indoor average mean velocity (m/s) profile of lines along the building. 75
Figure 5-9: Mean streamlines velocity in the horizontal plane (y/H=0.56). 76
Figure 5-10: Variation of the dimensionless ventilation rate over time steps. 78
Figure 5-11: Comparison of dimensionless ventilation rate. 79
Figure 5-12: Distribution of dimensionless turbulent kinetic energy around the building (k/U^2_{ref}) in the horizontal plane (y/H=0.56). 80
Figure 5-13: Distribution of dimensionless indoor turbulent kinetic energy (k/U^2_{ref}) in the horizontal plane(y/H=0.56). 81
Figure 6-1: The front view of the building (dimensions in meters). 84
Figure 6-2: Average wind temperature, speed and relative humidity of Kirkuk, Iraq [161]. 84
Figure 6-3: The room average PMV, PPD, velocity and temperature in the seated plane for Case-I, Case-II and Case-III. 91
Figure 6-4: The room average PMV, PPD, velocity and temperature in the standing plane for Case-I, Case-II and Case-III. 92
Figure 6-5: PMV contours in the horizontal plane (seated level) for Case-I, Case-II and Case-III. 93
Figure 6-6: PMV contours in the horizontal plane (standing level) for Case-I, Case-II and Case-III. 94
Figure 6-7: Temperature contours in the horizontal plane (seated level) for Case-I, Case-II and Case-III. 95
Figure 6-8: Temperature contours in the horizontal plane (standing level) for Case-I, Case-II and Case-III. 96
Figure 6-9: The room average PMV and PPD in the seated horizontal plane for Case-III. 99
Figure 6-10: The room average velocity and temperature in the seated horizontal plane for Case-III. 100
Figure 6-11: The room average PMV and PPD in the standing horizontal plane for Case-III. 101

Figure 6-12: The room average velocity and temperature in the standing horizontal plane for Case-III. 102
Figure 6-13: PMV contours in the horizontal plane (seated level) for Case-III at different wind velocity. 103
Figure 6-14: PMV contours in the horizontal plane for Case-III at U_{ref} = 3 m/s. 104
Figure 6-15: The room average PMV and PPD in the seated horizontal plane for Case-III. 106
Figure 6-16: The room average PMV and PPD in the standing horizontal plane for Case-III. 107
Figure 7-1: The layout of the furniture in the building. 110
Figure 7-2: Computational domain and the mesh layout of the grid (Top view). 112
Figure 7-3: The mesh layout of the building with furniture. 112
Figure 7-4: The room average velocity, temperature, PMV and PPD in the seated plane for Case-F and Case-FF. 115
Figure7-5: The room average velocity, temperature, PMV and PPD in the standing plane for Case-F and Case-FF. 116
Figure 7-6: Contours of dimensionless velocity magnitude ($|V|/U_{ref}$), temperature and PMV in the seated plane. 117
Figure 7-7: PMV contours in the standing plane for Case-F and Case-FF. 118
Figure 7-8: The room average PPD in the seated and the standing planes for Case-F2 at different wind temperature. 122
Figure 7-9: The room average temperature, PMV and PPD in the seated plane for Case-F1, Case-F2 and Case-F3. 123
Figure 7-10: The room average temperature, PMV and PPD in the standing plane for Case-F1, Case-F2 and Case-F3. 124
Figure 7-11: Temperature and PMV contours in the seated plane for Case-F1 and Case-F2. 125
Figure 7-12: Temperature and PMV contours in the standing plane for Case-F1 and Case-F2. 126
Figure 7-13: Temperature and PMV contours in the seated plane for Case-F2 and Case-F3. 127
Figure 7-14: Temperature and PMV contours in the stand plane for Case-F2 and Case-F3. 128

Figure 7-15: The room average velocity, temperature, PMV and PPD in the seated and the standing planes. 130
Figure 7-16: Contours of dimensionless velocity magnitude ($|V|/U_{ref}$), temperature and PMV in the seated plane and the standing plane. 131

List of Tables

Table 1-1: Dimensions of the rooms.......... 9
Table 2-1: Overview of wind-induced ventilation in building.......... 16
Table 5-1: Cases description.......... 66
Table 5-2: Mean indoor velocity (m/s). 70
Table 7-1: Dimensions of the furniture and the human bodies in meters. 110
Table 7-2: Heat loads of the study cases.......... 111

Nomenclatures

Abbreviations

AIJ	Architectural Institute of Japan
ASHRAE	The American Society of Heating, Refrigerating and Air-Conditioning Engineers
BSI	British Standards Institution
CFD	Computational Fluid Dynamics
COST	European Cooperation in Science and Technology
HVAC	Heating, ventilation, and air conditioning
ISO	International Organization for Standardization
LES	Large Eddy Simulation
LES_IQ	Large Eddy Simulation index of quality
PISO	Pressure implicit with splitting of operator
PMV	Predicted Mean Vote
PPD	Predicted Percentage of Dissatisfied
Pr	Prandtl number
Pr_t	Turbulent Prandtl number
RANS	Reynolds-Averaged Navier-Stokes
Re	Reynolds number
Re^*	Turbulent Reynolds number ($k^{0.5}y/v$)
RMSE	Root-mean-square-error
RNG	Renormalization Group

SGS	Subgrid Scale
SIMPLEC	Semi-Implicit Method for Pressure Linked Equations-Consistent
SET	Standard Effective Temperature
UDF	User-Defined-Function

Variables

a, b	Near–wall model constants
A	Area (m^2)
C_s	Dynamic Smagorinsky coefficient
$C_{1\varepsilon}$, $C_{2\varepsilon}$,	*RNG* k- ε model constants
C_p	Dimensionless pressure coefficient ($(P-P_o)/0.5\rho U^2_{ref}$)
C_μ	Model constants
D	Distance(m)
F_i	External body force
f_{cl}	Clothing area factor (1 *clo* = 0.155 m^2 K/W)
g_i	Component of the gravitational vector
G_b	Production of k due to buoyancy
G_k	Production of k due to velocity gradients
H	Height of the building (m)
h_c	Convective heat transfer coefficient (W/m^2 K)
h_j	Subgrid-scale heat flux
I_u	Turbulence intensity (u_{rms}/u_{mean})

I_{cl}	Resistance to sensible heat transfer
k	turbulent kinetic energy (m^2/s^2)
k_{res}	Resolved turbulent kinetic energy (m^2/s^2)
k_{num}	Numerical dissipation turbulent kinetic energy (m^2/s^2)
k_{sgs}	Subgrid scale turbulent kinetic energy (m^2/s^2)
k_t	Total turbulent kinetic energy (m^2/s^2)
L_D	Length of the domain (m)
L_s	Mixing length for sub-grid scales
L_{ij}	Leonard stress tensor
L_{th}	Thermal load (W/m^2)
M_{ij}	Germano stress tensor
N	Vortex number
P_o	Reference pressure (Pa)
$\bar{p}$	Resolved pressure (Pa)
p_a	Partial water vapor pressure (kPa)
P_k	Shear production of turbulence (kg/m.s)
Q	Ventilation rate (m^3/s)
q_{cw}	Convective heat flux at the surface (W/m^2)
Q^*	Dimensionless ventilation rate
$\overline{S}_{ij}$	Rate of strain tensor
$\tilde{\bar{S}}_{ij}$	Filtered strain rate tensor
T	Temperature (K)

$\bar{T}$	Resolved temperature (K)
T^*	Dimensionless time period
T_{cl}	Surface temperature of the clothing (°C)
T_c	Adaptive comfort temperature (°C)
T_r	Mean radiant temperature (°C)
T_o	Operation temperature (°C)
T_{om}	Monthly mean outdoor temperature (°C)
T_w	Wall temperature (°C)
T^+	Dimensionless temperature $(\rho c_p u_\tau (T_w - T)/q_{cw})$
u, v, w	velocity components (m/s)
u_i	Velocity (tensor form m/s)
$\bar{u}_i$	Resolved velocity component (tensor form m/s)
u'_i	Fluctuating component of velocity (tensor form m/s)
u_τ	Friction velocity (m/s)
$U(y)$	Mean velocity at height y above the ground (m/s)
U_{ref}	External wind speed at the building height (m/s)
u^+	Dimensionless mean air speed (u/u_τ)
V	Volume of the computational cell
W	Active work (W/m^2)
y^+	Dimensionless wall (normal) distance$(u_\tau y/\upsilon)$
y_o	Aerodynamics roughness length (m)

Greek symbols

α	Molecular thermal diffusivity (m^2/s)
α_t	Subgrid-scale eddy diffusivity (m^2/s)
β	Model constant
δ_{ij}	Kronecker delta
ε	Rate of dissipation of turbulent kinetic energy (m^2/s^3)
θ	Wind angle
κ	Von Karman constant
λ_t	The turbulent thermal conductivity
μ	Dynamic viscosity (kg/m.s)
μ_t	Turbulent viscosity (Pa.s)
υ	Kinematic viscosity (m^2/s)
υ_{sgs}	Subgrid-scale (kinematic) eddy viscosity
ρ	Density (kg/m^3)
σ_k	Turbulent kinetic energy Prandtl number
σ_ε	Turbulence dissipation Prandtl number
τ_{ij}	Subgrid-scale stress tensor
Γ	Blending function

Chapter 1 Introduction

1.1 Background

Energy consumption is an important issue and has become a great concern during the last few decades because of rising energy costs and mounting scientific evidence of global warming. World energy consumption has increased around 50% between 1990 and 2010, and the energy demand is expected to increase at a rate of 1.8% per year according to U.S. Energy Information Administration (2013). In the building sector, the energy consumption related to the operation of heating, ventilating and air-conditioning (HVAC) systems is significant and according to recently published data, nearly 40% of the total energy used in the EU building sector in the provision of heating, cooling lighting and appliances [1]. The energy required for cooling purpose in a hot climate has been predicted to be more than double the energy required for heating [2]. Although the energy utilization of the buildings represents a large portion of overall energy consumption, most of the energy is used for space heating and cooling purposes, and including 51% of energy consumption in residential buildings according to the annual review by U.S. Department of Energy [3].

One approach to reducing the energy consumption of the building is to minimize the amount of energy required for ventilation by designing buildings ventilated naturally even in a wide range of climates. One key building type that is responsible for this problem is a low-cost family house, which has become popular in Iraq. Such buildings are mostly partitioned into five rooms with external boundary wall, almost all units using air-condition systems and these systems are energy expensive. Moreover, previous works relating to passive cooling strategies for this building type in Iraq are still rare. In this thesis, a comfort natural cross-ventilation is proposed and its performance to improve indoor air velocity and thus provide thermal comfort for the occupants' comfort is investigated in detail. The main intention for proposing such a strategy is to reduce the high electricity demand due to natural ventilation in the typical average family house in Iraq.

Kurdistan is the north part of Iraq and has a cold weather in winter and hot weather in summer whilst in spring and autumn the weather is warm, windy, the temperature between 20-30°C and there is a potential to utilize natural cross-ventilation in the domestic buildings to reduce using air-conditioning systems. Increase in ventilation rates could significantly improve the indoor environmental quality of the dwellings [2]. Natural ventilation should be considered at the early stages of design as well as during refurbishment studies of existing buildings to ensure resilience to future climates. To accomplish such objectives, the study provides a holistic look at wind-driven ventilation using various research techniques, then to leverage the information learned to develop a novel prediction method. Utilizing the environment conditions to provide a proper thermal comfort of the low-cost average family house. Furthermore, examination of thermal comfort may help in recognizing the factor of thermal comfort problems in buildings. Despite studies regarding the efficiency of passive ventilation strategies in buildings, only limited research has been carried out in domestic buildings and specifically in the Middle East Region. A considerable gap in knowledge remains for a natural ventilation study of multi-storey, free-running, urban, domestic buildings in the Middle East that could provide guidance for future projects.

1.2 Natural ventilation

Natural ventilation has become an increasingly attractive proposition for the reduction of energy usage and cost whilst still providing an acceptable quality indoor environment and preserving a comfortable, healthy, and productive indoor climate rather than the more prevalent approach to the use of heating, ventilation and air-conditioning (HVAC) systems that in turn fail to reduce carbon emissions [4]. Natural ventilation can provide thermal comfort inside buildings for residents by supplying fresh air without fans. For warm and hot climates, it can help meet a building's cooling requirements without using mechanical air conditioning systems, which make up a large fraction of a building's total energy use. In addition, it is an important factor in the development of the sustainable sector. Successful ventilation is determined as having high thermal comfort, lower contaminant concentrations, adequate fresh air for ventilated spaces and having little or no energy use for active heating, ventilation and air conditioning (HVAC).

Natural ventilation is the use of natural forces, including both wind and thermal buoyancy, to regulate a building's indoor climate, therefore, the flow will be more complex compared to mechanical systems and hence more difficult to predict thus, a natural ventilation strategy should be carefully designed, and the physics understood. As the weather outside often changes, it can be difficult to maintain stable conditions inside a building [5]. As mentioned in previous studies, there are a number of factors which need to be considered for this type of ventilation due to limited natural driving forces some of them are related to outside climatic conditions, such as the wind speed, wind direction and temperature, while others are related to the building design, such as building form and dimension, shape and size of openings, construction methods, internal spaces, and internal heat load [6-8].

In the field of natural ventilation, there are typically three basic types of ventilation, depending on the position of the openings in the outer walls: single-side ventilation, cross ventilation and stack ventilation. In cross-ventilation there are openings in more than one wall so that the air crosses the room and usually used for cooling purposes whilst in single-sided ventilation there is only one opening in one wall. In stack ventilation, there are openings at the high level and openings at the lower level as shown in Figure 1-1. The driving forces in natural ventilation are temperature differences and wind pressure differences. In cross-ventilation, the main driving force will be the wind as long as the openings are at the same height whilst with a difference in height the thermal buoyancy will also impact the air flow rate. For single-sided ventilation, the air-change rate is much dependent on the height and the shape of the opening, wide openings will be more influenced by the wind than small openings, whereas high openings will be more affected by temperature differences than low openings. Regarding the stack ventilation, the higher internal pressure occurs at the upper section of the openings due to a higher temperature, which drives outflow whilst the lower internal pressure at the lower section of the opening drives inflow and this works on the same principle as above (utilizing both cross and single ventilation).

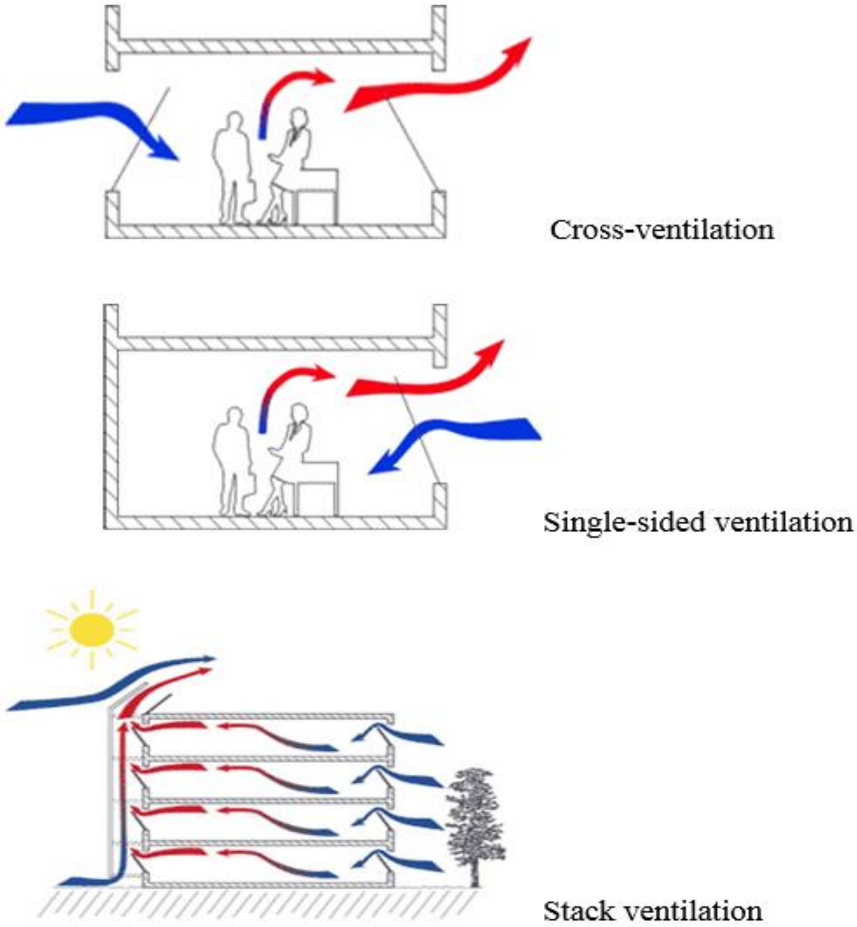

Figure 1-1: The principle of natural ventilation [9].

1.3 Thermal comfort

Thermal comfort is one of the most important indices that are widely used by researchers to evaluate and develop ventilation system in addition to the indoor air quality and energy saving. Defining the thermal comfort can be difficult as you need to take into account a range of factors such as environmental condition, work-related and personal factors when deciding what makes a comfortable workplace temperature and can be different from one person to another within the same space. For example, a person walking upstairs in a cool environment whilst wearing a jacket might feel hot, whilst someone sat still in a shirt in the same environment might feel cold. Thermal comfort is the pleasant environmental conditions that are able to provide a human's thermal preference. In this study, thermal comfort is the main criterion for assessing the performances of natural ventilation enhancement strategies in average family house.

According to the British Standards Institution (BSI), the thermal comfort can be defined as "that condition of mind which expresses satisfaction with the thermal environment"

[10]. It can be achieved by maintaining a thermal equilibrium between the human body and the environment where the condition when someone is not feeling either too hot or too cold. Indoor thermal comfort is not measured by room temperature only, there are another three environmental factors that related directly to the thermal comfort; radiant temperature, air velocity, humidity and two personal factors; clothing insulation and metabolic heat [11]. These factors are interconnected and their effects in comfort cannot be considered independently. Moreover, there are found to be other factors that may affect a person's perception of climatic comforts such as age, sex, state of health and acclimatization.

When the building ventilated naturally, the thermal comfort will be affected by all factors that effect on the natural ventilation such as the wind speed and direction, the building configurations, outdoor and indoor temperature, etc. [12]. Among these factors, the role of wind speed is significant, and the airflow encourages heat transfer between the human body and its ambient environment where the skin will lose heat by convection when fresh cold air passes over it. All these factors make the design of building under natural ventilation complex, therefore, a balancing energy efficiency, architectural requirements, and users' thermal comforts is not an easy task for the engineers.

Numerous indices have been proposed for the assessment of thermal comfort. Commonly used indices based on the estimate of the heat flow between the human body and its environment includes the well-known Fanger's method, also known as the PMV-PPD thermal comfort model: the Predicted Mean Vote (PMV) and the Predicted Percentage of Dissatisfied (PPD). PMV refers to the thermal scale that runs from Cold (-3) to Neutral (0) then to Hot (+3). The original data was collected by subjecting a large number of people to different conditions within a climate chamber and having them select a position on the scale the best described their comfort sensation. A mathematical model of the relationship between all the environmental and physiological factors considered was then derived from the data. The recommended acceptable PMV range for thermal comfort from ASHRAE 55 is between -0.5 and +0.5 for an interior space [13]. Predicted Percentage of Dissatisfied (PPD) predicts the percentage of occupants that will be dissatisfied with the thermal conditions and it is a function of PMV, given that as PMV moves further from 0, or neutral, PPD increases. The recommended acceptable PPD range for thermal comfort from ASHRAE 55 is less than 10% persons dissatisfied for an interior space.

1.4 Computational Fluid Dynamics (CFD) for indoor air simulation

The complex flows of natural ventilation can be explored using three techniques: analytical methods; full-scale or wind-tunnel experiments; and numerical modelling such as Computation Fluid Dynamics (CFD)[14]. For the evaluation of the numerical simulation, it is necessary that all the errors and uncertainties that cause the results to deviate from the true or exact values are identified and treated separately if possible. The sources for the numerical errors and uncertainties are computer programming, spatial discretisation, temporal discretisation, and iterative convergence [15]. The spatial and temporal discretisation are the most crucial sources of numerical error and these errors describe the difference between the exact solution of the basic system of partial differential equations and the numerical solution obtained with finite discretisation in space and time [16].

CFD numerically solves the conservation equations of mass, momentum and energy. CFD methods are convenient to access for design practice and can simulate the flow field about a building and predict parameters of interest such as velocity, pressure, and temperature fields [17], and now commonly applied in a number of industries. The most accurate and popular numerical method to predict the air movement in naturally ventilated buildings is CFD modelling and it provides many details of the airflow both inside and outside the buildings in both a steady and a transient manner [18, 19]. The results from CFD simulations during the schematic design stage can help architects or designers to improve the indoor and outdoor environment for the planned building at the schematic design stage [20].

CFD can be less expensive, both in time and resources, relative to traditional wind tunnel testing and large scale experiments, as the computer costs continuously decrease, unlike the cost of materials [1]. Therefore, the CFD has seen widespread use in predicting ventilation performance and in the last decade, many studies of CFD applications exist, concerning the flow field in naturally ventilated buildings, and refer both to experiment and real-scale buildings. In addition, the implementation of well-known thermal comfort indices in a CFD code provides local thermal comfort predictions [21].

On the other hand, it is important to know that there are some errors and uncertainties of the results of the CFD codes that cause deviation from the exact values such as simplification of physical complexity, usage of previous experimental data, geometric and physical of boundary conditions, and initialization [15]. The physical complexity of turbulent flows is reduced by using the averaged Navier-Stokes equations where averaging is performed in space for Large Eddy Simulations and in time for the Reynolds-Averaged approach. The solution of these averaged equations, however, requires turbulence closure models that describe the influence of the unresolved scales on the resolved flow field. These approximate models then introduce errors and uncertainties to the results of the numerical solution. When performing validation simulations it is mandatory to quantify and reduce the different errors and uncertainties originating from these sources [22]. CFD is difficult to use in the architectural design process because of its relatively complicated process and time consuming aspects such as the generation of complex geometries. Various calculation conditions should be set by users, such as the size of the computational domain, grid resolution, boundary conditions, and selection of the turbulence model. Moreover, the selection of the boundary conditions is not a simple matter in the numerical solution of turbulent flow [20].

Although numerous numerical studies on building performance have focused on the quantitative aspects of the problem, far fewer have reported qualitative investigations into the effectiveness of adopting CFD as a tool for design assistance. Instead, most CFD publications have conducted straightforward quantitative comparisons of model predictions against experimental observations [20].

CFD calculations can be either steady state or transient, for the evaluation of static conditions or time-varying processes respectively, of buoyancy and wind driven forces. The most common CFD mode is the RANS approach (Reynolds Averaged Navier-Stokes equations) which is usually used for steady state application. An alternative mode that predicts with high accuracy natural ventilation is large eddy simulation (LES). LES adequately evaluates unsteady turbulent flows of buoyancy-driven ventilation. LES filters the time-dependent equations, resolves the large-scale eddies and models the small scale eddies [23]. However, due to the assumptions used in the CFD modelling and dependency of CFD accuracy on specific simulation parameters, every CFD study requires accompanying validations to demonstrate the correctness of the simulation results.

1.5 Characteristics of region study

The typical Kurdistan region (Iraq) weather is defined by hot, dry summer and cold, rainy winter, the annual cycle can be divided into three main weather seasons: the cold and rainy (December-February), the hot and dry season (June-August) and warm and relatively dry in other six months[24, 25] . In mid of summer, high air temperatures can reach up to 45°C and low as -10°C in the mountainous regions during winter. Generally, the Köppen-Geiger map classified the weather in north part of Iraq (Kurdistan region) as a cold semi-arid climate[26]. During the warm months (spring and autumn) the weather is stable, clear skies windy and the temperature is around (20-30) °C.

1.6 Description of average family house

A typical averaged family house was used for the investigation and the typical size of the house is about 8m in width and 10m in depth. The house consists of five rooms: kitchen (A), sitting room (B), living room (C), and two bedrooms (D & E), as shown in Figure 1-2. This layout is simple and represents an average low-income house for an average family in Iraq [27]. The height of the building (H) was 3m, with two square openings (0.6 m) in the front wall and two openings at the rear of the building, and the wall porosity (opening area divided by wall area) was 3%. The building has an external boundary wall and the height of the wall was 1.0 m. The thickness of the walls was 0.2m. Ventilation is achieved with the wind, and the windows are fully open.

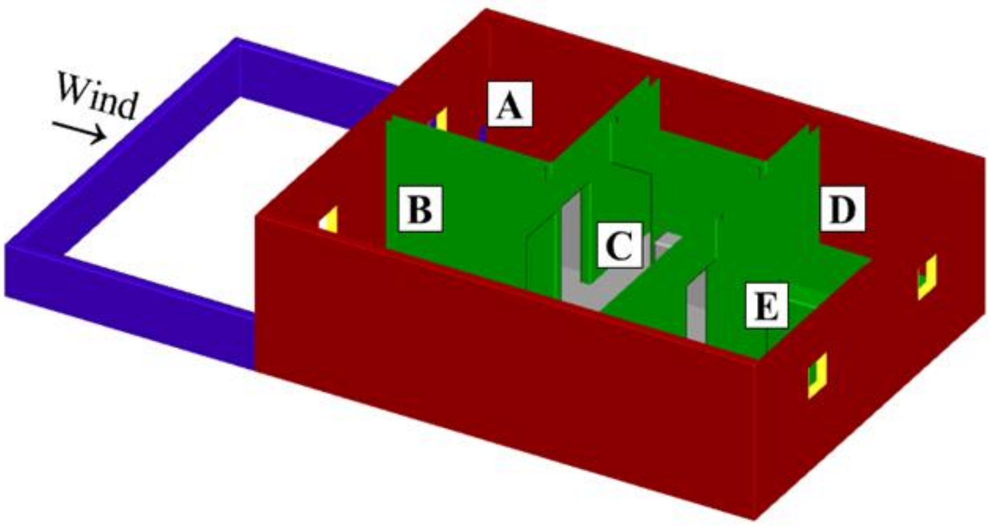

Figure 1-2: The geometry of the building model

Table 1-1: Dimensions of the rooms

Room	Room type	Dimension size (Length×Width) in meters
A	Kitchen	(3.2×3.4)
B	Sitting room	(3.2×4.0)
C	Living room	(3.0×5.9)
D	Bed room I	(3.0×3.4)
E	Bed room II	(3.0×4.0)

1.7 Aims and objective

The aim of this research project was assessing the indoor thermal comfort and indoor airflow characteristics of natural cross-ventilation solutions for an average family house city based on CFD simulation. The assessment includes analysing some elements of the building envelope that influence building performance and thereby make recommendations on viable options to solve the inadequacies. Moreover, assessing the sensitivity of these elements using representative passive design parameters to understand the use of passive design techniques as a low-cost design for more sustainable housing supply. Consequently, developing a detailed analysis of the performance of key design of government provided low-income housing in order to understand contextual aspects of thermal comfort. The main objectives of the thesis can be specified as:

1. To study the impact of the windward inlet opening positions on fluctuation characteristics of wind-driven natural cross-ventilation.
2. To examine the impact of an external boundary wall on indoor flow field and natural cross-ventilation.
3. Evaluating the thermal comfort condition under a naturally ventilated environment in a hot climate.
4. To study the effect of heat loads and furniture on the thermal comfort under a naturally ventilated environment.

This work provides new information and a novel method for assessing of natural cross-ventilation based on indoor thermal comfort indices (PMV and PPD) which in turn can help the engineers and architects for designing energy efficient building under natural cross-ventilation in consideration of the Iraqi context.

1.8 Thesis outline

The thesis is subdivided into eight chapters: starting with an introductory chapter; a literature review chapter; a chapter on numerical methods; four performance evaluation chapters; and the concluding chapter. The contents of the thesis chapters are surmised below:

Chapter One

The background of the research, introduction of the natural ventilation and the thermal comfort in buildings, the aims and objectives of the project are presented in this chapter.

Chapter Two

This chapter reviewing all strategies and modelling techniques that relevant to the current study. In the first part of this chapter, the influences of the openings position on the cross-ventilation are briefly reviewed. The second part introduces the studies which concerned with the external factors (non-climate) that effect on the natural ventilation. Finally, the chapter reviewing the studies that evaluate natural ventilation based on the thermal comfort.

Chapter Three

This chapter presents the method which adopted in the current study and the modelling techniques which used. In addition, the validation case and a comparison study between RANS and LES are reported in this chapter.

Chapter Four

This chapter investigates the impact of the windward inlet opening positions on fluctuation characteristics of wind-driven natural cross-ventilation of the case study using LES technique.

Chapter Five

Impact of an external boundary wall on indoor flow field and natural cross-ventilation of the case study is presented in this chapter by using LES technique.

Chapter Six

Thermal comfort evaluation of the case study under a naturally ventilated environment in a hot climate is investigated in this chapter by using steady RANS model.

Chapter Seven

This chapter presents the effect of heat loads and furniture on thermal comfort under a naturally ventilated environment using RANS model.

Chapter Eight

This chapter presents the conclusions, limitations of the research and provides recommendations for future research.

Chapter 2 Literature Review

2.1 Introduction

This chapter provides a review of literature relevant to this dissertation, with primary emphasis on wind-driven cross-ventilation and as part of the analysis, results obtained using different methods (e.g. full-scale, wind tunnel, CFD, and analytical). The literature review is divided into three major sections. The first section describes the current knowledge of the contributing factor of wind-driven cross ventilation, the resulting indoor air distribution and particular emphasis is given to parameters such as openings position. The second section describes the influence of the configuration of the surrounding neighbourhood on the airflow over and through naturally ventilated buildings. In the third section, the previous studies of evaluation indoor thermal comfort of different buildings under natural ventilation are presented and discussed. In addition, the gap in previous research methods and current knowledge are also addressed as motivations for this dissertation.

2.2 The role of openings position in natural ventilation

The current methods to study wind driven cross-ventilation can be divided into analytical models, full-scale field experiments, small-scale wind tunnel studies and computational fluid dynamics (CFD) modelling. Many studies have often selected two of these methods for comparison and validation. Many researchers have utilized the aerodynamic potential of building façades to investigate their enhancement effect on indoor and outdoor airflow exchanges for both single-sided and cross ventilation buildings. Table 2-1 presents an overview of wind-induced cross-ventilation of buildings in the previous studies.

Studying natural ventilation by experimental methods has been tested in many types of buildings for numerous reasons, though usually through two principal, though complicated and expensive, methods during research: wind tunnels [8, 28-35] and field measurements for existing buildings [36-38]. Karava et al. [35] examined five cases of inlet-outlet vertical opening positions (Figure 2-1) on opposite walls and four cases on adjacent walls in natural cross ventilation; they found that the inlet-to-outlet ratio and the relative location of openings on a building's façade are important parameters that must be considered in addition to wall porosity. Tominaga et al. [33] analysed five configurations of inlet-outlet vertical configuration on field flow and dispersion of contaminants in cross-ventilated buildings and their results provide new insights into the flow and dispersion processes inside naturally cross-ventilated buildings, and can be used in computational fluid dynamics (CFD) validations of flow and dispersion.

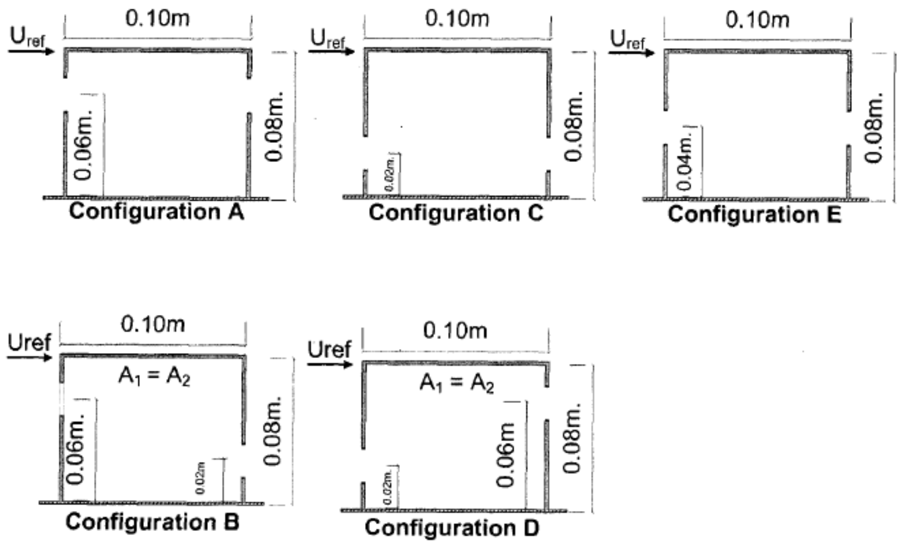

Figure 2-1: Basic openings configurations of Karava's study [35].

Due to providing many details of airflow both inside and outside buildings in both a steady and a transient manner, the CFD has seen widespread use in predicting ventilation performance. Reynolds-Averaged Navier-Stokes (RANS) is the most widely used CFD method in wind engineering [32] [27, 36-45]. This approach provides appropriate cross-ventilation flow characteristics with a relatively economical computational cost, but such models are less satisfactory in their description of turbulent features within and around buildings. An alternative approach, such as large eddy simulation (LES), can predict information on flow structure, including turbulence statistics, and describe the flow field variation over a given period of time. Jiang and Chen [46] performed cross- and single-sided ventilation of a cube building (Figure 2-2) using two subgrid-scale models, namely the Smagorinsky subgrid-scale (SS) and filtered dynamic subgrid-scale (FDS) models. Subsequently, Jiang and Chen [47] focused on the impact of the fluctuation of wind-driven, natural cross ventilation in four apartments. Their results showed the important role of the fluctuating flow field in determining an accurate ventilation rate through the openings. In 2003, Jiang et al. [48] concluded that the two models, SS and FDS, provide almost the same results when compared with those of physical wind tunnel measurements, and explained that most of the energy of the airflow around a building is contained in large eddies, which are known to have a greater effect than small eddies. Unsteady cross-ventilation flow modelling was performed by Hu et al. [49] on a small building using a sub-grid Smagorinsky model with constant $C_s = 0.12$ applied to it. Driver domain, which was proposed by Lund et al. [50], was used to generate flow fluctuations. Their results showed that the standard deviation of the fluctuation flow rate was small when the wind direction is normal to the aperture.

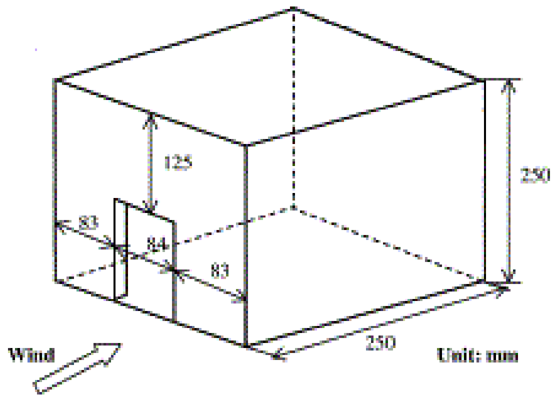

Figure 2-2: A schematic view of the building model [46-48].

Chu and Chiang [51] investigated the influences of internal resistance on wind-driven cross-ventilation by LES and wind tunnel experiments (Figure 2-3). The ventilation rate in a building with a rectangular plate inside was measured, together with the impact of plate size and location, on the external pressure and ventilation rate. The results showed that the resistance factor is a function of internal blockage ratio and location, but is independent of external wind speed, building size and opening configuration. Furthermore, LES and wind tunnel experiments were used by the same authors [7] to study the effect of building length on natural ventilation rate. The numerical results revealed that ventilation rate decreases as building length increases due to a reduction in the pressure difference. The other reason for the decline in ventilation rate was that the internal friction from turbulent flow caused a 'sluggish zone' with a low wind speed inside the building when the building length was greater than five times its height. Tuan et al. [52] used LES to investigate the impact of the downstream construction of terraced houses on nearby, upstream houses, and the flow patterns inside them. Recently, an in-depth comparison between five different steady RANS models and LES has been performed by van Hooff et al. [53] to determine which CFD model is the most suitable for cross-ventilation flows in a generic, isolated building. The study shows that the five steady RANS models failed to reproduce any turbulent kinetic energy, whilst LES shows a better reproduction of velocity, turbulent kinetic energy, and volume flow rate parameters.

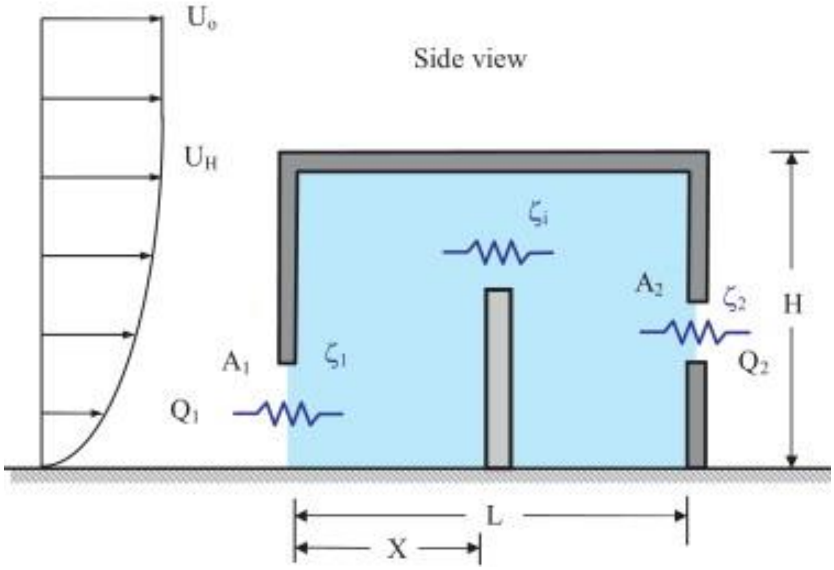

Figure 2-3: Schematic diagram of resistances in a building with internal obstacles [51].

In summary, the majority of the previous studies have investigated only the time-averaged ventilation rates using the steady RANS method by testing different heights of the opening positions, whereas other studies have employed the transient models to focus on fluctuating ventilation rates of the openings located at the middle of the building. There is limited knowledge about the impact of turbulence and fluctuation of the flow from the windward openings of the building at different horizontal locations that cannot be predicted by the steady methods. In addition, the position of the windward inlet openings in the buildings has a major role in the natural ventilation processes and not only changes the appearance of the building, but can also influence the efficiency of the natural ventilation and the thermal comfort. Therefore, investigating the impact of the horizontal position of the windward inlet openings on the fluctuation of the cross ventilation and the flow-field inside the building is considered in the current project using the LES technique.

Table 2-1: Overview of wind-induced ventilation in building.

Authors	Ref.	Physical model	Technique
Murakami et al.(1991)	[54]	A specific room of a building	Wind tunnel and full-scale experiments
Ernest(1992)	[29]	Rectangular building	Wind tunnel
Kato et al.(1992)	[28]	Cube building	Wind tunnel and CFD simulation (LES)
Kindangen et al. (1997)	[30]	Square-base building	Wind tunnel and CFD simulation (Standard k-ε)
Kato et al.(1997)		large-scale market building	Wind tunnel and CFD simulation
Straw(2000)	[36]	Cube building	Full-scale experiments and CFD simulation (Standard k-ε , RNG k-ε)
Li and Delsante (2001)	[55]	Single-zone building	Theoretical analysis
Jiang and Chen(2002)	[46]	A specific room of a building	CFD simulation (LES)
Jiang et al. (2003)	[56]	Cube building	Wind tunnel and CFD simulation (LES)
Elmualim et al. (2002)	[31]	Cube building	Full-scale experiments and CFD simulation (Standard k-ε)
Yang(2004)	[37]	Cube building	Full-scale experiments, Wind tunnel and CFD simulation (Standard k-ε , RNG k-ε)
Heiselberg et al. (2004)	[57]	Cube building	Wind tunnel and CFD simulation
Karava et al. (2004)	[58]	Cube building	Theoretical analysis
Sawachi et al. (2004)	[59]	Multi-room building	Full-scale experiments
Etheridge (2004)	[60]	Rectangular building	Wind tunnel
Evola and Popov (2006)	[32]	Cube building	CFD simulation (Standard k-ε , RNG k-ε)

Larsen (2006)	[8]	Multi-room building	Full-scale experiments
Wright and Hargreaves (2006)	[61]	Cube building	CFD simulation (DES)
Kotani and Yamanaka (2016)	[62]	Rectangular building	Wind tunnel
Livermore and Woods(2007)	[63]	Two floors with atrium	Theoretical analysis and small-scale experiments
Karava et al. (2007)	[64]	Cube building	Wind tunnel
Fitzgerald and Woods(2008)	[65]	Isolated room	Theoretical analysis and small-scale experiments
Horan and Finn(2008)	[66]	Two- storey building	Full-scale experiments and CFD simulation (Standard k-ε , RNG k-ε)
Stavrakakis et al.(2008)	[38]	One-room building	Full-scale experiments and CFD simulation (Standard k-ε , RNG k-ε , Realizable k-ε)
Hu et al. (2008)	[49]	Isolated room	CFD simulation (LES)
Visagavel and Srinivasan(2009)	[67]	Isolated room	CFD simulation (Standard k-ε)
Meroney(2009)	[68]	Rectangular building	CFD simulation (RANS, LES , DES)
Chu et al.(2010)	[69]	Partition building	Wind tunnel
Bu et al. (2010)	[70]	Residential basements	Wind tunnel
Nikas et al.(2010)	[71]	Square base building	CFD simulation (Standard k-ώ)
Kurabuchi et al.(2011)	[72]	Isolated house	CFD simulation (LES)
Li et al. (2011)	[73]	Cube building	Wind tunnel
Bangalee et al.(2012)	[74]	Isolated room	CFD simulation (RNG k-ε)
Karava et al. (2011)	[75]	Cube building	Wind tunnel

Karava and Stathopoulos (2011)	[75]	Cube building	Wind tunnel
Ramponi and Blocken (2012)	[39]	Rectangular building	Wind tunnel and CFD simulation (SST k-ω)
Chu and Chiang (2013)	[7]	Long building	Wind tunnel and CFD simulation (LES)
Lo & Novoselac (2013)	[76]	Multi-room building	Full-scale experiments and CFD simulation (Standard k-ε)
Chu and Chiang (2014)	[51]	Building with internal obstacle	Wind tunnel and CFD simulation (LES)
Martins & Carrilho da Graça (2016)	[77]	Long building	Wind tunnel and CFD simulation (Standard k-ε , RNG k-ε)
Tong et al. (2016)	[78]	Rectangular building	CFD simulation (LES)
Castillo and Huelsz (2017)	[79]	Rectangular building	CFD simulation (Realizable k-ε , RNG k-ε, SST k-ώ)

2.3 Impact of an external boundary wall on natural cross-ventilation

Many researchers have utilized the aerodynamic potential of building façades to 16investigate their enhancement effect on indoor and outdoor airflow exchanges for both single-sided and cross ventilation buildings. Typical building façades include a wind catchers [80-85] venturi-shaped roof [86-88] wing walls [89], a ventilation shaft [90-92], a balcony [93-96] and eaves [30, 40, 41, 97], while other researchers focused on the influences of external factors on ventilation rates and indoor air patterns such as sheltering building [29, 52, 98-101] and external landscape [6, 102].

Fred et al. [101] used both computational and experimental methods to investigate the performance of natural ventilation in long rows of buildings. Their study concluded that the best options for flow inlets and outlets depend on the building spacing and wind direction. The solid wall windbreak was tested by Ikeguchi et al. [103] who examined the ability of windbreaks to control air contaminants from livestock buildings (Figure 2-4). The air pollutant which accumulates behind the solid wall can be emitted from the building by spraying with water. Aynsley [104] concluded that vegetation can improve external wind direction and increase the rate of ventilation. The effects of some environmental factors on air flow in and around buildings were examined by Lam et al. [99]. They concluded that any change in these factors can significantly affect the boundary conditions and consequently the indoor airflow parameters such as pressure, velocity magnitude and distribution pattern.

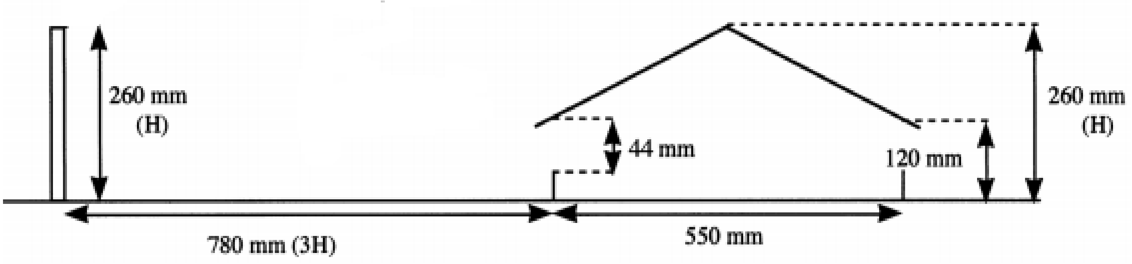

Figure 2-4: Scale model of windbreak studied by Ikeguchi et al. [103].

Tuan et al. [52] investigated the impact of the sheltered building on the natural ventilation and flow pattern of a downstream building in tropical regions (Figure 2-5). It was found that the possibility of ventilation was increased by increasing the sheltered distance. Some studies mentioned that obstacles around buildings, such as trees, block wind flow, reduce wind velocity and increase average pollutant concentrations [105, 106]. Ai et al.[93] studied the effect of balconies on the indoor ventilation performance of low-rise building by examining mass flow rate and average velocity on the working plane, the numerical results indicated that, for single-sided ventilation, the provision of balconies increased mass flow rate and reduced average velocity on the working plane in most rooms, while for cross ventilation, this provision had no significant effect under normally or obliquely incident wind conditions.

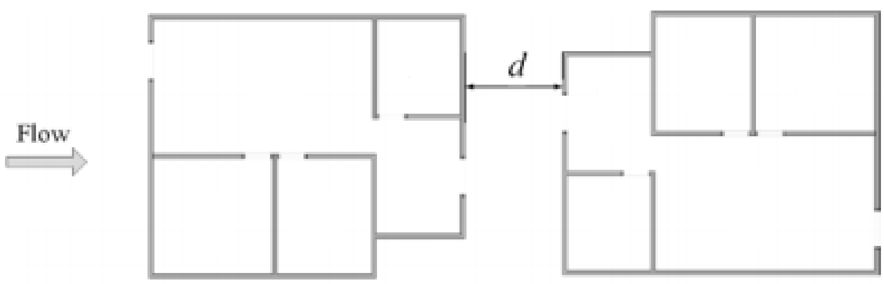

Figure 2-5: Model layout of the buildings studied by Tuan et al. [52].

Mohamed et al. [96] suggested that balconies could improve the level of thermal comfort and indoor air quality of apartments for high-rise building by providing higher indoor air velocity and better ventilation performance, respectively. Amos et al. 6 tested the impact of two different boundary walls, solid and perforated, on indoor airflow and patterns inside a typical residential building in Ghana with steady RANS simulations. The CFD results showed that the indoor airflow was significantly affected by the distance and height of the boundary wall and could be reduced to 40%. The effect of the surrounding buildings on the cross-ventilated flow was also investigated by Tong et al [100], and they concluded that the air flow rate was reduced to approximately 30% for the sheltered building due to the presence of the surrounding buildings.

The external boundary wall is a commonly used feature in low-rise buildings in Iraq and some other countries. A typical envelope design for residential buildings in Iraq is limited between 1 and 1.5 m in height with a thickness of 0.2 m. A higher wall than this limit will effect on the features of the building and reduce the ventilation rate considerably while lower wall than this limit is undesirable.

Generally, there is limited knowledge and understanding of the impact of external boundary walls on indoor air patterns and flow rates. In addition, not enough studies have focused on their influence on unsteady cross-ventilation, where the flow with the presence of a wall is high turbulence with more unsteadiness. Therefore, this paper focuses on investigating the impact of an external boundary wall on improving indoor mean velocity, flow pattern inside rooms and natural cross-ventilation in an isolated residential house in Iraq using the LES method with a dynamic sub-grid scale model. In addition, the study examines the effects of two wall heights at 1 m and 1.2 m. The findings from this study are expected to improve the understanding about of the effect of external wall on natural ventilation and indoor air environment in residential buildings.

2.4 Thermal comfort evaluation under a naturally ventilated environment

Thermal comfort is the condition which expresses the level of satisfaction with the thermal environment and is usually assessed by subjective evaluation; there are many factors that affect thermal comfort such as heat conduction, convection, radiation, evaporative and heat loss [13]. In the building sector alone, the interest regarding energy-consciousness and sustainable eco-building development has increasingly grown to gain a better indoor environment and reduced energy consumption [107]. Therefore, there have been numerous indoor thermal environmental studies conducted for various types of buildings, including public buildings [108] [109] [110], transportation [111] [112], whole building environment [113] [114], offices [107] [115] [116] [117] and specific enclosed space [118], and one common feature of these studies is the evaluation of thermal comfort.

In general, thermal comfort can be assessed by available models such as comfort temperature[119], standard effective temperature (SET) [120], predicted mean vote (PMV) and predicted percentage of dissatisfied (PPD) [121]. ASHRAE standard 55-2004 provided an adaptive equation defining comfort temperature as[119]:

$$T_c = 0.31T_{om} + 17.8 \qquad (2\text{-}1)$$

where T_{om} is the monthly mean outdoor temperature (°C). The adaptive comfort standard has a mean comfort zone band of 5 K for 90% acceptance, and another of 7 K for 80% acceptance [119].

Standard effective temperature (SET) is a model of human response to the thermal environment, developed by A. P. Gagge and accepted by ASHRAE in 1986 [122]. With the effective temperature the thermal conditions can be compared to the conditions in a standardized room with a mean radiant temperature equal to air temperature and a constant relative humidity of 50% [123] . For the current study, PMV and PPD are considered. The PMV and PPD models stand amongst the most recognized thermal comfort models that have been developed using principles of heat balance and experimental data collected in controlled climate chambers under steady state conditions [13]. Occupants can control their thermal environment using clothing, operable windows, fans, heaters and sun shades. ASHRAE Standard 55 uses the PMV index to set the requirements for indoor thermal conditions and predicts the mean value of the votes of a large group of subjects for particular combinations of air temperature, mean radiant temperature, clothing insulation, metabolic rate, air speed, and relative humidity. Standard thermal comfort surveys ask subjects about their thermal sensation as rated by a seven-point scale of cold (-3) to hot (+3), where zero is the ideal value and has recommended limits of -0.5 to 0.5 [13].

The predicted mean vote for thermal comfort (PMV) is determined from the heat balance of the human being with his environment:

$$PMV = [0.303\ exp(-0.036M) + 0.028]\ L_{th} \qquad (2\text{-}2)$$

where M the metabolic rate (W/m^2) and L_{th} is the thermal load on the body expressed.

PPD predicts the percentage of occupants that will be dissatisfied with the thermal conditions and is a function of PMV. According to ASHRAE 55, the recommended acceptable PPD range of thermal comfort is less than 10% of persons dissatisfied with an interior space, since PPD is a function of PMV, it can be defined as:

$$PPD = 100 - 95e^{[-(0.03353PMV^4 + 0.2179PMV^2)]} \qquad (2\text{-}3)$$

In this context, Straw et al. [36] presented the results of experimental versus computational investigations of wind-driven ventilation with openings on the opposite walls of a room. Hunt et al. [124] examined ventilation driven by a point source of buoyancy on the floor of an enclosure in the presence of the wind. CFD simulations of the wind-assisted stacked ventilation of a single-storey enclosure with high- and low-level ventilation openings were presented by Cook et al. [125], the results of which are compared with both laboratory measurements and an analytical model of the flow and thermal stratification.

Hassana et al. [126] studied the impact of window combinations on thermal comfort index (PMV) for various wind speeds and directions (Figure 2-6); this study showed that two non-adjacent openings in a single-sided ventilation system result in better ventilation than with adjacent openings. Stavrakakis et al. [38] examined natural cross-ventilation with openings at non-symmetrical locations both experimentally and numerically (Figure 2-7). They concluded that the indoor thermal environment considered was unsatisfactory in terms of thermal perception and was 80% below the recommended levels. Milne and Kohut [127] focused on residential housing designed with high mass first floors, cross ventilation at each level and stack ventilation up the stairwell. The study concluded that the predicted percent dissatisfied (PPD) was 37%, implying that about 63% of the occupants would probably not find the prevailing conditions uncomfortable.

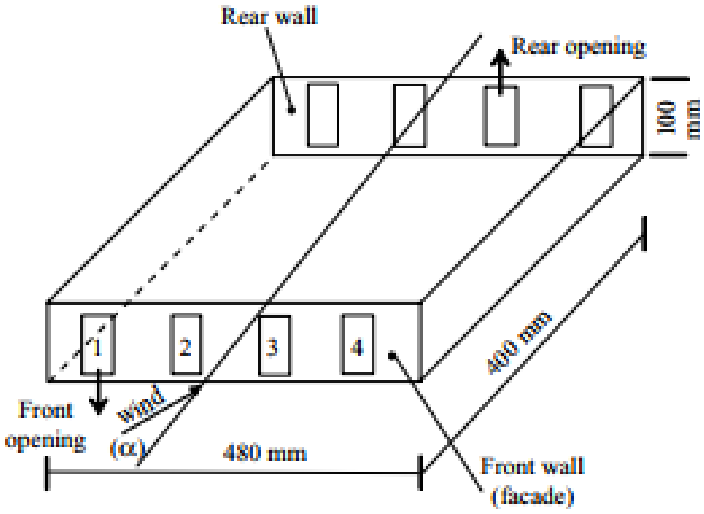

Figure 2-6: Test model studied by Hassana et al. [126].

Reduced-scale building models and numerical investigations of buoyancy-driven natural ventilation were used as the basis for a CFD simulation by Walker et al. [128] to investigate the buoyancy-driven ventilation of a scaled model with two configurations, namely those of the atrium stack vents being open and closed, and compared the results against the scaled model's measurements. Several aspects of the models were compared, including indoor temperatures, velocities, and airflow patterns.

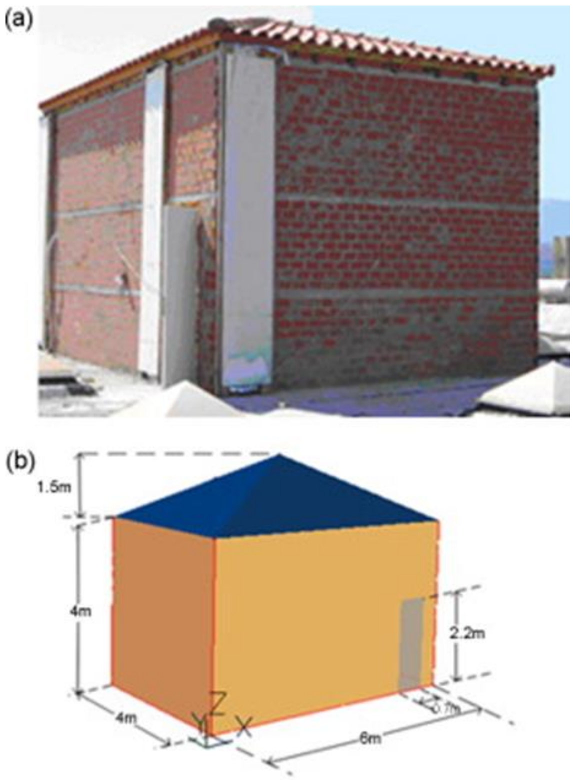

Figure 2-7: (a) Experimental chamber and (b) geometrical details [38].

Stavridou et al. [129] investigated the impact of outlet opening position on cross-natural ventilation due to buoyancy assisted by the wind using computationally and laboratory simulation techniques. A simple, empty small-scale building filled with ethanol as an operating fluid in open channel was used in this study and the thermal comfort assessment was made in terms of temperature and velocity only (Figure 2-8). Koranteng et al. [130] investigated the impact of opening size and position on indoor comfort for a residential room that was naturally single-side ventilated. It was found that to achieve comfortable indoor conditions, the ideal window-to-wall size ratio should be between 10 to 40%, and that the various positions of the windows did not seem to have any effect on indoor temperature. Prakash and Ravikumar [131] analysed thermal comfort for a residential building room under generalized window opening positions on adjacent walls and introduced a new set of strategies to find optimal window openings.

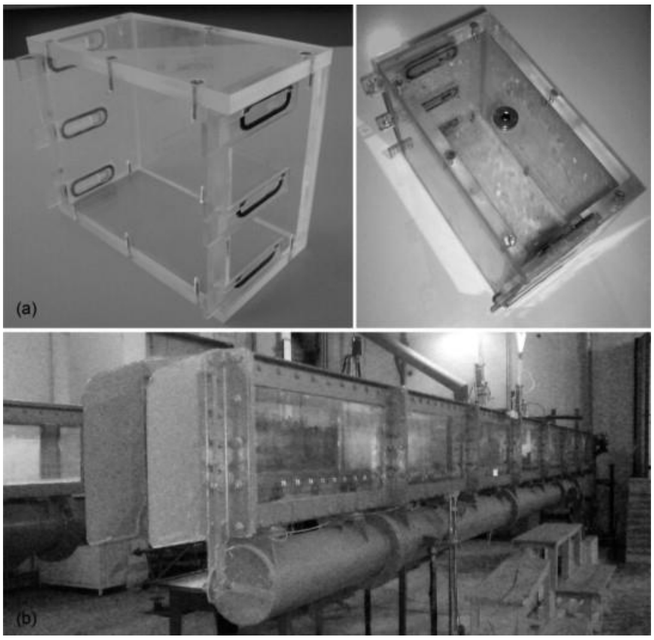

Figure 2-8: (a) Experimental model made of Plexiglas, (b) Open channel in the Laboratory of Hydraulics [129].

The natural ventilation design approach could reduce up to 1.13 kWh/m^2 the energy consumption of the building per annum with respect to an initial building design (Figure 2-9) in which natural ventilation has not been considered [132]. The combined operation of the wind-catcher and the dynamic façade can deliver operative temperature reductions of up to 7°C below the base-case strategy, and acceptable ventilation rates for up to 65% of the cooling period [133]. Lei et al. [134] showed that the indoor air quality generally was improved with an increase in natural ventilation area, whereas the thermal comfort level gradually declined. Baglivo et al. [135] evaluated the impacts of walls, slab-on-ground floors, roof, shading, windows and internal heat loads on the thermal behaviour of a building in a warm climate. Further study showed that the roof, floor, and the airtightness were the critical building parameters affecting the indoor thermal environment [136].

Figure 2-9: Building prototype render [132].

Most of the previous studies have investigated the effect of the opening positions on thermal comfort without coupling the flow between indoors and outdoors in one domain, with the latter representing a more realistic flow because of its fluctuation through the inlet and outlet openings [137]. There are a limited number of studies employing natural ventilation for the purpose of cooling in hot climates. In addition, very few studies have employed the human thermal comfort indices, PMV and PPD, in the analysis of the indoor environment, which in fact are more realistic than other indices. One of the main objectives of this study is to employ cross-ventilation through openings in the front and rear walls for passive cooling based on the human thermal comfort indices (PMV and PPD) of an isolated family house in a hot climate.

Moreover, there is a limited number of studies employing cross-ventilation for the purpose of cooling in hot climates have considering the impact of furniture and heat loads. Therefore, the study also focused on the impact of heat sources (e.g., TV, oven, and refrigerator) and furniture on the human thermal comfort indices (PMV and PPD) as well. The findings from the study are expected to improve our understanding and knowledge as to the impact of these parameters on the human thermal comfort indices in residential buildings.

Chapter 3 Numerical Methods

3.1 Introduction

Computational fluid dynamics (CFD) has become an essential tool and a detailed modelling technique widely used for investigating the airflow patterns through coupling indoor-outdoor microclimate by calculating velocities, temperatures and pressures. The CFD model has the ability to simulate a wide range of flow problems for different configurations and can be less expensive, both in time and resources, relative to traditional wind tunnel testing [1]. Furthermore, it can provide great design flexibility and has good correlation with experimental results in spite of having some uncertainties in the models, requiring sufficient knowledge on fluid mechanics from a user and demanding a high capacity computer [138]. The RANS models have been widely used to study indoor air quality, thermal comfort, HVAC system performance, etc. in various buildings (residential buildings, commercial buildings, health care facilities, schools, institutional buildings, and industrial buildings) [139]. Currently, the LES is mainly used as a research tool and it is an intrinsically accurate method for CFD simulations of wind flows [53]. The researchers were more satisfied with the results than a few years ago despite higher computing costs [139].

The commercial CFD software package FLUENT 16.2 is to perform the CFD simulations. The 3D steady Reynolds-Averaged Navier-Stokes (RANS) equations are solved in combination with the Renormalization Group (RNG) k-ε model. For time-depend approach Large Eddy Simulation (LES) are solved with the Smagorinsky-Lilly subgrid model. In this chapter, a brief description of the governing equations is given in the first part of the chapter, followed by the numerical models (RANS and LES) and finally a validation study are presented and discussed.

3.2 Governing equations

The fundamental governing equations of the fluid dynamics, i.e. the continuity, momentum and energy equations, are the mathematical statements of three fundamental physical principles, which can be regarded as follows:

- Conservation of mass (Continuity Equation)
- Newton’s Second Law (Momentum Equation)
- Conservation of energy (First law of thermodynamics)

Utilising the finite (control) volume method, the continuity equation is discretised by mass balance for a finite volume.

By applying Newton's Second Law of Motion, the relationship between the forces on a control volume of fluid and the acceleration of the fluid gives an expression for the conservation of momentum (Navier-Stokes equations).

Rate of increase of momentum of fluid particle	=	*Sum of forces on fluid particle*

The energy equation is derived from the first law of thermodynamics, which states that the rate of change of energy of a fluid particle is equal to the rate of heat addition to the fluid particle plus the rate of work done on the particle [140]:

Rate of increase of energy of fluid particle	=	*Net rate of heat added to fluid particle*	+	*Net rate of work done on fluid particle*

This would therefore allow the definitions of changes in fluid temperature within a control volume.

These fundamental principles can be expressed in terms of a set of partial differential equations as:

$$\frac{\partial(\rho u_i)}{\partial t} + \frac{\partial(\rho u_i)}{\partial x_i} = 0 \qquad \textit{(3-1)}$$

$$\frac{\partial(\rho u_i)}{\partial t} + \frac{\partial(\rho u_i u_j)}{\partial x_j} = -\frac{\partial p}{\partial x_j} + \frac{\partial}{\partial x_j}\left(\mu\left(\frac{\partial u_i}{\partial x_j} + \frac{\partial u_j}{\partial x_i}\right)\right) + \rho g_i + F_i \qquad \textit{(3-1)}$$

$$\frac{\partial T}{\partial t} + \frac{\partial(\rho u_i T)}{\partial x_i} = \frac{\partial}{\partial x_j}\left(\alpha\frac{\partial T}{\partial x_i}\right) + S_h \qquad \textit{(3-2)}$$

where g_i *and* F_i represent the forces due to gravity and external body force, respectively, and α is the molecular thermal diffusivity.

3.3 Turbulence models

In the current study, 3D steady RANS model and LES technique are applied to simulate the flow field and the heat transfer in the domain from Navier-Stoked equations. In addition, both models are used to validate the simulation results with the available wind tunnel experimental. The RANS simulation is conducted with the RNG k-ε turbulence model, whereas the LES is performed with the dynamic Smagorinsky subgrid-scale model.

3.3.1 Reynolds-Averaged Navier-Stoked model

The governing equations of continuity, momentum and energy for the steady incompressible flows and heat transfer with negligible radiation are expressed as follows [23]:

$$\frac{\partial(\rho u_i)}{\partial x_i} = 0 \qquad (3\text{-}3)$$

$$\frac{\partial(\rho u_i u_j)}{\partial x_j} = -\frac{\partial p}{\partial x_j} + \frac{\partial}{\partial x_j}\left(\mu\left(\frac{\partial u_i}{\partial x_j} + \frac{\partial u_j}{\partial x_i}\right) - \rho\overline{u_i' u_j'}\right) + \rho\beta(T - T_o)g_i \qquad (3\text{-}4)$$

$$\frac{\partial(\rho u_i T)}{\partial x_i} = \frac{1}{c_p}\frac{\partial}{\partial x_j}\left(\lambda\frac{\partial T}{\partial x_i}\right) + \frac{\partial}{\partial x_j}\left(-\rho\overline{u_j' T}\right) \qquad (3\text{-}5)$$

where $\overline{u_i' u_j'}$ is the Reynolds stress tensor, T_o is the operation temperature, β is the thermal expansion coefficient and where $\overline{u_j' T}$ is the turbulent heat flux. By relating the stress tensor and turbulent heat flux to the mean strain-rate and mean temperature gradients, respectively,
the two unknowns can be solved as follows:

$$-\rho\overline{u_i' u_j'} = \mu_t\left(\frac{\partial u_i}{\partial x_j} + \frac{\partial u_j}{\partial x_i}\right) - \frac{2}{3}\rho\delta_{ij}k \qquad (3\text{-}7)$$

$$-\rho c_p\overline{u_i' T} = q_c = \lambda_t\frac{\partial T}{\partial z} \qquad (3\text{-}8)$$

where μ_t is the turbulent dynamic viscosity, λ_t is the turbulent thermal conductivity ($\lambda_t = C_p\mu_t/Pr_t$), which is proportional to μ_t since the turbulent Prandtl number, Pr_t, ranges from 0.7 to 0.9 depending on the laminar Prandtl number of the fluid [141]. For the used RANS turbulence models, μ_t is related to the turbulent kinetic energy (k) and turbulent dissipation rate (ε) ($\mu_t = C_\mu \rho k^2/\varepsilon$) and the two-equation renormalized group *RNG k-ε* turbulence model was used to solve this relation. This model can produce an accurate prediction of indoor air flow and expressed as [23]:

$$\frac{\partial(\rho k u_i)}{\partial x_i} = \frac{\partial}{\partial x_j}\left[\left(\mu + \frac{\mu_t}{\sigma_k}\right)\frac{\partial k}{\partial x_j}\right] + G_k + G_b - \rho\varepsilon \qquad (3\text{-}9)$$

$$\frac{\partial(\rho \varepsilon u_i)}{\partial x_i} = \frac{\partial}{\partial x_j}\left[\left(\mu + \frac{\mu_t}{\sigma_\varepsilon}\right)\frac{\partial \varepsilon}{\partial x_j}\right] + C_{1\varepsilon}\frac{\varepsilon}{k}(G_k + C_{3\varepsilon}G_b) - C_{2\varepsilon}\rho\frac{\varepsilon^2}{k} - R_\varepsilon \qquad (3\text{-}10)$$

where

$$R_\varepsilon = C_\mu \rho \eta^3 (1 - \eta/\eta_\circ)\, \varepsilon^2/(1 + \beta\eta^3)k \qquad (3\text{-}11)$$

with $\eta = (\mathrm{S}k/\varepsilon)$ and $\mathrm{S} \equiv \sqrt{2\mathrm{S_{ij}}\mathrm{S_{ij}}}$

S is the modulus of the mean rate-of-strain tensor.

In *RNG k-ε* turbulence model, ($G_k = \mu_t\, \mathrm{S}^2$) represents the generation of turbulence kinetic energy due to the mean velocity gradients. G_b is the generation of turbulence kinetic energy due to buoyancy, calculated as:

$$G_b = \beta g_i \frac{\mu_t}{Pr_t}\frac{\partial T}{\partial x_j} \qquad (3\text{-}12)$$

where g_i is the component of the gravitational vector in the *i* th direction.

$C_{3\varepsilon}$ in Equation (3-10) is calculated according to the following relation:

$$C_{3\varepsilon} = tanh\left|\frac{v}{x}\right| \qquad (3\text{-}13)$$

The values of the constant in $RNG\ k - \varepsilon$ turbulence model are:

C_μ *=0.0845,* σ_k *=0.7194,* σ_ε *=0.7194,* $C_{1\varepsilon}$ *=1.42,* $C_{2\varepsilon}$ *=1.68,* $\eta_\circ$ *=4.38* and β *=0.012.*

Near-wall treatment is taken into consideration for the viscous sublayer by using a low-Reynolds number model instead of the wall functions and was suggested by Kader [142]. The enhanced wall treatment is a near-wall modelling method that combines a two-layer model with so-called enhanced wall functions. If the near-wall mesh is fine enough to be able to resolve the viscous sublayer ($y^+=1$), then the enhanced wall treatment will be identical to the traditional two-layer zonal model. In this approach, the whole domain is subdivided into a viscosity-affected region and a fully-turbulent region. The demarcation of the two regions is determined by a wall-distance-based, turbulent Reynolds number (*Re**).

In the fully turbulent region (Re* >200), the *RNG k-ε* model is employed whilst in the viscosity-affected near-wall region, the one-equation model of Wolfstein is employed [23], in which the turbulent Reynolds number Re∗ is smaller than 200.

To have a method that can extend its applicability throughout the near-wall region it is necessary to formulate the law-of-the wall as a single wall law for the entire wall region. ANSYS Fluent achieves this by blending the linear (laminar) and logarithmic (turbulent) law-of-the-wall using a function suggested by Kader [142]:

$$u^+ = e^{\Gamma} u^+_{lam} + e^{1/\Gamma} u^+_{turb} \qquad (3\text{-}14)$$

where the blending function of momentum equation (Γ) is given by [23]:

$$\Gamma = -a(y^+)^4/(1 + by^+) \qquad (3\text{-}15)$$

where a=0.01 and b=5.

Similar to the velocity a thermal boundary layer develops when a fluid at a specified temperature flows over a surface that is at a different temperature. In ANSYS Fluent's near-wall model, enhanced thermal wall functions follow the same approach developed for the profile of u^+ ($u^+=u/u_\tau$). The unified wall thermal formulation blends the laminar and logarithmic profiles according to the method of Kader [142].

$$T^+ = e^{\Gamma} T^+_{lam} + e^{1/\Gamma} T^+_{turb} \qquad (3\text{-}16)$$

where T_w is the temperature at the wall, T_P is the temperature at the first near-wall node P and $q^{\cdot}$ is the wall heat flux. Furthermore, blending function of energy equation (Γ) is given by:

$$\Gamma = -a(Pry^+)^4/(1 + bPr^5 y^+) \qquad (3\text{-}17)$$

where the coefficients a and b are defined as in Equation (3-15).

3.3.2 Large Eddy Simulation

In LES, the filtered continuity, momentum and energy equations are listed as follows [23]:

$$\frac{\partial \rho}{\partial t}+\frac{\partial(\rho \bar{u}_i)}{\partial x_i}=0 \qquad (3\text{-}18)$$

$$\frac{\partial \overline{\rho u_i}}{\partial t}+\frac{\partial(\rho \bar{u}_i \bar{u}_j)}{\partial x_j}=-\frac{\partial \bar{p}}{\partial x_i}+\frac{\partial}{\partial x_j}\left\{\mu\left(\frac{\partial \bar{u}_i}{\partial x_j}+\frac{\partial \bar{u}_j}{\partial x_i}\right)\right\}-\frac{\partial \tau_{ij}}{\partial x_j}+\rho\beta(\bar{\mathrm{T}}-\mathrm{T_o})\mathrm{g_i} \qquad (3\text{-}19)$$

$$\frac{\partial(\rho \bar{T})}{\partial t}+\frac{\partial(\rho \bar{u}_j \bar{T})}{\partial x_j}=\frac{\mu}{Pr}\frac{\partial^2 \bar{T}}{\partial x_i \partial x_j}-\rho\frac{\partial h_j}{\partial x_j} \qquad (3\text{-}20)$$

where $\bar{u}_i$ is the component of filtered instantaneous fluid velocity in the x_i direction, $\bar{P}$ is the fluid pressure, ρ is the fluid density, μ is the fluid dynamic viscosity, the bar '–' represents the spatial filtering and τ_{ij} represents the sub-grid scale tensor, the latter being modelled by the Smagorinsky model.

$$\tau_{ij}=\left(\frac{1}{3}\right)\tau_{kk}\delta_{ij}-2\mu_t\bar{S}_{ij} \qquad (3\text{-}21)$$

where τ_{ij} is the subgrid-scale stress tensor, $\bar{S}_{ij}$ is the rate of strain tensor of the resolved scale and μ_t is the viscosity of the sub-grid scale turbulence, which is defined as:

$$\mu_t=\rho L_s^2\sqrt{2\,\bar{S}_{ij}\bar{S}_{ij}} \qquad (3\text{-}22)$$

where L_s is the mixing length for sub-grid scales and can be calculated as:

$$L_s=min(\kappa d, C_s\,V^{1/3}) \qquad (3\text{-}23)$$

where κ is the Von Kármán constant, d is the distance to the closest wall, V is the volume of the computational cell and C_s is the dynamic Smagorinsky coefficient, which is computed during the simulation using the information provided by the smaller scales of the resolved fields. The dynamic Smagorinsky coefficient approach has been employed in the field of computational wind engineering by various other researchers [143, 144]. This coefficient varies with time and space, which allows the Smagorinsky model to cope with transitional flows and to include near-wall damping effects in a natural manner [145]. With this method, a second filter, referred to as the test filter (denoted with a curl), is applied to the once-filtered Navier-Stokes equations. The dynamic Smagorinsky coefficient can be calculated as:

$$C_s = \frac{L_{ij}M_{ij}}{2M_{ij}M_{ij}} \tag{3-24}$$

where

$$L_{ij} = \widetilde{\bar{u}_i \bar{u}_j} - \tilde{\bar{u}}_i \tilde{\bar{u}}_j \tag{3-25}$$

and

$$M_{ij} = \widetilde{|\bar{S}|\bar{S}_{ij}} - \tilde{\bar{\Delta}}^2 \, |\tilde{\bar{S}}|\tilde{\bar{S}}_{ij} \tag{3-26}$$

are the resolved stress and Germano rate of strain tensor, respectively [146].

The subgrid-scale heat flux, h_j, is equal to $\left(\overline{u_j T} - \bar{u}_j \bar{T}\right)$ and is modelled by the subgrid-scale eddy diffusivity (α_t) hypothesis with constant subgrid-scale Prandtl number, Pr_t, as follows:

$$h_j = -\alpha_t \frac{\partial \bar{T}}{\partial x_j} = -\frac{v_{sgs}}{Pr_t} \frac{\partial \bar{T}}{\partial x_j} \tag{3-27}$$

3.4 CFD model validation

Validation is obligatory to determine the accuracy and reliability of the results of CFD simulations and a general overview of the validation study will be provided in this section. The model selection is based on the accurate results obtained in similar studies of natural cross-ventilation [33, 40, 42, 53, 79, 100, 147]. This section first describes the experimental setup and then presents the numerical models, including the computational domain, boundary conditions and discretization scheme. In the last part of this section, detailed comparisons between CFD results and experimental data demonstrate the model accuracy.

3.4.1 Wind tunnel experiments

The CFD model is evaluated by measuring the flow over and through a cross-ventilation building model in a boundary layer wind tunnel (Ohba et al. [148]). The experiment was conducted in a wind tunnel of dimensions 1.2 m wide, 1.0 m high and 14.0 m long. As shown in Figure 3-1, the model was rectangular, measuring 1:2:2 with a height of 15 cm and a wall thickness of 0.75 cm, and where the inlet and outlet openings have the same dimensions (6 cm width and 3 cm height). The opening of the building model was placed perpendicular to the approaching flow and located at the centre of the windward and leeward sides of the building. The reference velocity was maintained at 7.0 m/s at the upwind edge of the model; further details can be found in a previous study by the authors [149].

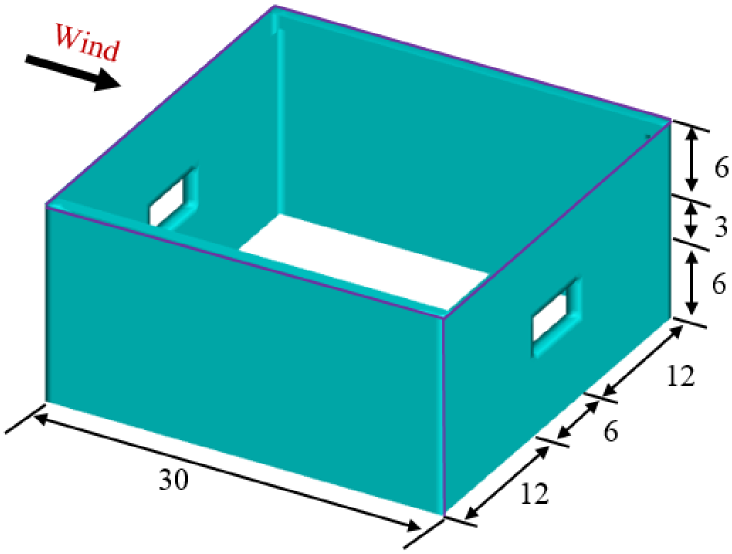

Figure 3-1: The geometry of the reduced-scale building model with dimensions (in meters) as studied by Ohba et al.[148].

3.4.2 CFD setting and parameters

The computational model represents the reduced-scale model used in the experiments and follows the two best-practice guidelines in wind engineering described by Franke et al. [39] and Tominaga et al. [40]. The dimensions of the domain are (22 x 5 x 12) H (Figure 3-2). The computational grid is created using hexahedral cells inside the building and domain, and a grid independence study is conducted to ensure that the results are independent of the mesh resolution and yield a fully structured hexahedral grid with 5.5×10^{6} cells (Figure 3-3). At the inlet of the domain, the vertical approach-flow profiles of wind speed, U, and turbulent kinetic energy, k, and specific dissipation rate, ε, are imposed, based on the measured incident profiles (Figure 3-4). The CFD code ANSYS Fluent 16.2 was used in the simulation. For the steady RANS model, the SIMPLEC scheme was imposed on the pressure–velocity coupling method, and the convective term was discretized by the bounded central-differencing scheme. The pressure was interpolated via a second-order scheme, whilst the spatial discretization of the convection terms of the momentum and the energy equations used the second-order upwind scheme. Regarding LES technique, the pressure-based solver was used in this study, where the flow was incompressible and the PISO algorithm was used for the pressure-velocity coupling. The second-order discretisation scheme was used for the pressure interpolation, whilst the bounded central-differencing scheme was used to discretise the convective term in the filtered momentum equation and time discretisation was the second-order implicit. A time-dependent inlet profile is generated by using the vortex method with the number of vortices N =190, and this setting was successfully tested in the previous LES validation studies for wind flows around buildings [53, 150].

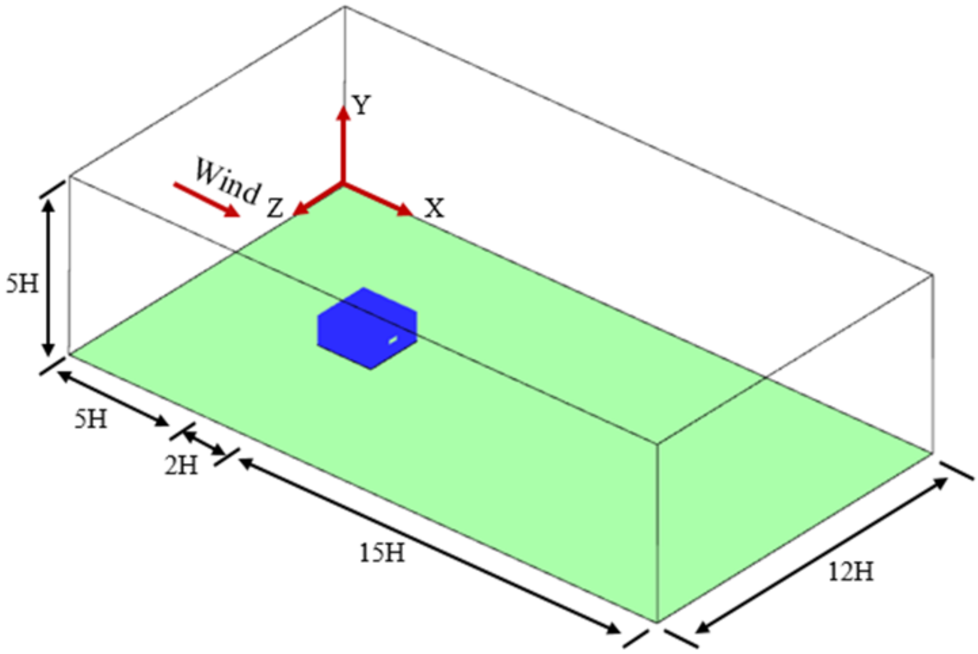

Figure 3-2: The building inside the defined duct.

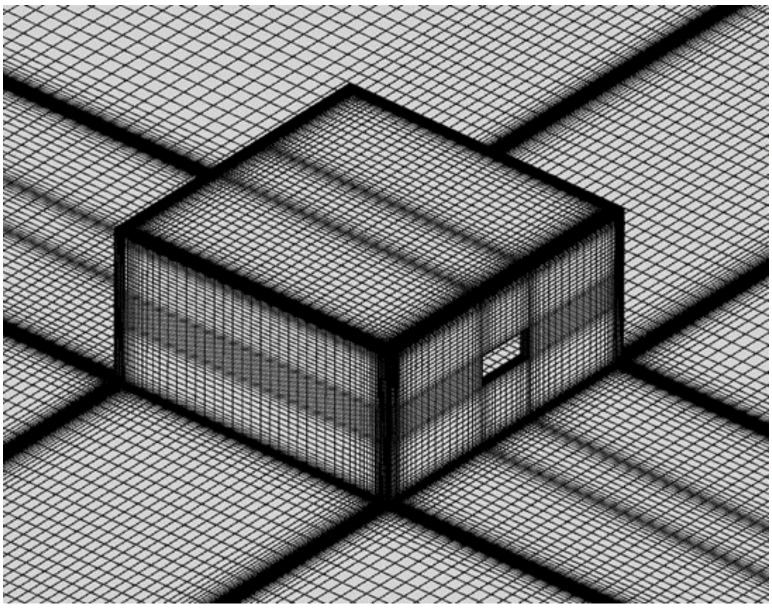

Figure 3-3: The mesh layout of the building.

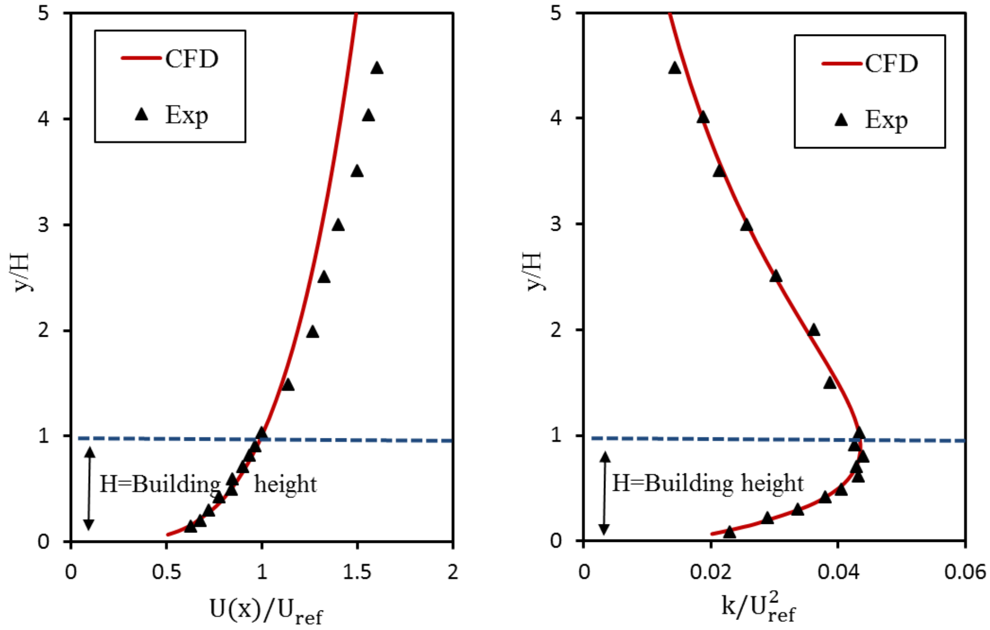

Figure 3-4: Comparison of dimensionless mean velocity and turbulent kinetic energy profiles of the approaching wind with experimental results of [148] at the inlet of the duct.

3.4.3 CFD model validation results and discussion

3.4.3.1 **Pressure coefficient**

The pressure coefficient profiles at the centrelines of the windward and leeward façade of the building obtained from the CFD simulations (RANS and LES) were compared with the experimental data reported by Ohba et al. [148], as shown in Figure 3-5. The LES simulation predicted closer results to those of the experiment than RANS. For the line of the front façade, the pressure coefficient of the flow in RANS deviated notably from the experimental results, especially, above the opening, while in LES the CFD simulation predicted results that were close to those derived from the experiment. As regards the leeward facade, the pressure coefficient along the line showed good agreement with the experimental results for LES. The steady RANS model predicted acceptable agreement with the experimental results above the opening, whilst under the opening, the data was close to the experimental results as LES results. Despite these differences, an overall good agreement is observed. The root-mean-square-error (RMSE) of RANS curves was 9% whilst for LES curves was 5%. This ratio is considered acceptable [151], especially if taking into account the deviation of the CFD values at the edges of the roof [7].

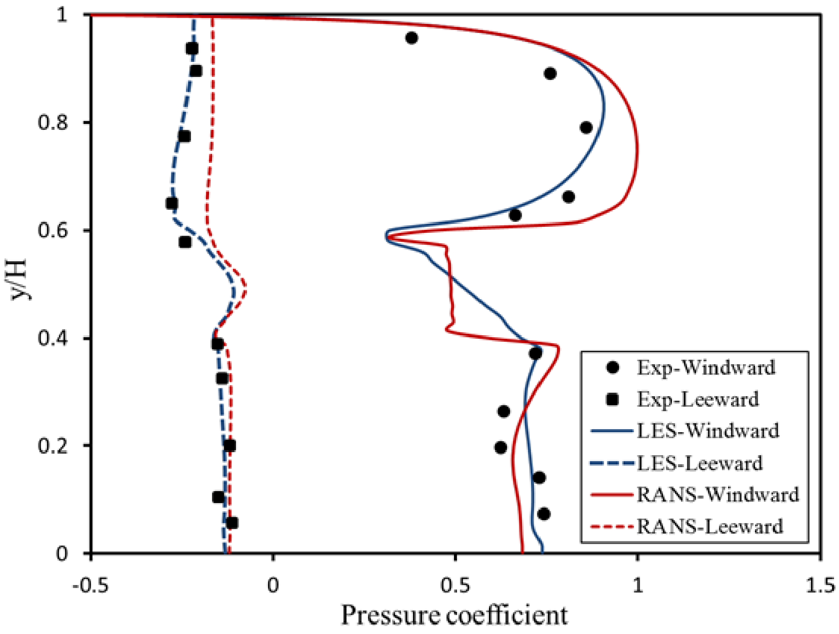

Figure 3-5: Pressure coefficient comparison between CFD and experimental results of [148] on the centrelines of the building external walls.

3.4.3.2 **Vector and mean velocity**

The comparison of the stream-wise wind speed ratio $U(x)/U_{ref}$ obtained with RANS and LES with the measurement data along a horizontal line through the middle of the two window openings is presented in Figure 3-6. The figure showed that there was good agreement between numerical and experimental results. The LES was more accurate than RANS to capture the flow acceleration near both openings, as well as deceleration inside the building. Moreover, the figure showed that the velocity of the incoming jet predicted by RANS model was higher than the experimental results, as found in other studies [100] [53] [79]. Overall, with the turbulence models selected, RNG k-ε model and LES, the average difference of the air velocity along, x, between the experimental, and the numerical results, RANS and LES, is around 10% and 6%, respectively. This difference is acceptable in similar CFD simulation studies [33, 40, 42, 53, 79, 100, 147].

The velocity vector field in the central plane of the building shows a close qualitative agreement between experimental and numerical results (Figure 3-7). The simulations reproduce the main vortexes of the flow, such as the one formed in front of the windward side of the building, the one formed at the leading edge of the roof and the windward wall, and the biggest one in the rear of the building. The wind velocities of the inflow stream accelerated and their directions changed downwards immediately inside the inflow opening. The internal air was then circulated by the incoming flows. At the exit of the outflow opening, the flows moved upwards and the velocities of the emitted air increased considerably. The averaged flow pattern calculated by RANS and LES exhibited the same flow behaviours as the experimental observations.

Generally, RANS models have been widely used in the ventilation sector for buildings in a cross flow, where the RNG k-ε model, in particular, provides high performance as the SST k-ω model in this kind of flow [39]. The LES simulation provides a very good agreement with the experimental data in cross-ventilation, both with respect to the mean velocities, flow pattern, and turbulent kinetic energy.

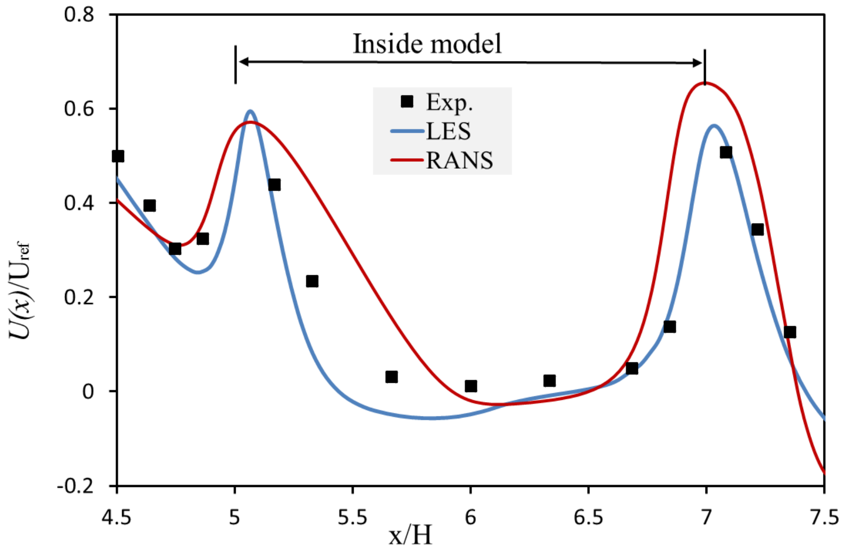

Figure 3-6: Comparison of experimental and CFD results for the stream-wise velocity ratio $U(x)/U_{ref}$ along the horizontal centreline of the openings.

3.4.4 Validation case versus case study

The geometry of the building that was used to validate the CFD model (Ohba et al. [148]) and that used in the current study (Figure 1-2) are not identical, but there are some similarities between the two geometries that allow the validation approach to be applicable for this type of building. For instance, both buildings are exposed to a wind direction normal to the façade. The atmospheric boundary layer is considered to be the approach-flow (Figure 3-4). Both buildings are isolated from the surroundings, and have a rectangular base. The roofs of both buildings are flat, without any external features such as gutters, shingles and eaves.

Regarding the CFD simulation, to minimize the differences between the CFD models of the validation case and the case study, the following steps are undertaken:

- The same boundary conditions of the computational domain (ground, top, outlet, and lateral sides) for both cases are used.
- The same numerical algorithms for both simulations are applied.
- Computational meshes for both geometries are generated using hexahedral unit cells keeping the same mesh parameters.

As a result, the notable features of the flow for the building studied by Ohba et al. [148] are also predicted for the building in the current study. The study of Ohba et al. [148] has been used in a number of other previous studies to validate the CFD models for different building geometries [43] [152]; for instance, those used by Cheung and Liu [152] to validate the standard k-ε model for a high-rise building with six inlet openings under a cross-ventilation. .

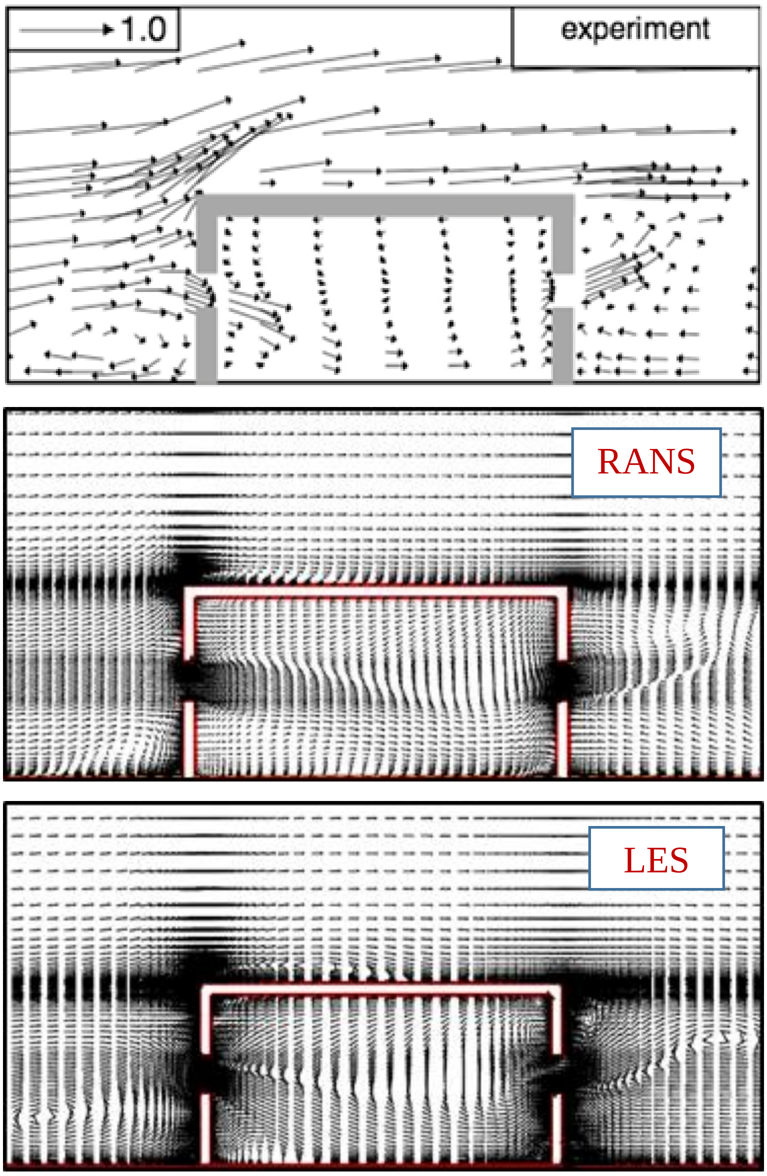

Figure 3-7: Comparison of the velocity vector field of measurements and the CFD simulations on the mid-plane of the building.

Chapter 4 Impact of windward inlet opening positions on fluctuation characteristics of wind-driven natural cross-ventilation

4.1 Introduction

This chapter presents a CFD simulation of coupled outdoor wind flow and indoor air flow in the investigation of the horizontal positions of openings on the fluctuation of cross-ventilation and flow field inside an isolated family house. Two inlet-opening positions located at the same height are used to investigate the impact of the position of windward inlet openings on ventilation rate and flow field inside the building. Due to unsteady flow and high turbulence near the openings, the study employed the large eddy simulation (LES) with the dynamic Smagorinsky subgrid-scale model techniques. The details of the CFD model and of the boundary conditions that are used for the domain airflow modelling are presented. The computational mesh dependence of the CFD predictions is tested in this chapter. The impact of the two inlet opening positions on the flow fields is evaluated and discussed in details in this chapter. The material reported herein has been published in the International Journal of Ventilation [19].

4.2 Case description

An isolated building model in cross-turbulent flow was considered for the computational analysis of wind-induced natural ventilation. Figure 4-1 shows a schematic of the studied model, which includes an isolated house with a height (H=3m) with two square openings (*0.2 H*) on the front wall of the house and two openings at the rear. The wall porosity (opening area divided by wall area) was 3%. Two different configurations of inlet openings, Case-I and Case-II, were used in this study. The base of the house had dimensions 8×10 m (Width ×Length) and the length of the building was less than the maximum length (5H) suggested by Chu et al. [7] to obtain effective wind-driven cross ventilation. The building is partitioned inside as shown in Figure 4-1; this layout is simple, and representative of an average family house in Iraq [27]. To simulate different window opening positions, two inlet-opening positions were used, as shown in Figure 4-2a, with the front view of the building cases including dimensions shown in Figure 4-2b. In both cases, the wind speed at the height of the building (U_{ref}) was 7 m/s with an angle of incidence of 0°.

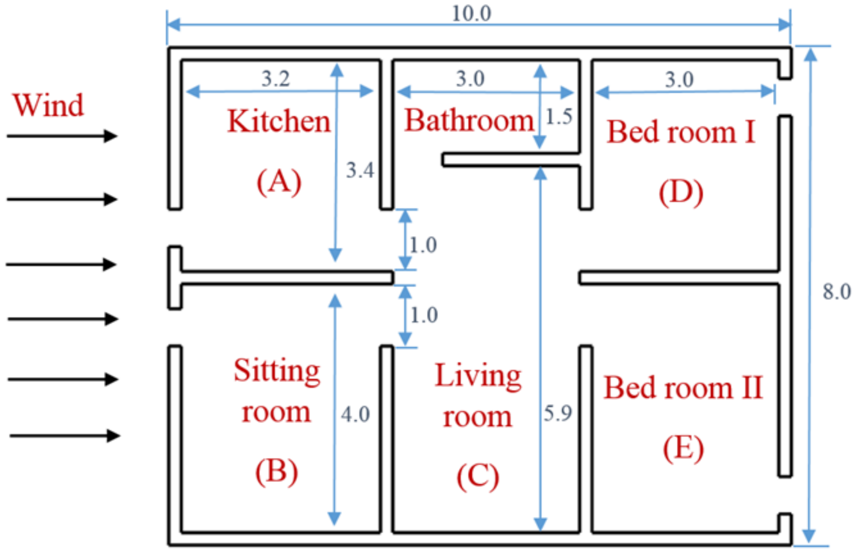

Figure 4-1: The layout of the building models (dimension in meters).

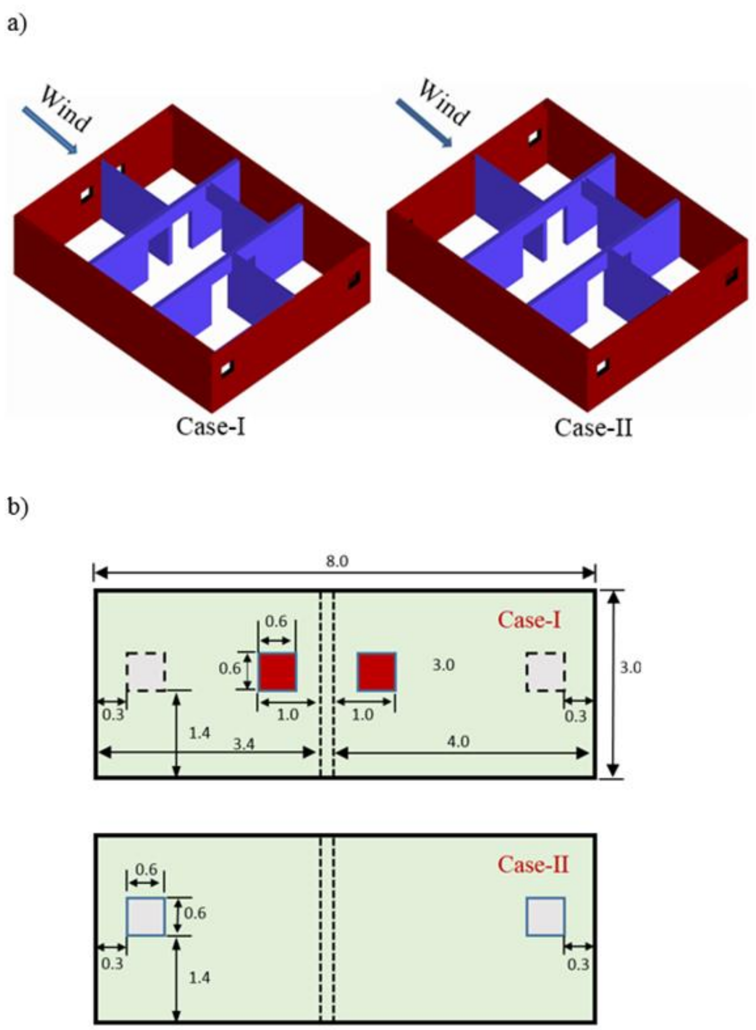

Figure 4-2: The geometry of the building models; (a) Perspective view and (b) Front view (dimension in meters).

4.3 CFD cases study: setting and parameters

In this section, the computational geometry, domain grid, boundary conditions and solver settings for the evaluation of the horizontal inlet opening position of an isolated family house are presented.

4.3.1 Computational geometry, domain and grid

A *3-D* computational domain was constructed based on COST [22] and AIJ [153] guidelines, consisting of a rectangular house with height *H* inside a duct (23.3×5×12.6) *H*, as shown in Figure 4-3. The blockage ratio was 4.2%, which is within the range recommended in the guidelines. A distance of 5*H* was set between the inflow boundary and the building, whilst the outflow boundary was positioned 15*H* behind the building to allow the flow to redevelop in the wake region.

The numerical grid was generated by ICEM and hexahedral cells were used inside the house and domain. A fine mesh was constructed near the walls because the dynamic Smagorinsky model in the LES method requires a very high grid resolution in these regions, whilst a coarse mesh was used away from the walls and in all directions. The space between the walls of the house and the centre of the first cell was 0.005*H*; the same distance was used for the ground, which is small enough to obtain y^+ around 1.4 and capture a laminar sub-layer. A grid expansion ratio of 1.15 or 1.2 was used between consecutive cells for the generation of the grid used in the simulation (Figure 4-4).

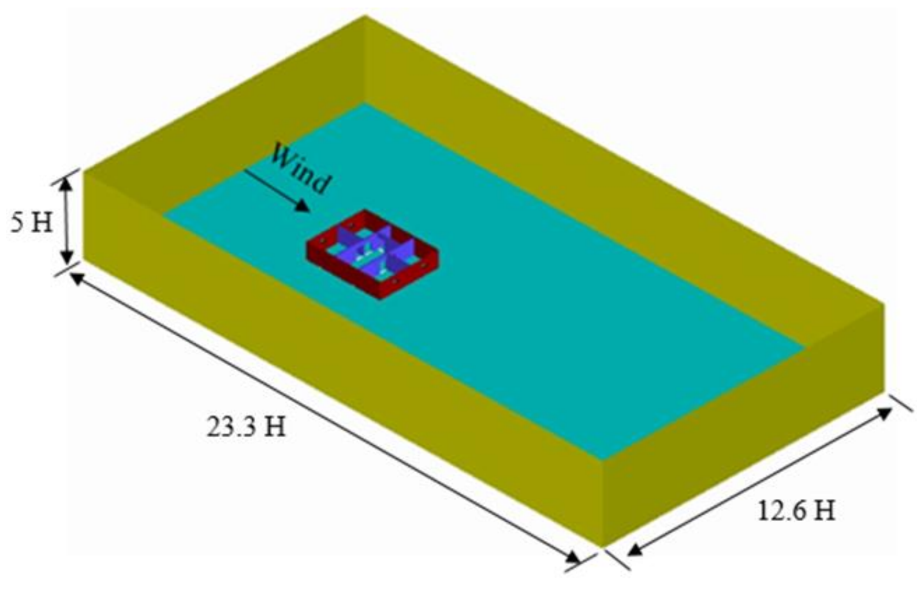

Figure 4-3: The building inside the defined duct.

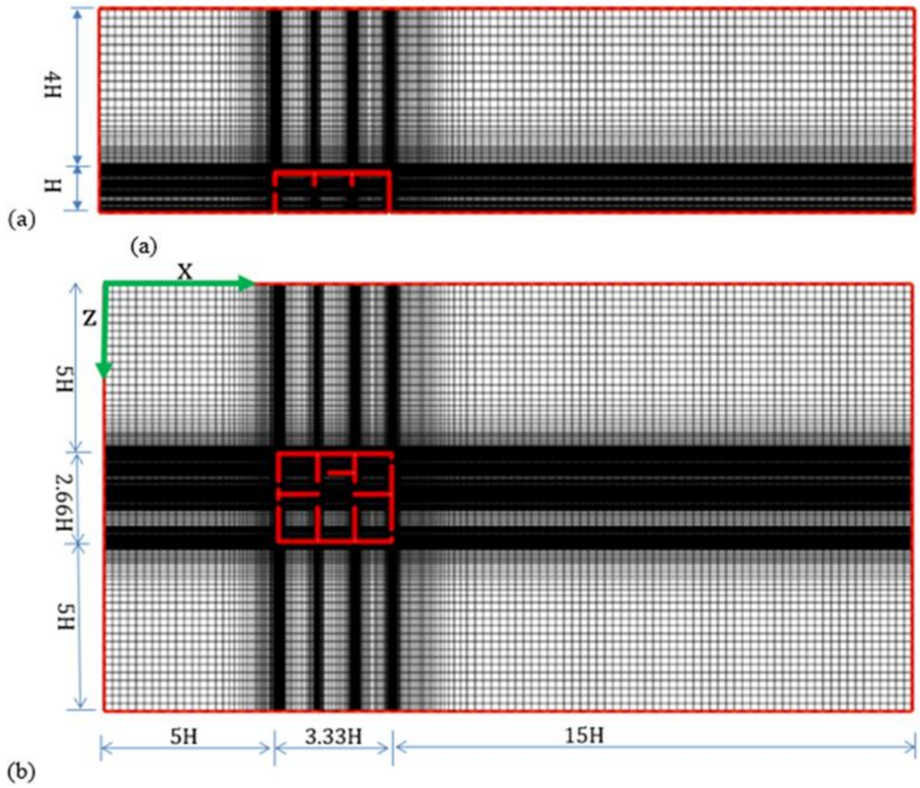

Figure 4-4: Computational domain and the mesh layout of grid (a) Side view and (b) Top view.

4.3.2 Grid independence

Grid independence is an important factor in numerical simulations and is selected to find the effect of mesh size on results. The LES index of quality proposed by Celik et al. [154] is used to test the grid, and is dependent on the calculation of turbulent kinetic energy. The total kinetic energy, k_t, includes a resolved part, k_{res}, a subgrid scale part, k_{sgs}, and the numerical dissipation, k_{num}

$$LES\_IQ = \frac{k_{res}}{k_t} = \frac{k_{res}}{k_{res} + k_{SGS} + k_{num}} = 1 - \frac{k_t - k_{res}}{k_t} \qquad (4\text{-}1)$$

According to Pope [155], when 80% of the turbulent kinetic energy is resolved, a LES computation is considered to be well-resolved. The combined turbulent kinetic energy of numerical dissipation and the *SGS* model based on Richardson extrapolation are assumed to scale with grid size/filter length [154]:

$$k_t - k_{res} = a_k \Delta^n \qquad (4\text{-}2)$$

where ak is a coefficient that can be determined by running the LES on two grids with different resolutions, and where n = 2 is the order of accuracy of the numerical scheme. The grid sensitivity analysis is performed for Case-I and two grids were chosen for this purpose: a coarse mesh (Grid A) with 3.5×106 cells, and a fine mesh (Grid B) with 6×106 cells. The profiles of LES_IQ along lines x/H = 4.6, 9 and 12 are shown in Figure 4-5. The LES for the fine mesh (Grid B) resolved on average more than 80% of the turbulent kinetic energy, whilst the course mesh (Grid A) resolved less than that proposed by Pope [155]. Therefore, the fine mesh with 6×106 cells was chosen for the simulation of Case-I, whilst for Case-II the grid sensitivity analysis was not performed, as this latter case has almost the same number of grids (6.1×106 cells) as Case-I.

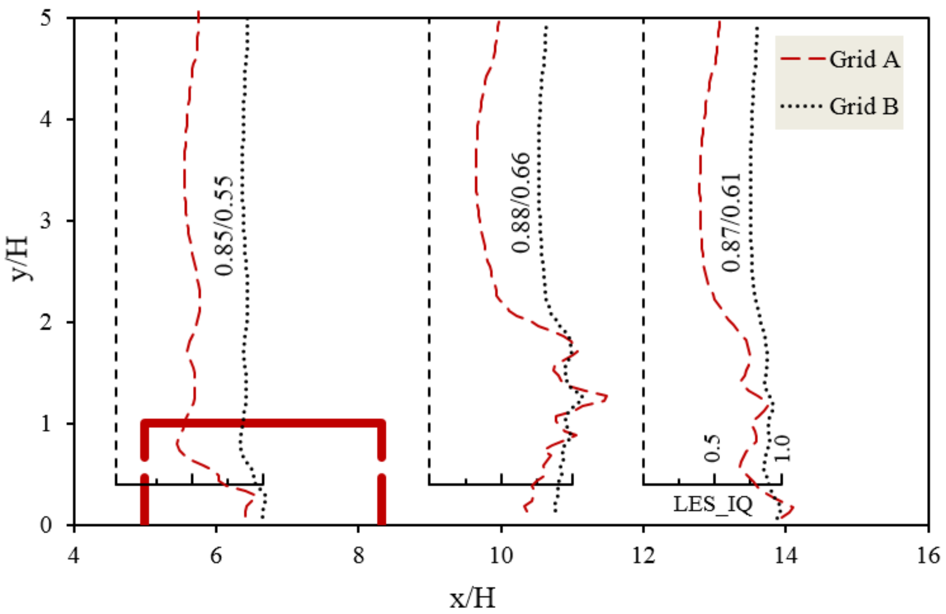

Figure 4-5: Profiles of LES_IQ for Grid A and Grid B in the vertical lines for the Case-I.

4.4 Boundary condition and solver settings

The inlet boundary conditions were based on the measurement incident profile of mean wind velocity. The inlet wind velocity profile is defined according to the logarithmic law. According to Richards and Hoxey [156], the vertical profiles of the mean wind velocity, turbulent kinetic energy and turbulent dissipation rate are imposed at the inlet of the domain. The equations used for the profiles are:

$$U(y) = \frac{u_\tau}{\kappa} ln\left(\frac{y + y_o}{y_o}\right) \tag{4-3}$$

$$k = a\ (\ U\ I_u\ )^2 \tag{4-4}$$

$$\varepsilon = \frac{{u_\tau}^3}{\kappa(y + y_o)} \tag{4-5}$$

The inlet boundary conditions were used with equations (4-3), (4-4) and (4-5) and the parameter, a, in eq. 12 is limited to 1.5 [149]. The value of u_τ is determined based on the values of the reference velocity (U_{ref} = 7 m/s) at a building height, H, and the aerodynamic

roughness length, yo. A time-dependent inlet profile at the inlet of the domain was generated by the vortex method, where the number of vortices was N= 190, this setting having been successfully tested in previous LES validation studies for wind flow around buildings[143, 149]. The lateral and the top sections of the domain were modelled as symmetry conditions, i.e., zero normal velocity and normal gradients for all variables. The surfaces of the house and the ground of the domain were modelled as no-slip boundaries, whilst at the outlet of the domain the zero-gradient condition was used [56].
The CFD package, FLUENT R16.3, was used for numerical simulation prediction. The pressure-based solver was used in this study, where the flow was incompressible. The PISO algorithm was used for the pressure-velocity coupling and the second-order discretization scheme for the pressure interpolation. The bounded central-differencing scheme was used to discretize the convection term in the filtered momentum equation. Time discretisation was second-order implicit, and the convergence criterion was 10^{-5} for all terms. The time-step was set to Δt = 0.0000075 s and kept constant during the simulation, which ensured that the Courant number was always smaller than 0.3 in most of the grid points with a maximal value of 0.6. The flow was initialized until the flow was fully developed and then, time-averaging and statistics collections are made for all the intended quantities were started. The initial transient conditions from the inlet of the duct and the total simulation time were continued until such a time as the flow became statistically steady. At this point, the total time for the simulation was found as 135,000 time-steps, which was equal to five time periods ($10T^*$), where dimensionless time, T^*, is defined as:

$$T^* = t\, U_{ref} / L_D \qquad (4\text{-}6)$$

where L_D is the length of the domain. The convergence of root-mean-square (RMS) quantities in unsteady flow was used for steady-state convergence. The transient run continued for a sufficiently long period of time until a statistically steady state was reached. To assess the quality of the LES analysis, a spectral analysis of certain quantities of interest were used. The way to achieve this is to extract a turbulent energy spectrum from the time history of the flow by performing a Fourier transform of the turbulent energy recorded over a long period of time. Examples of temporal evolution of the power density spectra (*PSD*) at points near the building are shown in Figure 4-6. The spectra in this figure show that the flow approaches fully turbulent and has a gradient of -5/3 in the roll-off.

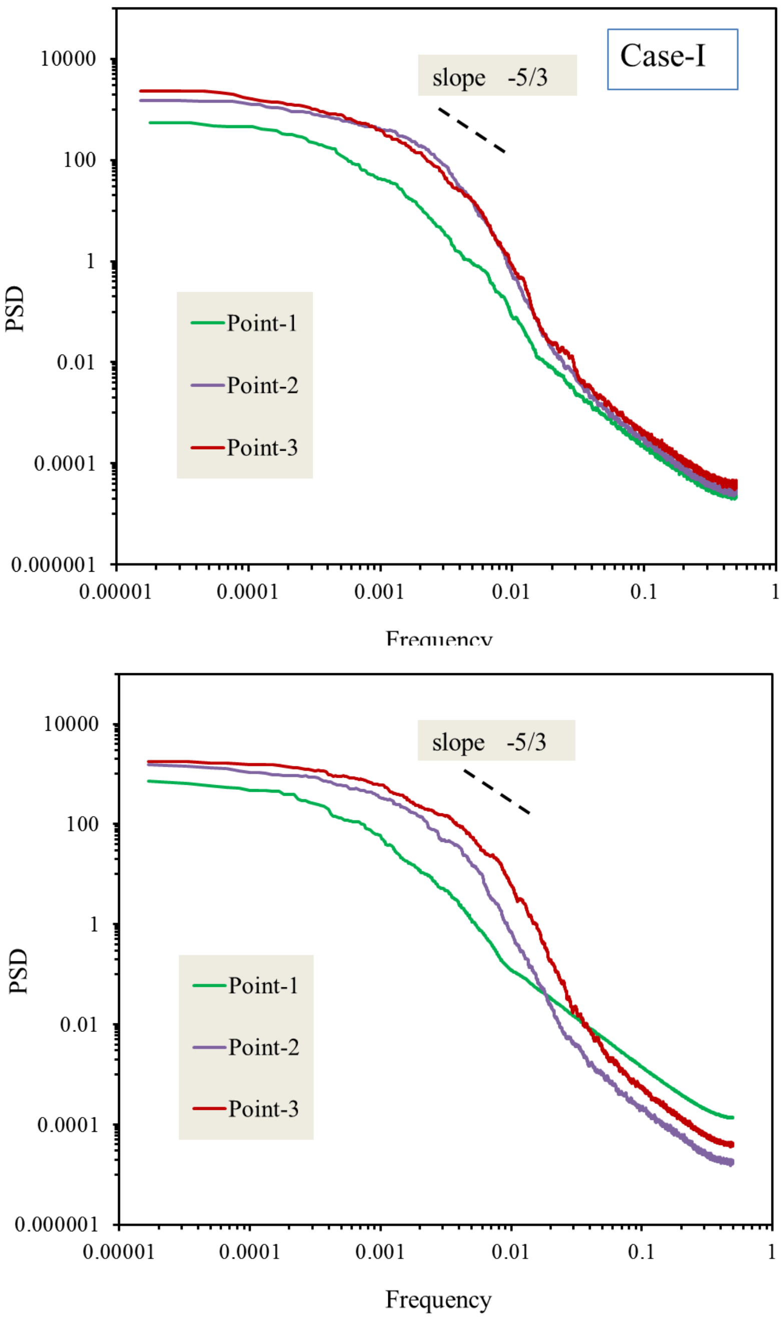

Figure 4-6: Power spectral density of the turbulent kinetic energy.

4.5 Results and discussion

The present study investigated the natural cross ventilation of a small-scale family house to ensure the physical comfort of the occupants. Two different inlet-opening configurations (Case-I, and II) were used to examine the impact of the windward inlet opening positions on the recirculation areas, flow pattern, and the ventilation rate inside a family house in order to determine which configuration is better. The inner layout of the building was kept the same for both configurations, and the schemes used for each case are shown in Figure 4-1and Figure 4-2. The flow enters from two openings in the front wall and exits from two openings in the rear wall of the house. The two inlet openings in Case-I are positioned near the centre of the building, whilst in Case-II the flow enters from openings near the sides of the building, whilst discharge is from openings located near the sides of the building for both cases. These four openings provide a high ventilation rate for the building. In order to investigate the impact of the positions of the inlet openings on cross ventilation, the area of the openings was kept constant in both cases, as was the wind speed at a constant of 7 m/s at the height of the building, with wind direction normal to the openings.

4.5.1 Mean flow and streamlines around the building

The mean velocity and streamlines around the building in the vertical and horizontal planes for both cases are presented in Figure 4-7 and Figure 4-8, respectively. The major feature shown outside the building is the formation of three main recirculation zones at the two side walls and the roof of the building because of the low-pressure zones produced in these regions, as shown in Figure 4-9. In addition, the low-pressure zone behind the building also produced a large circulation zone in both cases. The two kidney vortices covered one-third of the length of the right and the left side of the building, and seemed to be equal in their dimensions due to the almost-symmetrical flow. The third kidney vortex covered one-third of the length of the roof of the building near the edge of the roof itself. The upstream airflow is accelerated because it hits the edges of the roof and laterals of the building, reaching a maximum velocity of 9.2 m/s. Generally, these figures showed the same patterns of flow around the building in both cases, where the size of all vortices was found to be approximately the same. These results show that the position of the inlet openings has no significant effect on the flow behaviour around the building for these configurations, and most of the impact will probably occur inside the building.

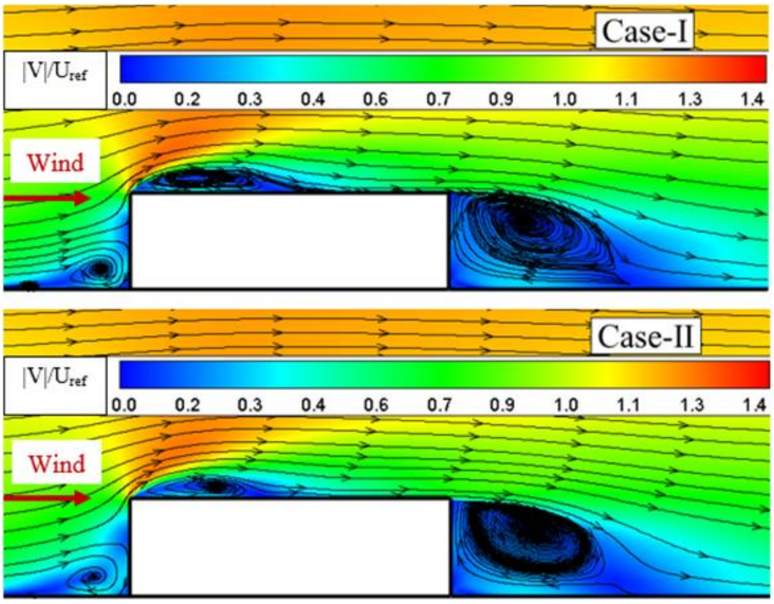

Figure 4-7: Contours of dimensionless mean velocity magnitude ($|V|/U_{ref}$) and streamlines around the building in the vertical plane at the middle of the building.

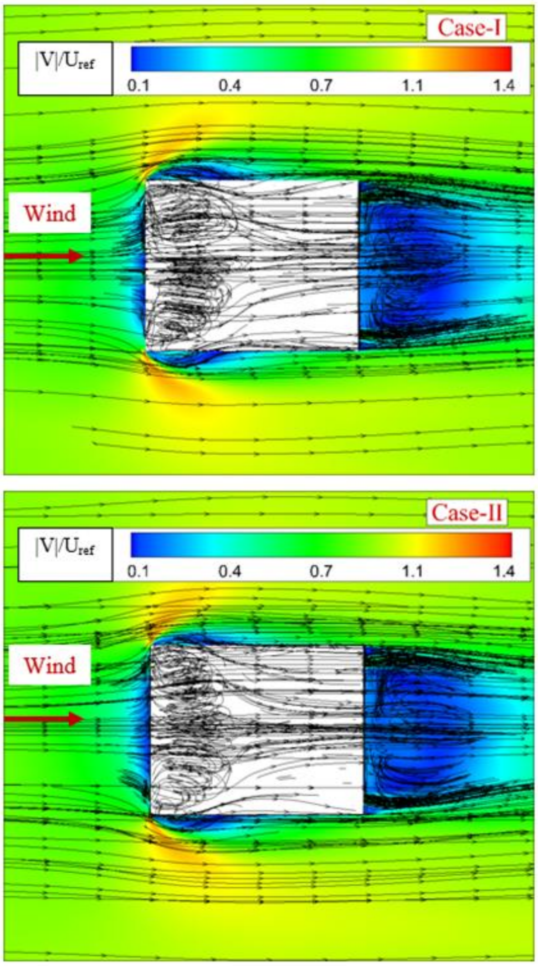

Figure 4-8: Contours of dimensionless mean velocity magnitude ($|V|/U_{ref}$) and streamlines around the building (y/H = 0.5).

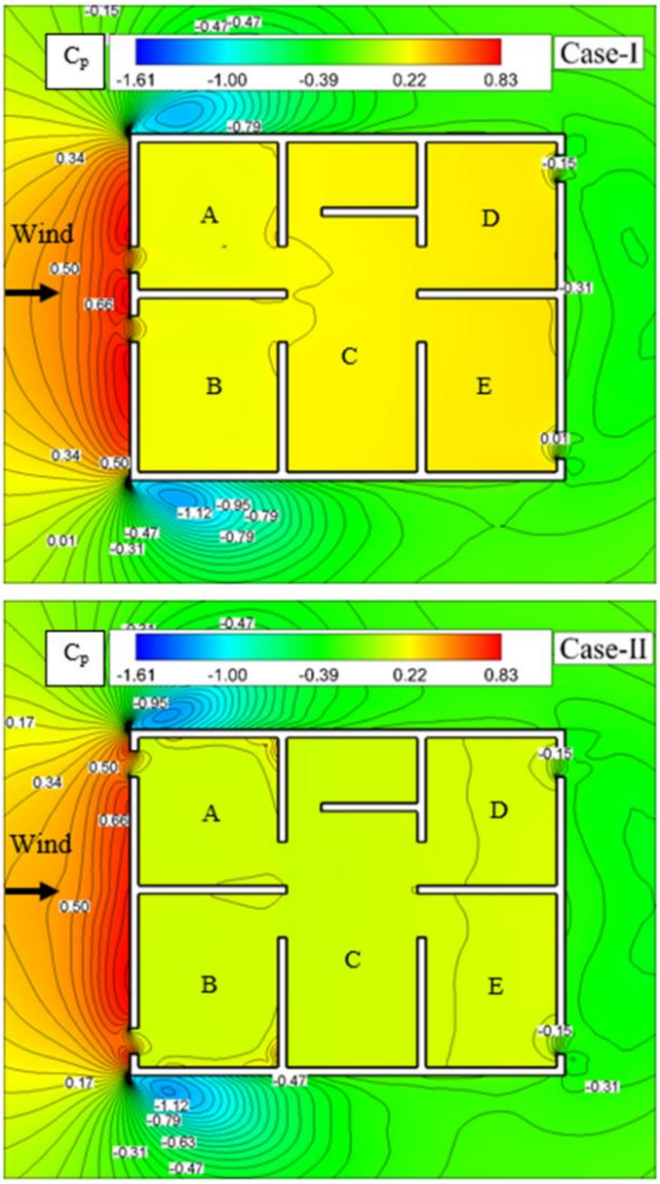

Figure 4-9: Contours of mean pressure coefficient C_p around the building (horizontal plane y/H = 0.56).

4.5.2 Mean flow pattern inside the building

Air velocity countours of a horizontal plane at 1.7 m are presented in Figure 4-10. The main feature of the indoor flow for both cases is the momentum of the incoming airflow, which is hindered by the interior walls of rooms A and B in the streamwise direction, thus causing the airflow paths to change direction. The airflow swerves to the z- and x-directions, the flow in the x-direction moves directly to the leewards rooms and represents the main cause of high indoor turbulent kinetic energy, whilst the air flow in the z-direction rotates inside rooms A and B, creating a circulation zone inside these two rooms. The airflow in Case-II swerves towards the z-direction and then moves to the other rooms; whilst the flow path in the lateral direction in Case-I is lower, the inflow stream coming from rooms A and B is restricted to flowing leeward (rooms D and E) and can thus supply high ventilation to the leeward rooms. Air velocity is an important factor in determining the levels of indoor thermal comfort [157], and the velocities of the zones near the inner walls in rooms A and B for both cases are higher than the maximum acceptable velocity (0.8 m/s) recommended by ASHRAE guidelines. Therefore, it will be difficult for the designer to create acceptable indoor thermal comfort for the occupants of these rooms. In room C, the airflow velocity is low for both cases, with the area of high velocity (green area > 0.3) in Case-I being higher than for Case-II; a still-air zone is produced in the middle of the room, and a high concentration of CO_2 may result from the presence of people. Regarding rooms D and E, the two cases show the same patterns, with half of the rooms showing very low air velocities because of weak circulation in these zones. These zones will become stagnation zones with low ventilation rates resulting in less mixing of air, and therefore inner re-topology is necessary for rooms D and E.

4.5.3 Streamlines inside the building

Figure 4-11 presents the mean average velocity streamlines of the airflow at the plane crossing the middle of the inlet openings. In addition, the mean average velocity streamlines in the vertical section (*xy*) in the middle of rooms A and room B are presented in Figure 4-12. For both cases, the first figure shows that a recirculation zone forms, especially in rooms A and B, in which the flow enters the house directly through the two openings, whilst the recirculation is weaker in rooms D and E. The strong circulation inside rooms A and B is due to the low-pressure regions at their centres and high-pressure regions near the interior walls, as shown in Figure 4-12. Regarding Case-I, the streamlines of the flow are normal to the openings, producing two circulation zones in opposite directions (clockwise in room B and anticlockwise in room A), whereas in Case-II the flow enters near the lateral walls at an angle of approximately 45^o to the inner walls, producing large circulation zones inside the two rooms that flow in opposite directions to those in Case-I due to the flow hitting the windward wall and separating on both sides of the building as a result of low-pressure zones at the lateral sides of the building (Figure 4-8 and Figure 4-9). As the positions of the inlet openings are located near the centre of the building in Case-I, this configuration can supply more air to the other rooms, which would be of interest to architects who want high aeration inside buildings. The results of both cases show that the recirculation zone in room A is more intense than in room B due to the fact that room B is smaller than room A. Furthermore, the gradient of the pressure coefficients for room A is larger than that for room B in Case-I, which increases the rotation of the flow as shown in Figure 4-13. The vertical section through the streamlines shows that the recirculation zones in each case are different, especially in rooms A and B. Regarding Case-I, two large circulation zones are formed that divide the room into two zones, whilst a large circulation zone is formed in Case-II, mixing air from the bottom to the top. The circulation inside room C is the same in both cases, but in Case-I is more intense at the centre, which may cause a high concentration of CO_2 at the middle of the room. Regarding room D, a circulation zone, which is produced at high level in Case-II, is larger and more intensive than Case-I, whereas in room E (Case-I) a full circulation zone is produced and covers the room. In general, most of the rooms in Case-II show airflow mixing that is better than Case-I, and it could therefore be easier for a designer to obtain proper thermal comfort inside the rooms in Case-I.

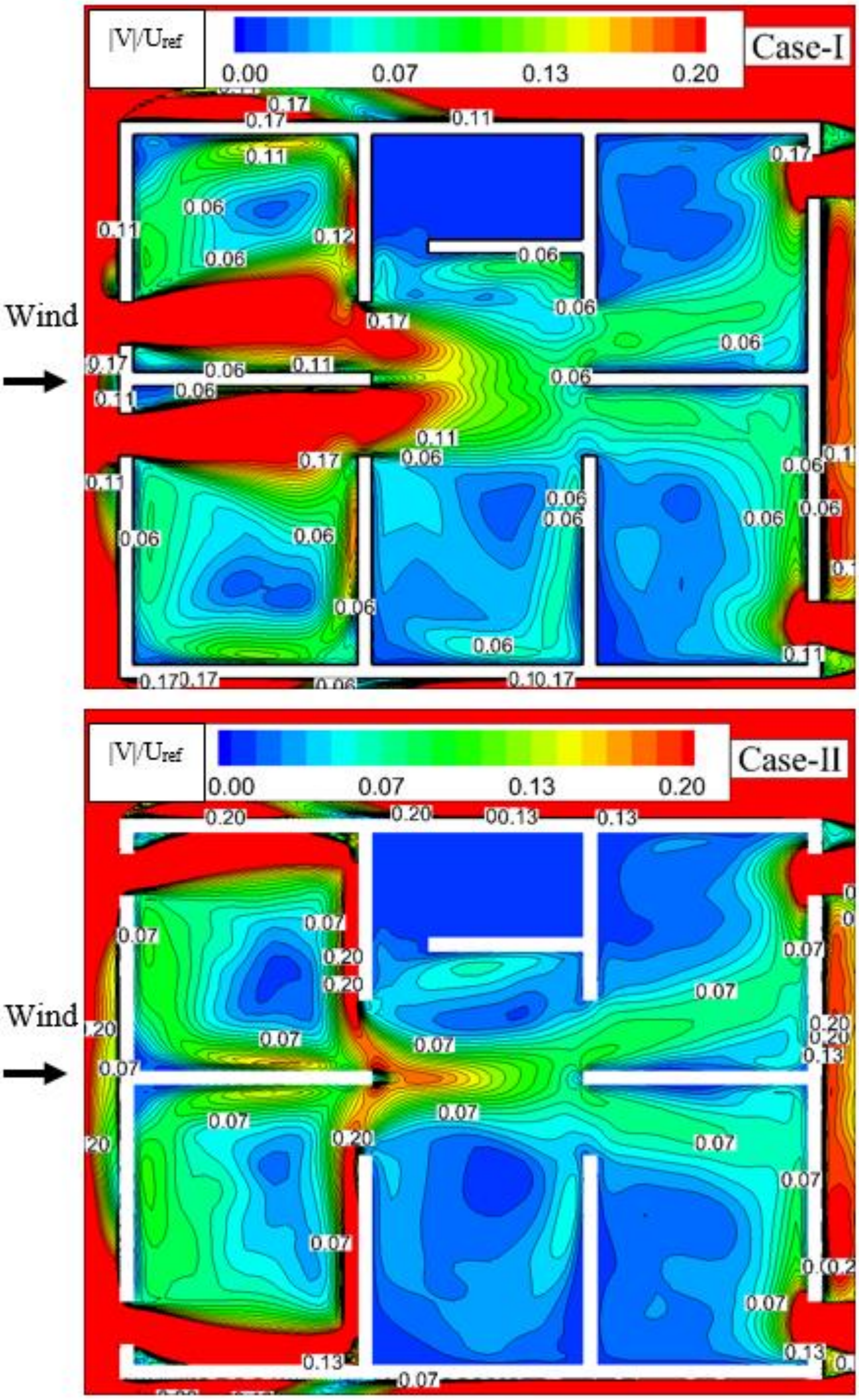

Figure 4-10: Contours of dimensionless mean velocity magnitude ($|V|/U_{ref}$) inside the building in the horizontal plane ($y/H = 0.56$).

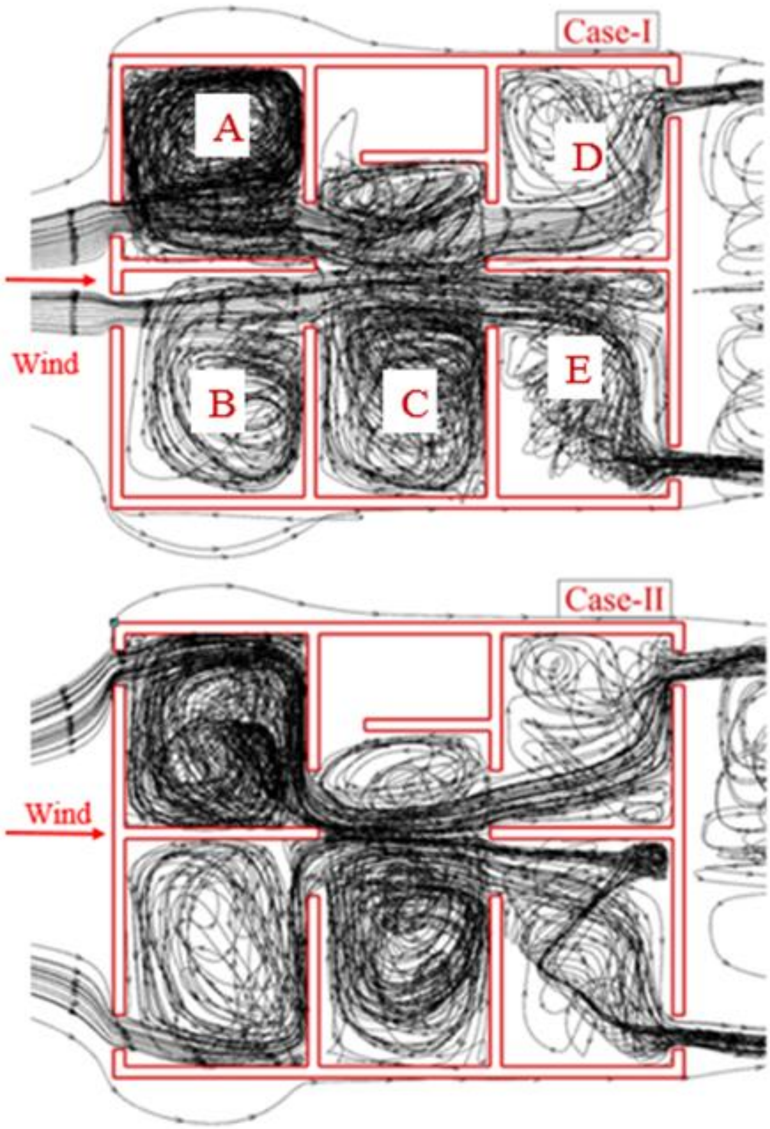

Figure 4-11: Mean streamlines velocity in the horizontal plane (y/H = 0.56).

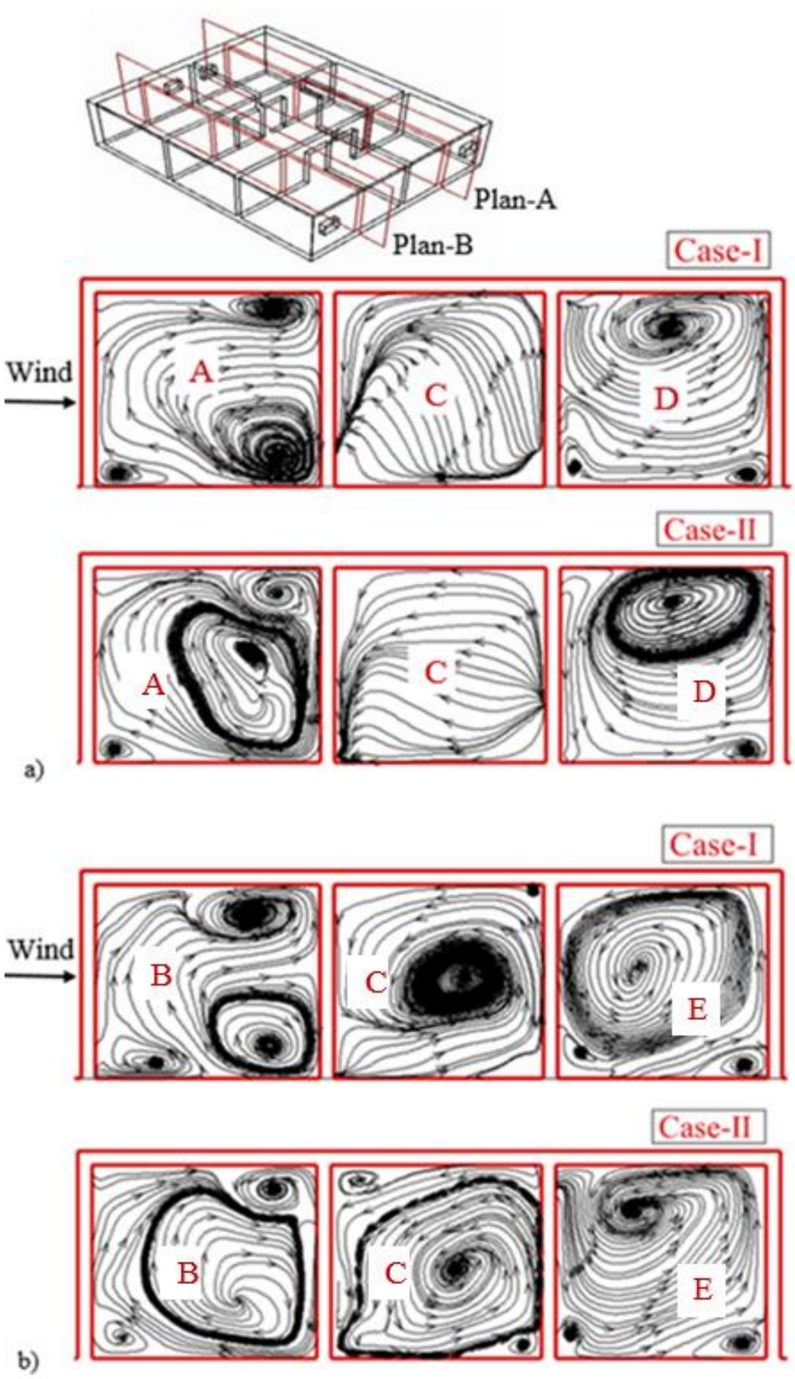

Figure 4-12: Mean streamlines velocity in the X-Y section in (a) Plane-A and (b) Plane-B.

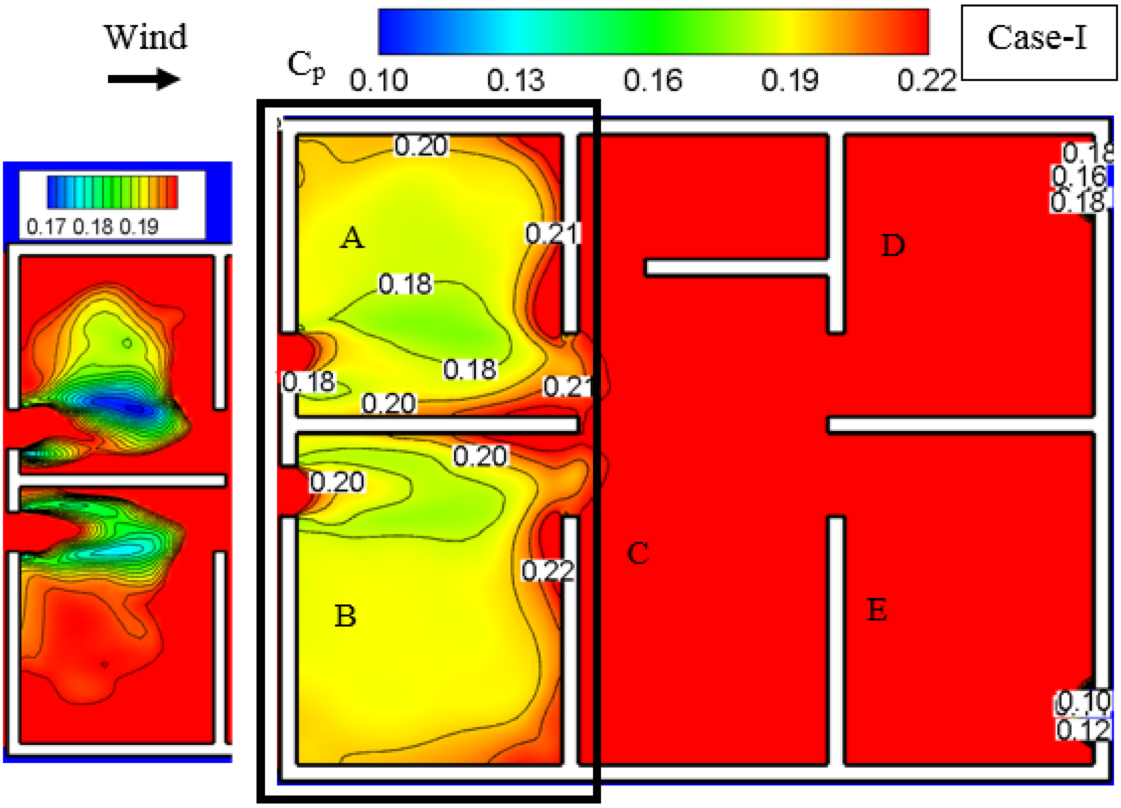

Figure 4-13: Contours of mean pressure coefficient C_p inside the building (horizontal plane y/H = 0.56).

4.5.4 Instantaneous wind flow pattern

Instantaneous wind flow patterns can be obtained from the LES, Figure 4-14 and Figure 4-15 show the flow pattern at different flow times for both cases. They dominate the flow structure in and around the building at different instants in time for Case-I (2.6T^*, 3.5T^*, 4.1T^*), and Case-II (2.5T^*, 3.6T^*, 4.5T^*). It can been seen that the flow patterns are irregular and complicated in the horizontal plane. The flow changes its direction with time and this has a significant impact on the flow pattern inside the building, subsequently affecting the strength of circulation areas inside rooms.

4.5.5 Fluctuating ventilation rate

Generally, the ventilation flow rate always fluctuates through openings, especially for wind-induced ventilation; thus, the description of ventilation flow rate may be insufficient if the scale of the fluctuations in the flow rate are large [47]. As shown in Figure 4-16, large fluctuations can be found near the leeward side, and the top and lateral walls of the building due to high-frequency flow and separating flow at the leading edges. The transient evolution of the ventilation rates through the two inlet openings is provided in Figure 4-17 for both cases, where the dimensionless ventilation rate, $Q*$, based on the reference velocity, is defined as:

$$Q^* = Q/U_{ref}A \tag{4-7}$$

in which A is the opening area. Comparison of openings aerating flow can be very important when one wishes to design houses with high ventilation efficiencies. The standard deviation denotes the fluctuating turbulence intensity of the instantaneous ventilation. Figure 4-17 shows that the maximum standard deviation is 0.16 at opening-2 (Case-II) whilst the minimum is 0.11 at the same opening for Case-I. Although large fluctuations can be found in both cases, the influence of small-scale fluctuations is greater due to the low frequency of the flow. In addition, the turbulence intensity (ratio of the RMS of the velocity fluctuations in the x-direction, u_{rms}, to the local mean flow velocity, u_{mean}, in the x-direction) at both openings was higher for Case-II than for Case-I, as shown in Figure 4-18, which indicates that the flow is more turbulent near the openings in Case-II than Case-I. Straw [36] mentions that the standard deviation of ventilation rates can be considered to be induced by turbulence since the fluctuation of a wind-induced ventilation rate is caused by the turbulence impact of wind. Consequently, the ratio of the standard deviation to the dimensionless ventilation rate indicates the magnitude of the turbulence-induced component in the total ventilation rate.

The ratios of the standard deviation to the dimensionless ventilation rates of openings 1 and 2 for Case-I are about 23% and 21%, respectively, which indicates the extent of the impact of the flacuations in the total ventilation rate, whilst for Case-II this ratio is higher, and represents about 33% for both openings. Accordingly, as the mean stream of the flow provides at least 67% of the total ventilation rate in Case-II and more than 78% in Case-I, it can be concluded that the main source of momentum for air exchange is provided by the mean flow.

As a result, the largest ventilation rate occurs in Case-I because the ratio of mean flow to turbulent flow in this case is larger than for Case- II, as shown in Figure 4-19. In additon, In comparision with Case-II, Case-I has less resistance to the incoming air flow, where the two windward inlet openings are aligned with the corridors that go into rooms D and E, which is another reason why Case-I reaches the highest volume flow rate. In general, the results showed that the rate of ventilation of Case-I is higher than for Case-II by 10%, and this configuration would interest any designer seeking a higher ventilation rate.

Comparison of aerating flow openings can be very important for designers who want to design houses with high ventilation efficiencies.

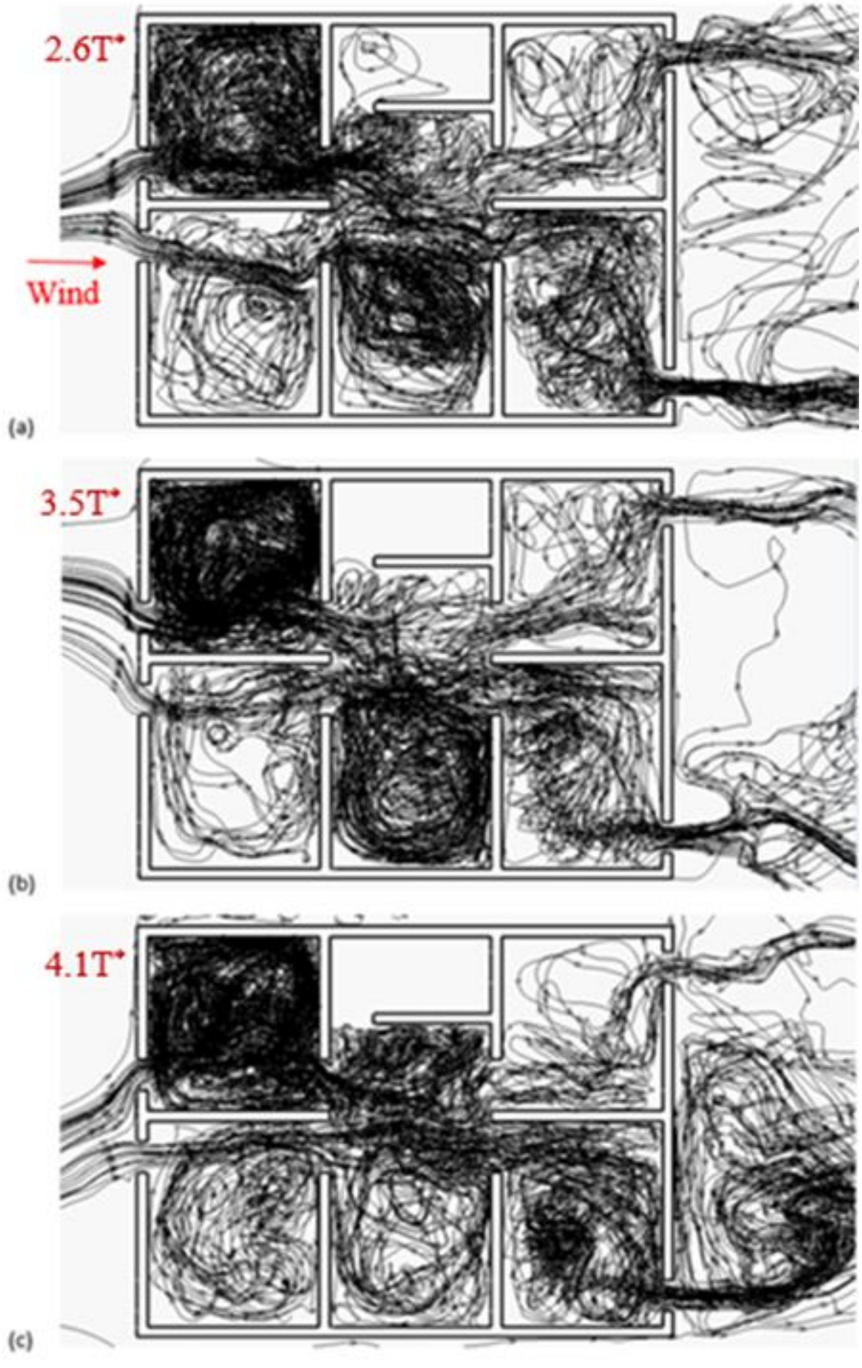

Figure 4-14: Instantaneous wind streamlines for Case-I in the horizontal plane (y/H = 0.56).

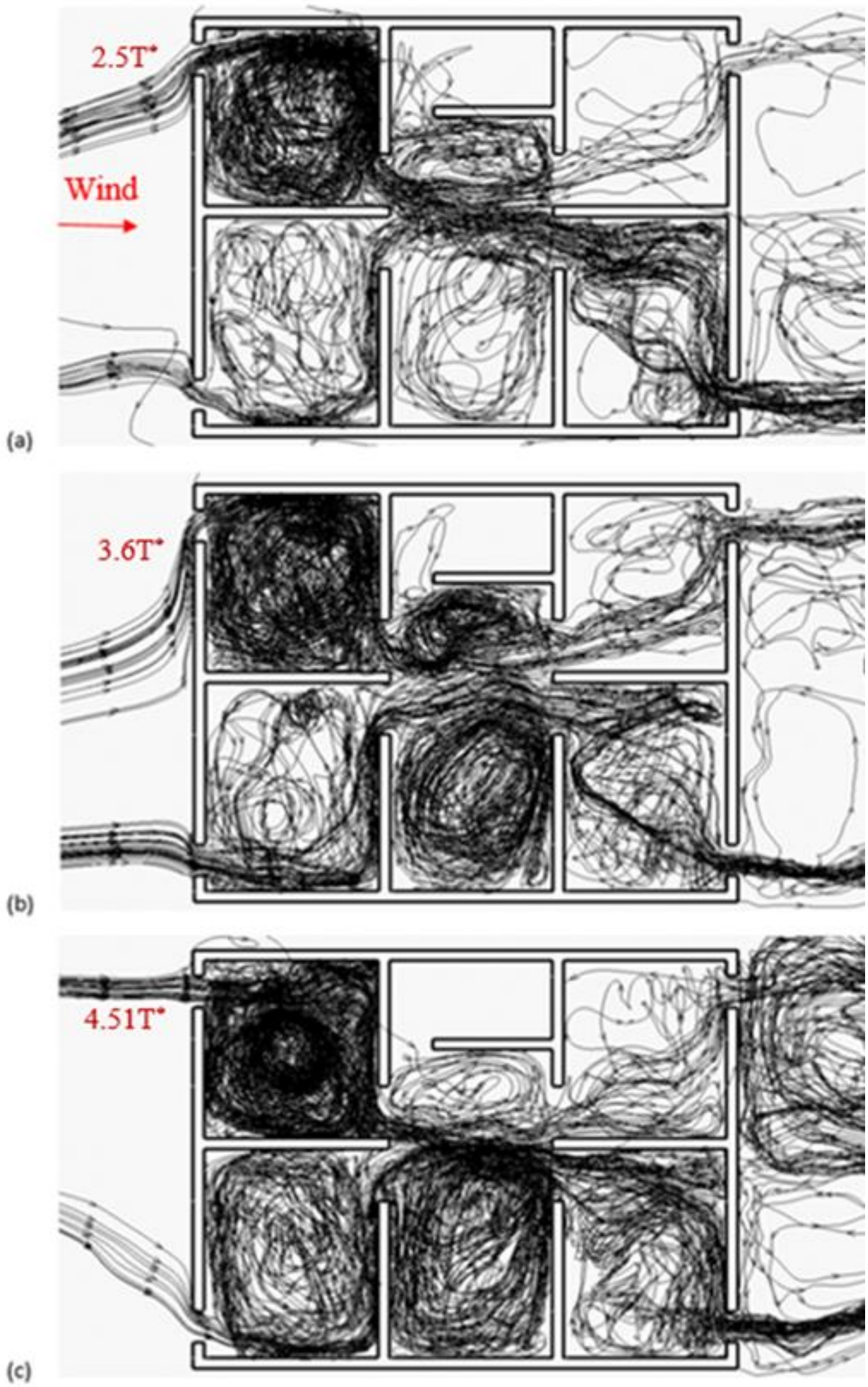

Figure 4-15: Instantaneous wind streamlines for Case-II in the horizontal plane (y/H = 0.56).

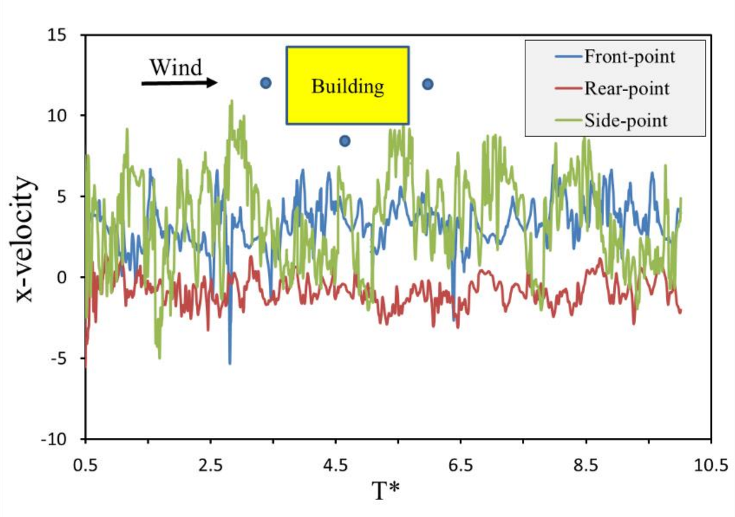

Figure 4-16: Time history of velocity, x-velocity, at the monitoring points near the building.

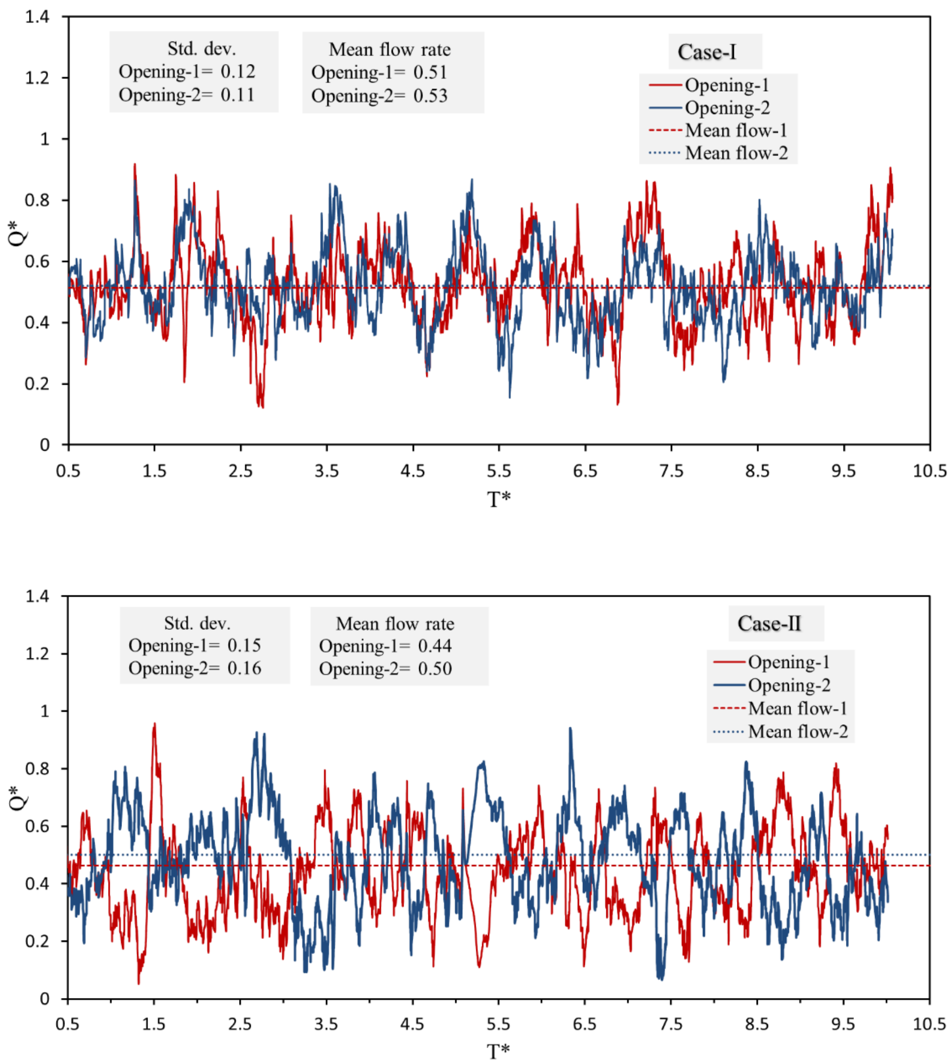

Figure 4-17: Variation of the dimensionless ventilation rate over time steps.

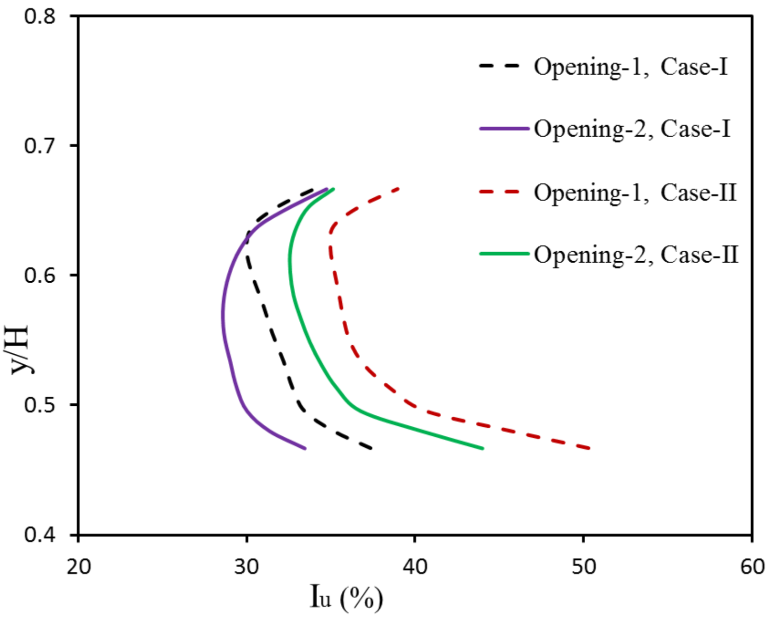

Figure 4-18: Turbulence intensity in the centreline of openings.

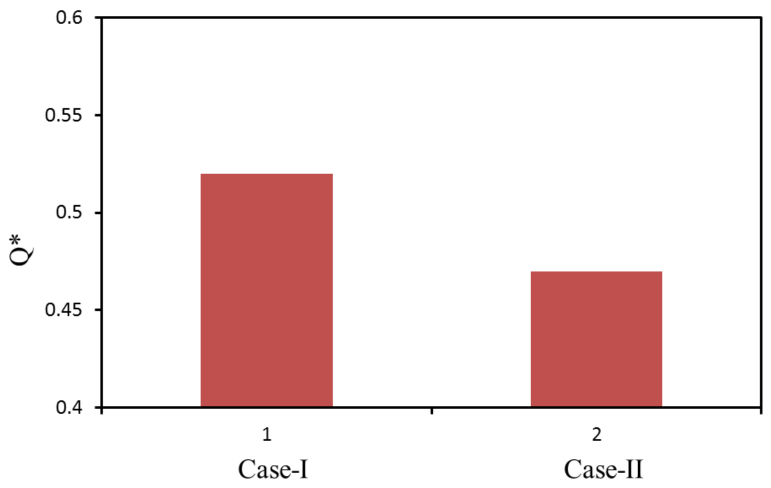

Figure 4-19: Comparison of dimensionless ventilation rates.

4.5.6 Turbulent kinetic energy

Figure 4-20 compares the distribution of the turbulent kinetic energy fields in the horizontal section perpendicular to the openings for the two cases. In front of the building, the turbulent kinetic energy in Case-II is higher than for Case-I, and therefore, the flow at the openings is more turbulent in Case-II than in Case-I. Furthermore, the turbulent intensity profile shows the same trend, which explains the larger spread of the mixing layer observed in Case-II than in Case-I (Figure 4-18).

Regarding the indoor turbulent kinetic energy, the figure shows that the turbulent kinetic energy in Case-I is higher than in Case-II. Therefore it seems that the indoor turbulent kinetic energy depends on the rate of ventilation because the indoor turbulent kinetic energy represents the airflow power of the entire building space transported from the ambient wind through the openings and thus accounts for the characteristics of the indoor airflow, such as with a low speed and high turbulence intensity [158].

This relationship implies the conclusion that openings near sides windward of the building result in less fluctuation of indoor turbulent kinetic energy than openings located in the middle. As the wind comfort inside the building can be more easily achieved when the air has lower indoor kinetic energy [149], so the first configuration (Case-I) would not be chosen by a designer who wanted comfortable rooms because of the high amount of air movement inside the rooms. In contrast, Case-I could be better for hot and/or humid weather conditions where higher air velocities are needed to obtain thermal comfort.

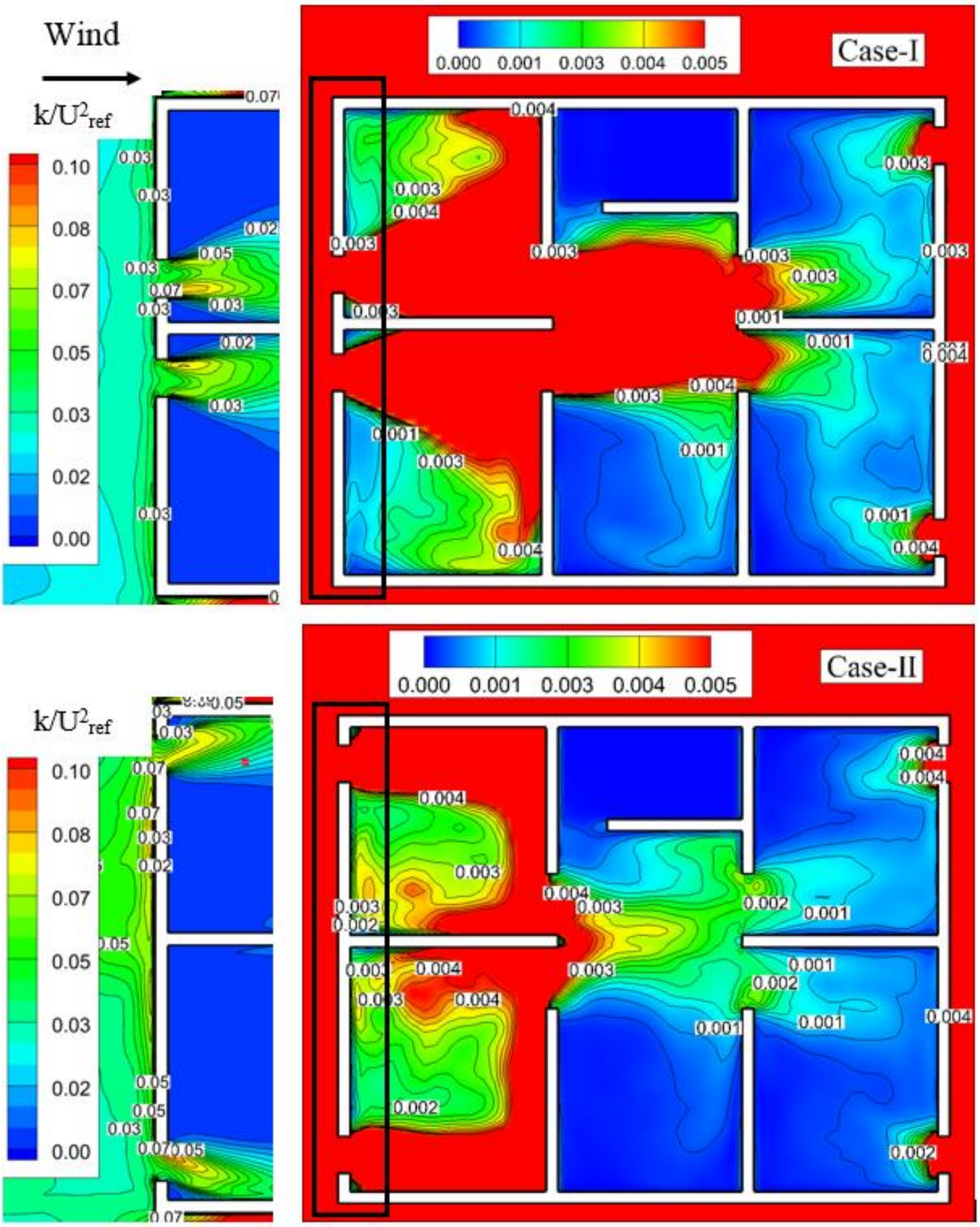

Figure 4-20: Contours of dimensionless turbulent kinetic energy (k/U^2_{ref}) in the horizontal plane (y/H = 0.56).

4.5.7 Comparison with previous work

A comparison between the two geometries of the current study and previous studies from the literature is difficult due to various differences in geometry, which are complicated even further due to the different geometries used, different velocity profiles and turbulence levels being compared, etc. In addition, the partitions inside the geometry (multi-zones) make the comparison even more difficult when comparing the current geometry with a one-zone geometry or with a building with different internal partitioning. Despite these differences, there are some points that can be contrasted and discussed. First, the current study agrees with those of Karava et al. [35] and Tominaga et al. [33] regarding the nature of the recirculation region in terms of vortex centre, size, and sense of rotation being mainly governed by inlet opening position. Second, the study focuses on the openings position concluding that the rate of ventilation through openings located near the centre of the building is higher and more steady than the flow rate of openings located near the sides of the building. It should be pointed out that the two references mentioned above focused on the vertical location of openings and concluded that the opening located at the centre of the front façade of the building provides a lower flow rate than an opening located at a higher level.

4.6 Conclusion

Natural cross ventilation in a small-scale building exposed to outdoor conditions was investigated numerically using CFD analysis. In this study, openings were shown to be an important design factor in terms of its effect on the air-stream pattern inside a building. The numerical approach used in such studies gives the architect the best view of the natural mechanisms of ventilation in a building by providing further insight into the induced flow-field inside and around it, with information that would not otherwise be produced by experimental methods. Despite certain limitations to this study, such as the impacts of direction and speed of the wind, shape of the openings, surrounding buildings, etc., the following conclusions were obtained:

- The rate of fluctuations of the flow rate through the inlet openings depends on the position of the openings. In Case-II, where the openings were near the side wall, this rate was 33%, whereas in Case-I was around 22% when the openings were in the middle of the front wall.

- In agreement with previous studies [35], the indoor air flow pattern changes when the positions of the inlet openings are changed, which also changes the direction of circulation inside a room from clockwise to anticlockwise or from horizontal to vertical circulation.
- The flow rates of openings located near the centre of the building were steadier than the flow rates of openings located near the sides of the building.
- The ventilation rate depends on the positions of the windward inlet openings; the geometry of Case-I provides higher rate that of Case-II by 10%.
- Based on the results, strong recirculation formed in rooms A and B with weaker recirculation formed in rooms D and E; this is better for a designer who desires weaker recirculation in a building.

Chapter 5 Impact of an external boundary wall on indoor flow field and natural cross-ventilation

5.1 Introduction

In this chapter, the impact of an external boundary wall on natural cross-ventilation and flow patterns inside an isolated family house was analyzed using CFD simulations. The wall was located in front of the building and three different conditions were tested: basic case (without a wall) and two cases using walls of different heights. The study employed the techniques of large eddy simulation (LES) with the dynamic Smagorinsky subgrid-scale model because of the unsteady flow and high turbulence around the building. The details of the CFD model and =3mof the boundary conditions that are used for the domain airflow modelling are presented. The impact of an external boundary wall on the flow fields and natural cross-ventilation is evaluated and discussed in details in this chapter.The results of this study are expected to inform building designers of the impact of an external boundary wall on the flow patterns in relation to the rate of ventilation and indoor mean velocity. The chapter`s content has been published in Journal of Building Engineering [159].

5.2 Case description

The basic configuration of the studied model was an isolated house without a boundary wall, including partitions from inside; this layout is simple and represents an average house for an average family in Iraq. The height of the building was (*H=3m*) and had base dimensions of 8×10 m (Width × Length). The ratio of openings to façade of the building was 0.03. There were two square openings (*0.2H*) on the front wall and two openings at the rear of the building as shown in Figure 5-1. The front view of the building model with the sizes and dimensions of the openings are presented in Figure 5-2. Three cases were used in this study and the details are provided in Table 5-1. The first case was the basic case, while the second and third cases were based on the same basic model, but with the addition of an external boundary wall with height 0.333*H* and 0.40*H* respectively. The wind speed at the height of the building (U_{ref}) was 7 *m/s* with an angle of incidence of 0^o.

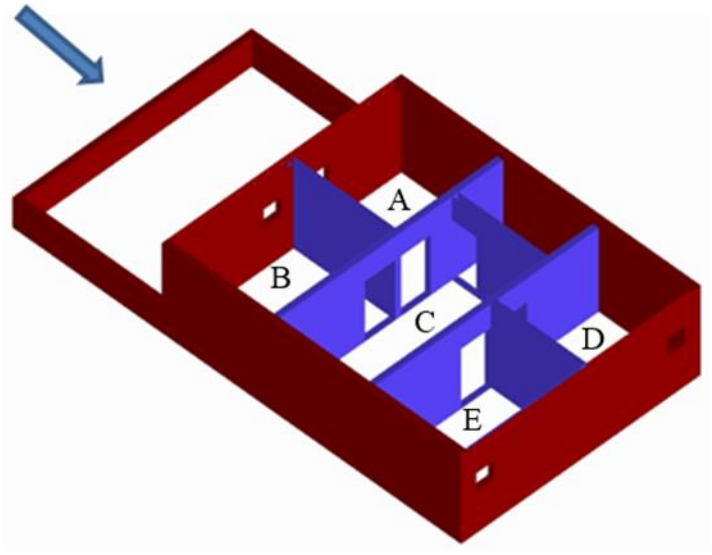

Figure 5-1: Schema of the case used in the study.

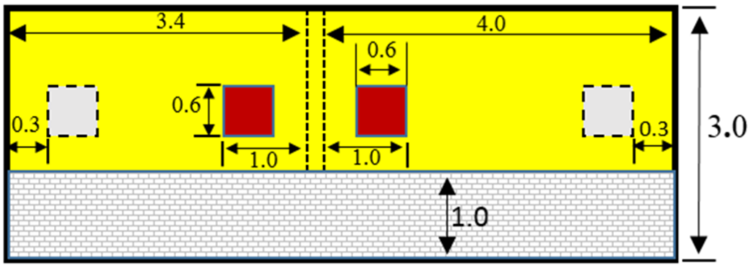

Figure 5-2: The front view of the building with opening sizes and dimensions (m).

Table 5-1: Cases description

Cases	Case description	Height of boundary wall
Case-I	Basic case	0.00H
Case-EF	Basic case+ boundary wall	0.33H
Case-EFH	Basic case+ boundary wall	0.40H

5.3 CFD case study: computational domain and grid

The computational domain of this study followed the recommendation of the European Cooperation in Science and Technology (COST) [22] and the Architectural Institute of Japan (AIJ) [153] guidelines. The building was set inside a duct (23.3×5×12.6) H, as shown in Figure 5-3 and the blockage ratio was 4.2% which is within the range recommended in the guidelines. These guidelines suggest at least 5H as a distance between the inflow boundary and the building, whereas *15H* was set as a distance between the outflow boundary and the building, which is enough to allow the flow to redevelop in the wake region. The numerical grid used for the basic case examined consists of around 6×10^6 hexahedral computational cells. A fine mesh was structured near the walls, while coarse mesh was used away from the walls in all directions. The Y^+ used for the first cell near the wall was 1.4, which was enough to capture a laminar sub-layer and the minimum grid spacing used in the present computations was $0.005H$ in all directions with a non-uniform grid of stretching ratio of 1.15-1.20.

5.4 Boundary condition and solver settings

The inlet boundary condition of wind velocity profile is defined according to the logarithmic law. The vertical profiles of the mean wind velocity, turbulent kinetic energy and turbulent dissipation rate are imposed at the inlet of the domain (Eqs 4-3, 4-4 and 4-5) as described in chapter 4.

A time-dependent inlet profile at the inlet of the domain was generated by the vortex method, where the number of vortices was N= 190. The lateral and the top sections of the domain were modelled as symmetry conditions. The surfaces of the house and the ground of the domain were modelled as no-slip boundaries, whilst at the outlet of the domain the zero-gradient condition was used. The pressure-based solver was used in this study, where the flow was incompressible. The PISO algorithm was used for the pressure-velocity coupling and the second-order discretization scheme for the pressure interpolation. The bounded central-differencing scheme was used to discretize the convection term in the filtered momentum equation. Time discretisation was second-order implicit, and the convergence criterion was 10^{-5} for all terms. The time-step was set to Δt = 0.0000075 s and kept constant during the simulation, which ensured that the Courant number was always smaller than 0.3 in most of the grid points with a maximal value of 0.6. The initial transient conditions from the inlet of the duct and the total simulation time were continued until such a time as the flow became statistically steady. At this point, the total time for the simulation was found as 135,000 time-steps.

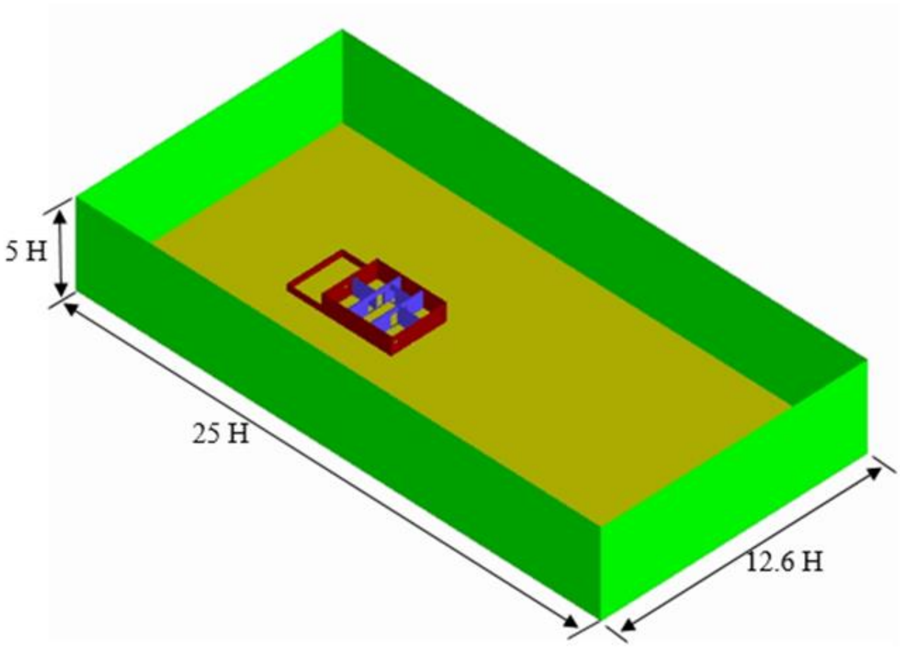

Figure 5-3: The building inside the defined duct.

5.5 Results and discussion

As defined in section 3, this study investigated the effect of an external boundary wall on the natural cross-ventilation of a small scale family house. Three different configurations of the models (basic case without a wall, and two cases with a wall) were used to examine the effects of an external boundary wall and its height on the recirculation area, flow pattern and the rate of ventilation inside the building, in order to determine the wind comfort of the occupants. The external boundary wall located in front of the building and the inner layout of the building was kept the same for the three configurations, and the schema of each case is shown in Figure 5-1 and Figure 5-2. The flow entered from two openings on the front wall and exited from two openings on the rear wall of the house. The areas of the openings were kept constant in all cases and the wind speed also remained constant at 7 m/s with wind incidence angle of 0^o.

5.5.1 Mean flow and streamlines around the building

The mean velocity and streamlines around the building for all cases are shown in Figure 5-4 and Figure 5-5 on the vertical and horizontal planes respectively. These figures show that an external wall has significant impact on the behaviour of flow around the building and this effect will extend to inside the building, changing the flow patterns and circulation zones inside the rooms. Regarding Case-EF and Case-EFH, the boundary wall caused a significant reduction in the mean pressure in front of the openings as shown in Figure 5-6, subsequently forming a large circulation zone. When the height of the wall is increased by 20%, the mean pressure also reduced and the circulation zone became larger and more intensive, whereas a small circulation near the ground formed in the absence of a wall (the basic case).

The large circulation in the presence of the wall reduces the mean x-velocity for two inlet openings considerably from 3.65 m/s in the basic case to 1.92 m/s in Case-EF and 1.24 in Case-EFH, whereas the mean y-velocity magnitude increases from 0.07 in Case-I to 3.4 in the other cases which has the main function of reducing the mean flow velocity inside the building (Table 5-2). This is because the flow is diverted upwards by the wall and then sweeps to the ground. The kidney shape vortex which covers one-third of the length of the building roof in the basic case almost disappears and causes the flow slipping on the roof of the building. The upstream flow accelerated when it struck the edges of the roof, reaching a maximum velocity of 9.1 m/s in the basic case and reduces to 8.6 and 8.4 m/s for Case-EF and Case-EFH respectively.

5.5.2 Mean flow patterns inside the building

Figure 5-7 presents the mean airflow velocity magnitude contours in a horizontal plane passing through the middle of the openings which is assumed to be user level. In addition, the profiles of mean velocity from the centre of the openings to the end of the building are provided in Figure 5-8. Regarding Case-I, the high velocity (the red area) near the inner walls in rooms A, B and C has a direct impact on the indoor discomfort and it would be difficult for a designer to provide proper thermal distribution inside these rooms. In the other two cases the mean velocity is considerably reduced to less than 0.3 m/s (the blue area) in most areas of all rooms and the difference between the front and rear rooms is small, therefore these two configurations could make it easier for a designer to attain proper thermal distribution than the basic case. In addition, Figure 5-8 shows that the airflow mean velocity in Case-I declines sharply to 0.5 m/s at the end of the building by two steps, whereas in the other two cases the velocity drops to less than 0.5 m/s directly after passing the openings and stays at the same level along the building. It can be concluded, therefore, that adding a boundary wall can improve the indoor environment considerably in terms of indoor airflow velocity. The figure also shows that increasing the height of the wall does not make any significant difference to the distribution of mean velocity in the rooms.

Table 5-2: Mean indoor velocity (m/s).

Cases	x-velocity	y-velocity	z-velocity
Case-I	3.65	-0.07	-0.32
Case-EF	1.92	-3.4	-0.11
Case-EFH	1.24	-3.4	0.03

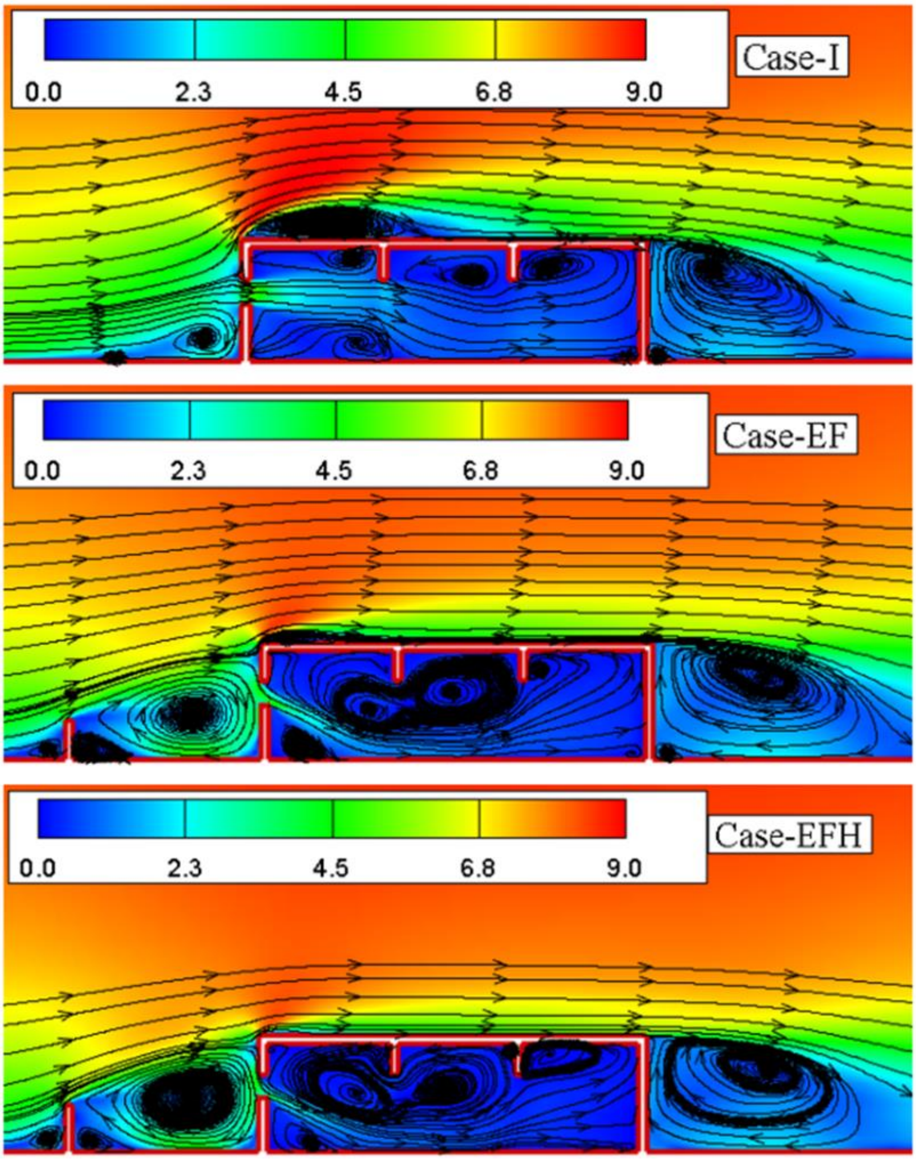

Figure 5-4: Mean velocity (m/s) and streamlines inside and around the building in the vertical plane and passing middle of opening-2.

Figure 5-5: Mean streamlines around the building in the horizontal plane (y/H=0.56).

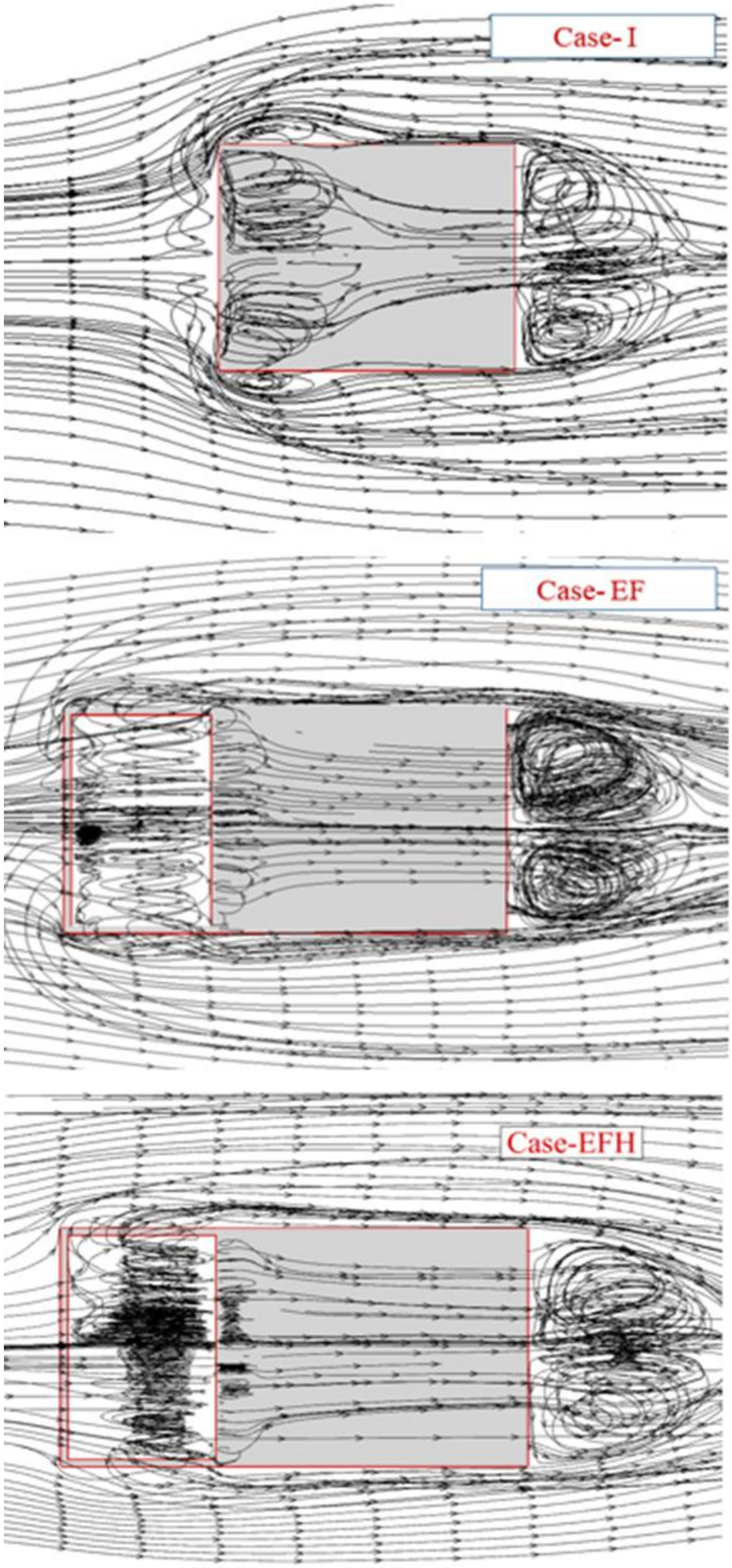

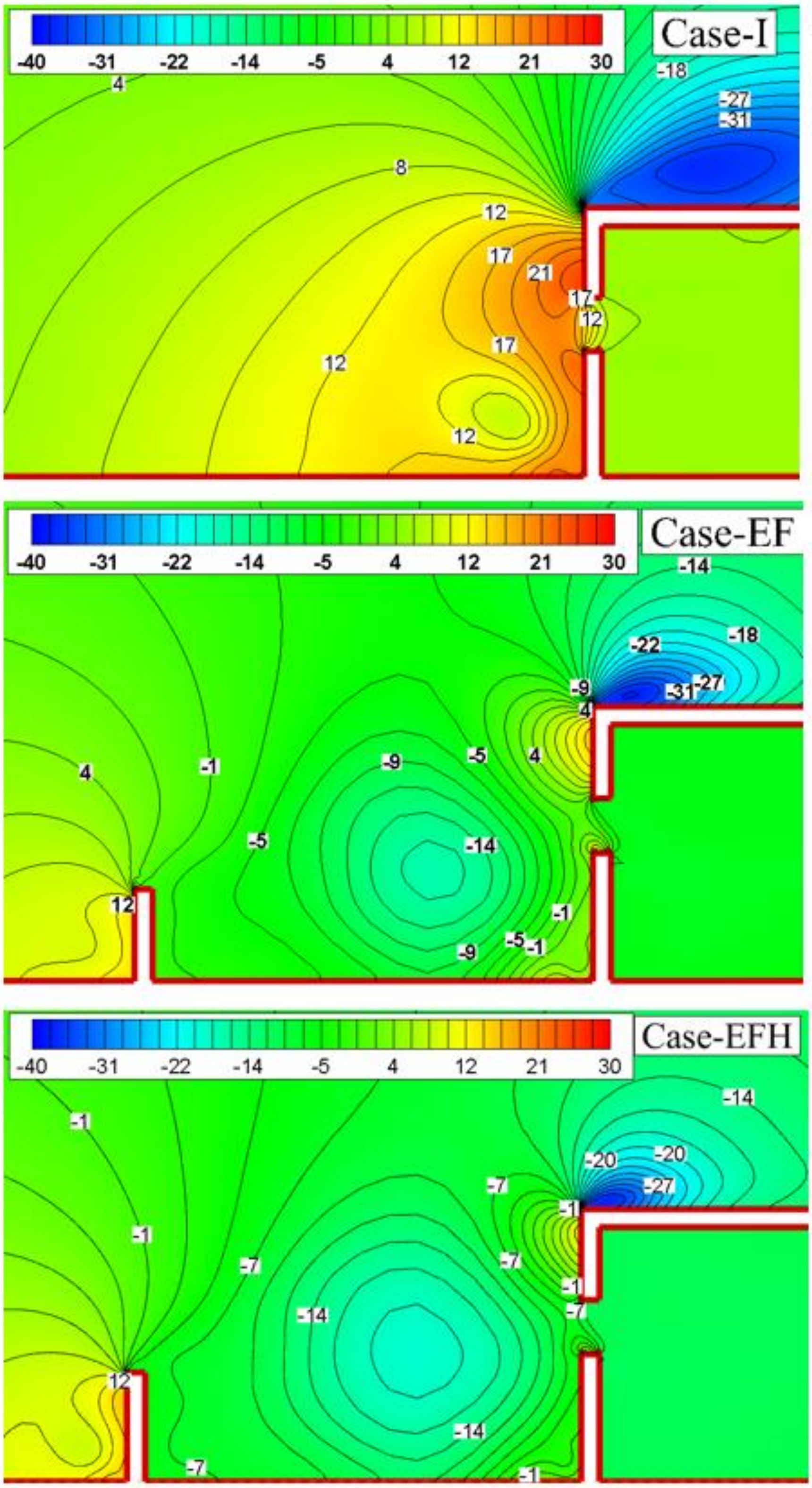

Figure 5-6: Mean pressure contours in front of the building in the vertical plane and passing middle of opening-2.

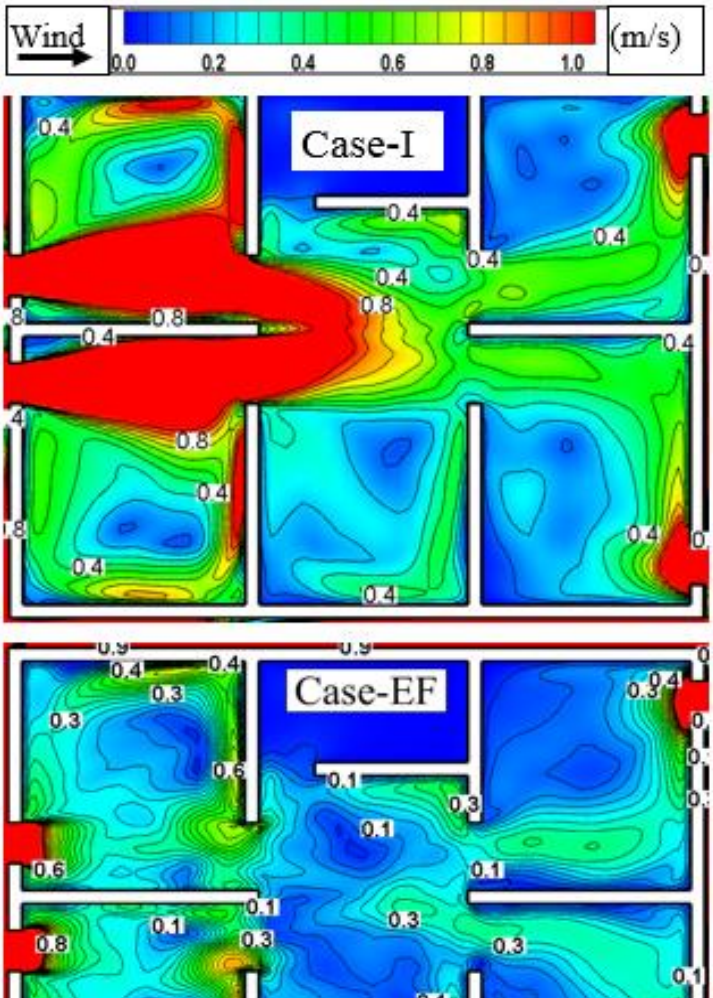

Figure 5-7: Mean velocity contours (m/s) inside the building in the horizontal plane (y/H=0.56).

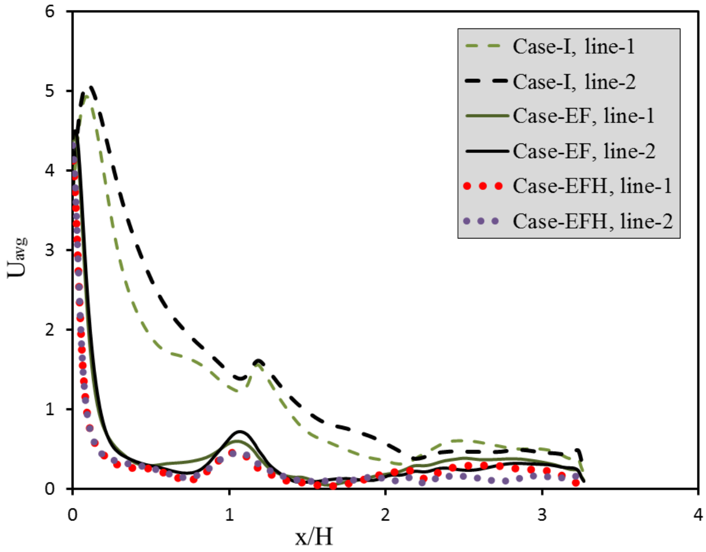

Figure 5-8: Indoor average mean velocity (m/s) profile of lines along the building.

5.5.3 Streamlines inside the building

Figure 5-9 presents the mean streamlines of the airflow at the horizontal plane crossing the middle of the inlet openings. The three cases showed almost the same pattern, a recirculation zone formed in each room for all cases, especially in rooms A and B, in which the flow enters the house directly through the two openings, while the recirculation is weaker in rooms D and E. The strong circulation inside rooms A and B is due to the high-velocity flow and intensity and the results of all cases show that the recirculation zone in room A is stronger than that in room B due to the fact that room B is smaller than room A. The horizontal plane figure showed that the streamlines of the flow in both cases are normal to the openings, producing two circulation zones in opposite directions (clockwise in room B and counter clockwise in room A) while the vertical section (Figure 5-6) presents different patterns between Case-EF and Case-EFH on the one hand and Case-I on the other hand. The flow enters in straight lines parallel to the ground in Case-I, forming a small circulation at a high level in the rooms while in the other two cases the flow enters the openings with an angle of 45^o, producing a large double circulation between the front rooms (A and B) and the middle room (C). The circulation provides good air mixing inside the building. The circulation inside the building became larger when the height of the wall is increased, which means that the formed circulation has a strong relation with the height of the boundary wall.

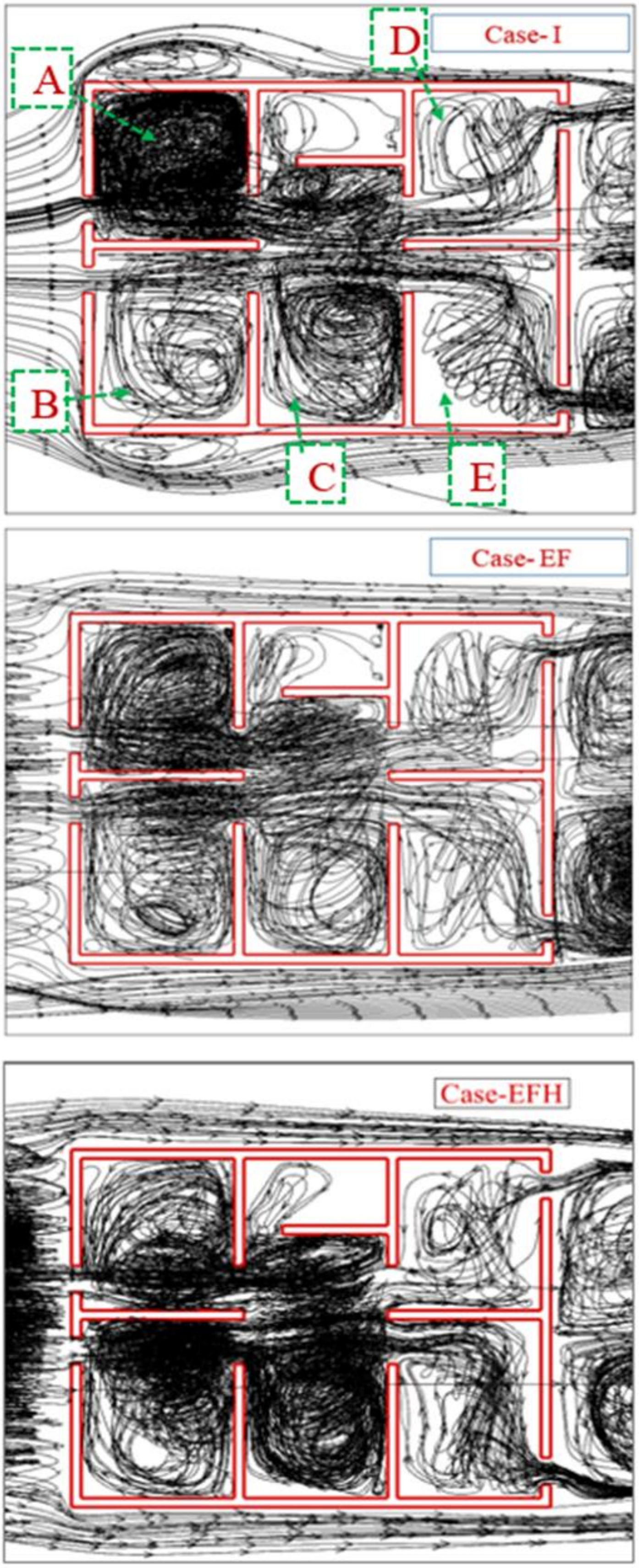

Figure 5-9: Mean streamlines velocity in the horizontal plane (y/H=0.56).

5.5.4 Fluctuating ventilation rate

An indication of the transient nature of the predicted flow through the two windward openings is given in Figure 5-10 for the three cases, where the dimensionless ventilation rate Q* based on reference velocity (U_{ref} = 7m/s). If the design is based on the rate of ventilation, the comparison of openings' aeration flow will be very important. The standard deviation of the ventilation rate is used to indicate the fluctuation intensity of the instantaneous ventilation rate [49, 137]. Because the fluctuation of a wind-induced ventilation rate is caused by the turbulence impact of wind, the standard deviation of the flow rate through the openings can be considered to be turbulence-induced ventilation rates [47, 137, 160]. Thus, the ratio of standard deviation to dimensionless ventilation rate refers to the role of the turbulence-induced component in the total ventilation rate [36]. The figure shows that the standard deviation predicted at both openings of Case-EF and Case-EFH was higher than Case-I because the boundary wall increased the intensity near the openings, therefore the flow became more turbulent near the openings than Case-I. The standard deviation of the ventilation rates can be considered to be turbulence-induced since the fluctuation of a wind-induced ventilation rate is caused by the turbulence impact of wind.

The figure shows that the ratios of standard deviation to the dimensionless ventilation rates of openings 1 and 2 for Case-EF and Case-EFH were about 53% and 82%, respectively, whereas for Case-I the ratio was small, around 22%, for both openings. This means that the mean flow stream provides at least 78% of the total ventilation rate in Case-I, while in the other two cases the mean stream provides less than 47% and 18%, respectively. In conclusion, the main source of momentum for the ventilation in Case-I was provided by the mean flow, while in the other two cases the fluctuating flows provided a greater source of momentum than mean flow especially in Case-EFH with 82%. Although the significant reduction in the ventilation rate was found to be between 33% and 52% of the case without a boundary wall, as shown in Figure 5-11, the solid wall offered the advantage of enhancing the indoor environment and made the design easier, as explained in the previous section. In addition, the figure shows that the rate of ventilation is inversely proportional to the height of the boundary wall and decreased by 36% when the height was increased by 20%. Therefore, the designer should be careful to set the height of the boundary wall in front of the building.

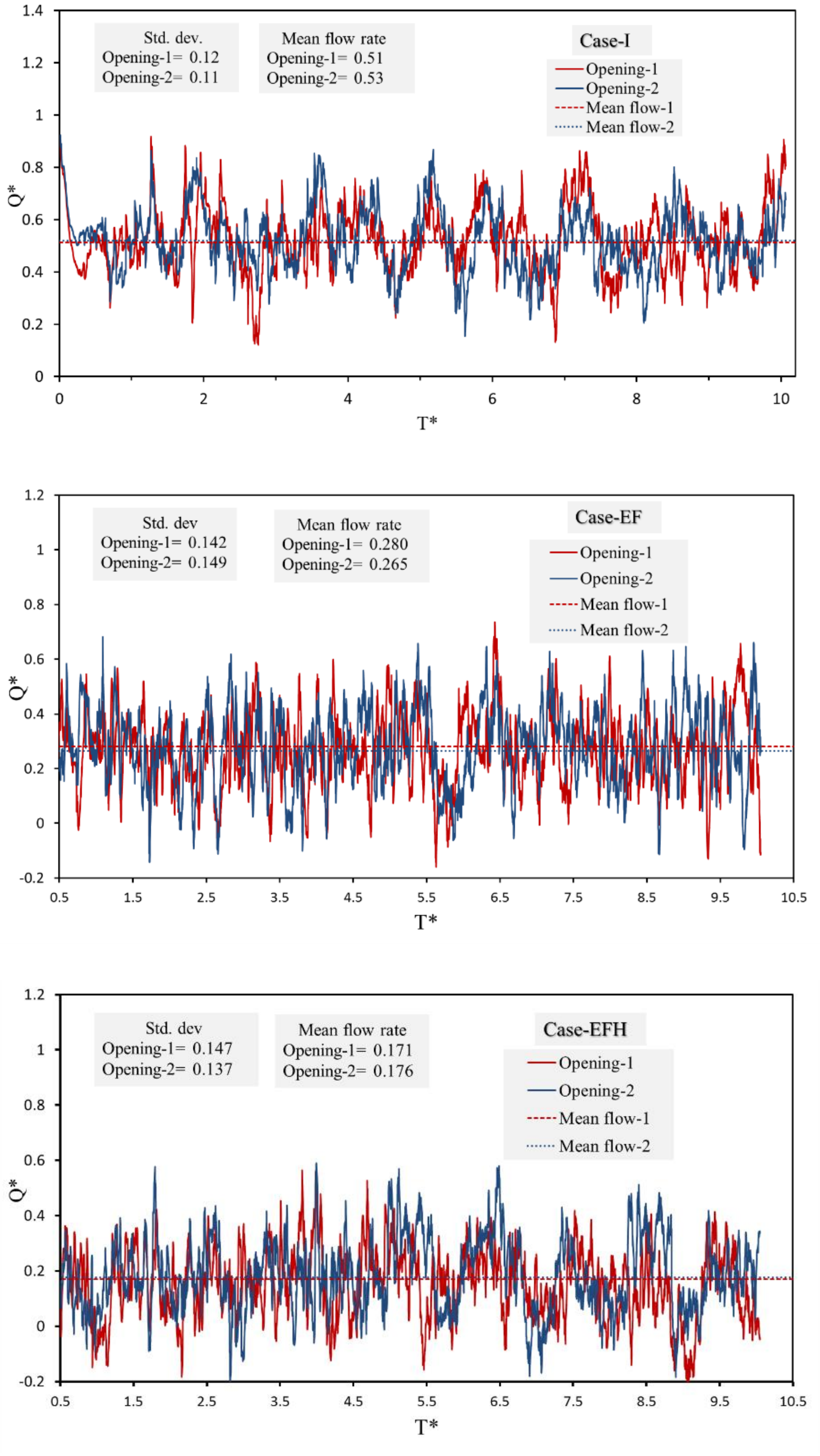

Figure 5-10: Variation of the dimensionless ventilation rate over time steps.

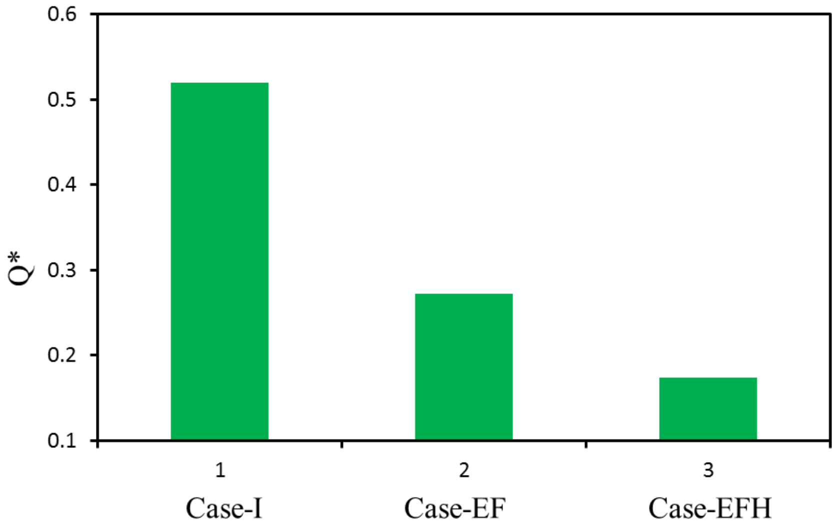

Figure 5-11: Comparison of dimensionless ventilation rate.

5.5.5 Turbulent kinetic energy

Figure 5-12 shows the horizontal plane at the centre of the openings with the distribution of the dimensionless turbulent kinetic energy k for all cases, which is calculated from the turbulent kinetic energy of the resolved scale and subgrid scale. Regarding Case-EF and Case-EFH, the simulation predicted higher k in front of the openings than that in the basic case, and the fluctuation of the flow at the openings increased as well. High fluctuation has a negative impact on the rate of ventilation, therefore, the ventilation rate decreases considerably when a wall is present, as shown in Figure 5-11[36]. On the other hand, the total indoor kinetic energy was reduced by around 20% with the addition of the wall in Case-EF and 42% in Case-EFH because of the lower flow rate through the openings, which has a proportional relationship with the indoor kinetic energy as discussed in previous studies [105]. Therefore it can be concluded that any boundary wall in front of an opening can lead to a decrease in the airflow rate through the openings, and there will be lower fluctuation of indoor kinetic energy (Figure 5-13). Therefore the velocity comfort inside the building can be more easily achieved when the air has lower indoor kinetic energy.

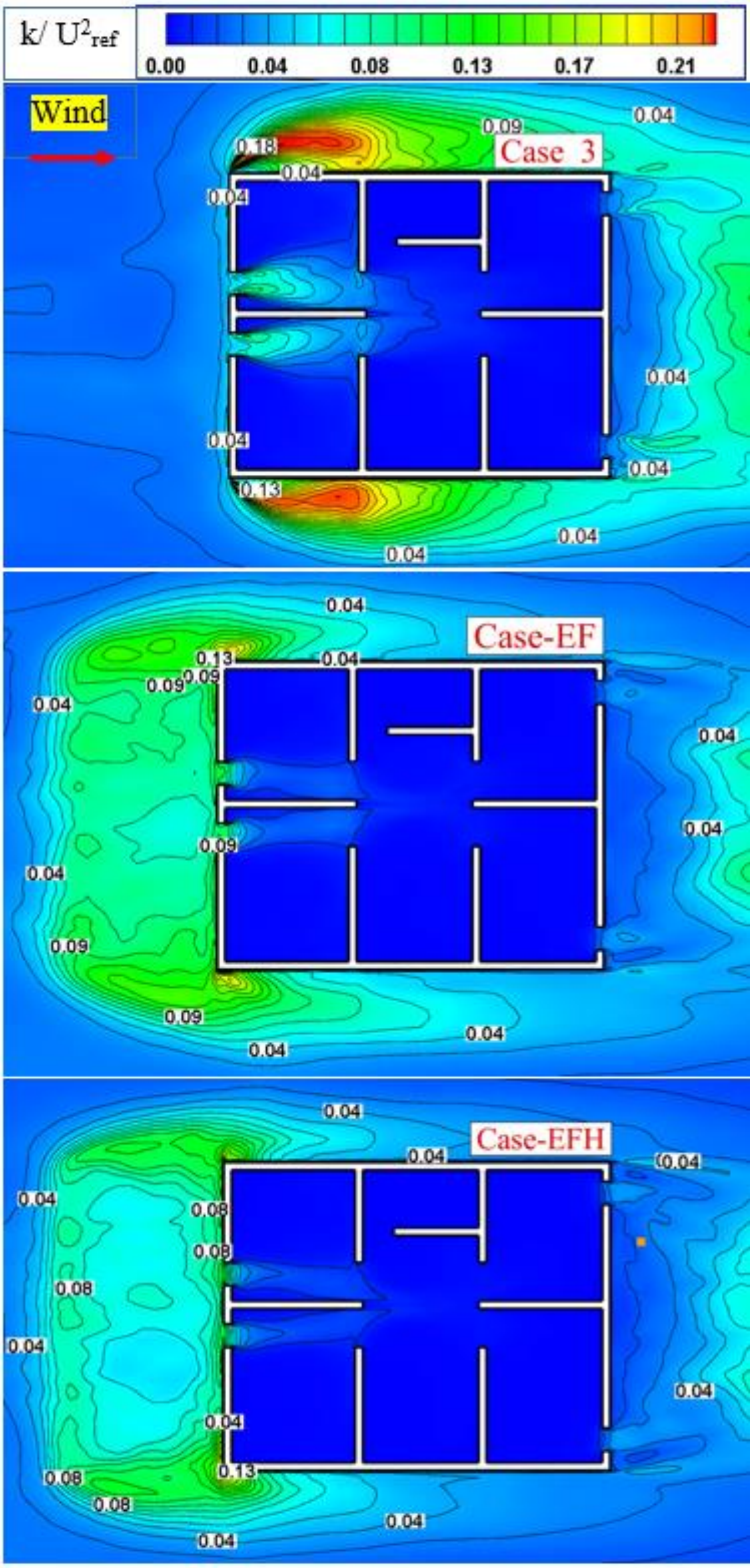

Figure 5-12: Distribution of dimensionless turbulent kinetic energy around the building (k/ U^2_{ref}) in the horizontal plane (y/H=0.56).

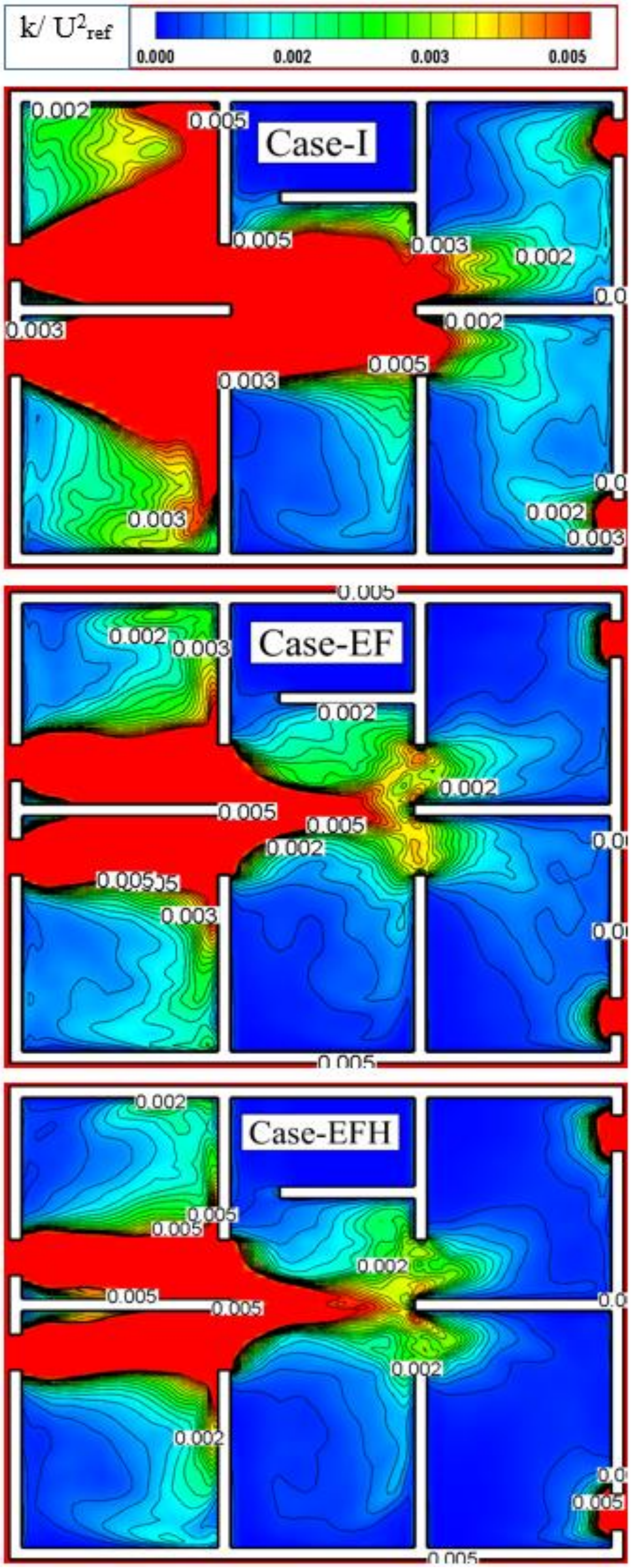

Figure 5-13: Distribution of dimensionless indoor turbulent kinetic energy (k/U^2_{ref}) in the horizontal plane(y/H=0.56).

5.6 Conclusion

This study examined the impact of an external boundary wall on the indoor ventilation performance of the building using the CFD analysis. The analysis on the three proposed cases included the average mean velocity, streamline distribution, and turbulent kinetic energy on the working plane of the CFD models exposed to the turbulent streams. The study found that the external wall, as an architectural element, helps to improve the distribution of indoor air flow by reducing the mean velocity and changing the airflow pattern within and around the building.

In summary, the following conclusions were reached:

- The study confirmed, in agreement with previous studies, that the type and placement of the external elements can affect indoor air flow rates and patterns.
- It was found that the boundary wall caused a reduction in the ventilation rate by around 48% in Case-EF and 67% in Case-EFH compared with the basic case without the wall.
- Adding the boundary wall to the building can provide uniform distribution of the indoor mean velocity, and subsequently enhancing the indoor environment for occupants in terms of indoor airflow velocity.
- Increasing the height of boundary wall by around 20% did not produce noticeable improvement on the indoor mean velocity distribution.

Chapter 6 Thermal comfort evaluation under a naturally ventilated environment in a hot climate

6.1 Introduction

This chapter focusses on the effects of different building parameters, such as the inlet horizontal openings position, wind speed, and outdoor temperature, on the human thermal comfort within an isolated family house using Computational Fluid Dynamics (CFD). The steady RANS simulation is conducted on the cases in this chapter and the next chapter to limit the computational cost. The thermal comfort indices will be described and explained in this chapter. Details regarding the impact of each parameter evaluated with regard to occupants' thermal comfort are further discussed. Then, the chapter concludes with the overall thermal comfort evaluation of the building.

6.2 Case description

The height of the building was H, with base dimensions of (3.33×2.66) H and there were two square openings (*0.2 H*) in the front wall and two openings at the rear of the building, and the wall porosity (opening area divided by wall area) is 3%. The building has an external boundary wall and the height of the wall is 0.33H. The thickness of the walls was 0.067 H. Three cases (I, II and III) with different opening positions were used in this study, and the details were provided in the front view of Figure 6-1 for the building model with the sizes and dimensions of the openings. In all cases, the wind speed was based on the reference at the height of the building (U_{ref}) with an angle of incidence of 0^o. The weather of Kirkuk city (north of Iraq) has been applied on the case study where the Köppen-Geiger map classified the weather in the north of Iraq as giving a cold, semi-arid climate and as being located in the temperature climate zone [26]. During the spring (March to May) and autumn (September to November), the weather in Kirkuk is stable, with clear skies, windy, and a mean relative humidity of around 30%; the mean velocity for this six months period is around 3 m/s, and the mean temperature is around 25°C, as shown in Figure 6-2 [161].

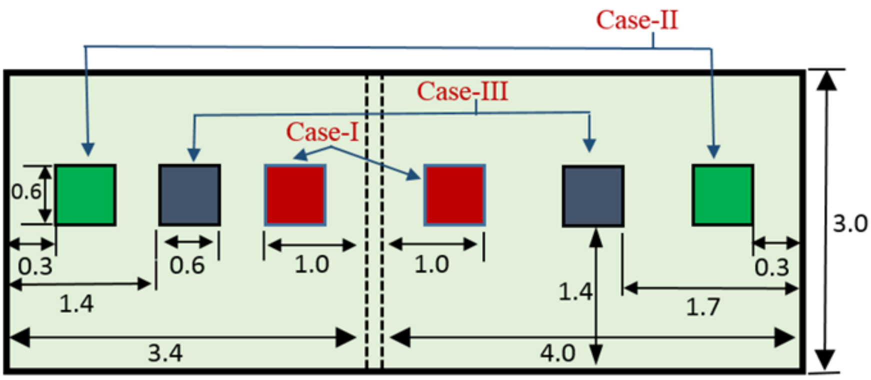

Figure 6-1: The front view of the building (dimensions in meters).

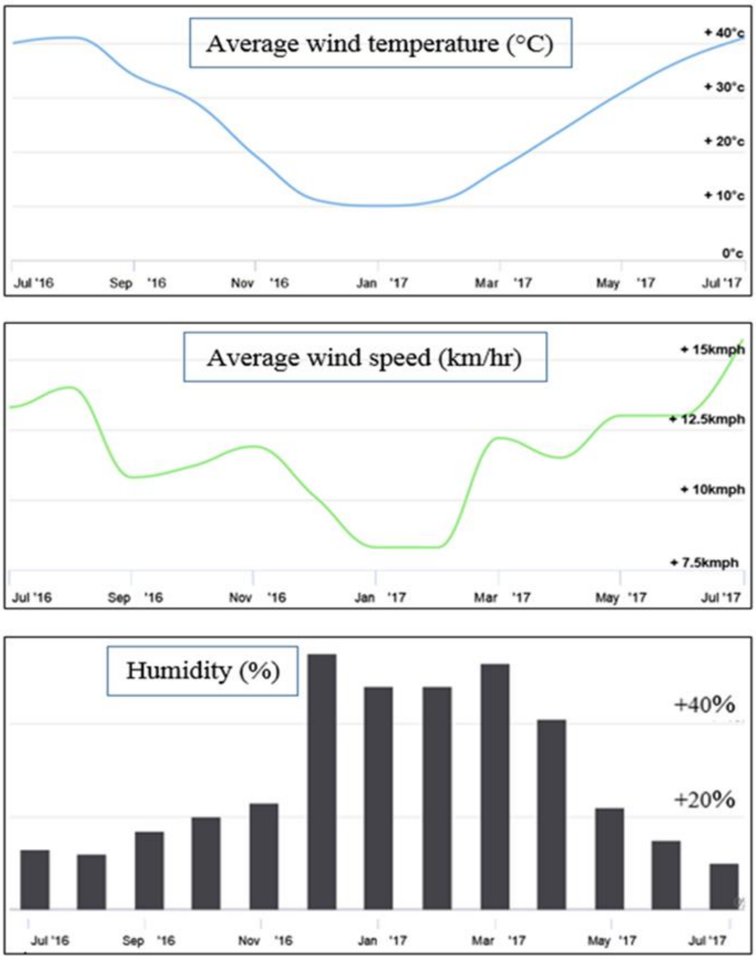

Figure 6-2: Average wind temperature, speed and relative humidity of Kirkuk, Iraq [161].

6.3 Computational domain and grid

The computational domain of the three Cases (I, II, and III) had dimensions (23.3×5×12.6) H, as shown in Figure 5-3. The building was set inside the duct; the blockage ratio was 4.2%, which was within the range recommended by the guidelines to avoid any effect of blocking and unphysical flow acceleration. The numerical grid used for all cases consists of around 6×10^6 hexahedral computational cells with a fine mesh structured near the walls, whereas a coarse mesh was used away from the walls in all directions. The minimum grid spacing used in each case was 0.005H in all directions to capture the laminar sub-layer. A grid independence study for Case-I was conducted to ensure that the results were independent of the mesh resolution as described in chapter 4, whilst for the other two cases the grid sensitivity analyses were not performed because they have almost the same number of grids (6.1×10^6 cells for Case-II and 6.05×10^6 cells for Case-III).

6.4 Boundary conditions and solver settings

The vertical profiles of the mean wind velocity, turbulent kinetic energy and turbulent dissipation rate are imposed at the inlet of the domain (Eqs 4-3, 4-4 and 4-5) as described in chapter 4. The surfaces of the house and the ground of the domain are modelled as no-slip boundaries, and symmetry boundary conditions are applied to the two sides and the top of the domain as slip walls with zero shear. The outflow boundary condition is specified at the end of the domain. A second-order discretization scheme was used in order to reduce the numerical diffusion effect. The family house analysed was comprised of several electrical appliances and the occupants of an average family; their generated heat value was assumed to be 25 W/m^2 which is equivalent to 1700 W and equal to the total heat generated by a TV, fridge, lights and four human bodies [131, 162]. The walls of the building were assumed adiabatic. This generated heat was uniformly applied to the floor of all rooms except bathroom as a heat flux boundary condition in all cases. A uniform temperature of 25°C was specified as the inlet boundary condition. For incompressible flow, the pressure-based solver was used in this study and the SIMPLEC scheme was imposed on the pressure–velocity coupling method. The pressure was interpolated by a second-order scheme. The spatial discretization of the momentum and the energy equations used the second-order upwind scheme.

6.5 Thermal comfort indices

The thermal comfort indices were evaluated using Fanger's comfort equations [121], i.e., predicted mean vote (PMV) and predicted percentage of dissatisfied (PPD), representing the thermal balance of a whole human body. The PMV parameter is an index representing the mean value of the voters of a large group of people in the same environment on a seven-point thermal sensation scale: cold (-3), cool (-2), slightly cool (-1), neutral (0), slightly warm (+1), warm (+2), and hot (+3). According to ISO 7730 (2005), an indoor environment is considered extremely comfortable when the values of the PMV index varied between [-0.5, +0.5] and is comfortable between [-1, +1] [10] . For the thermal comfort requirement, the appropriate range of PMV values was between -0.5 and 0.5, or -1 and 1, in which 90% and 80% of people claimed to be comfortable, respectively [163]. The mathematical expression of Fanger's PMV-PPD model is as given by Eqs. (6-1) and (6-6):

$$PMV = [0.303\, exp(-0.036M) + 0.028]\, L_{th} \tag{6-1}$$

where M the metabolic heat loss (W/m^2) and L_{th} is the thermal load on the body and calculated as:

$$\begin{aligned} L_{th} = (M - W) - 3.96E^{-8} f_{cl}[(T_{cl} + 273)^4 - (T_r + 273)^4] \\ - f_{cl} h_c (T_{cl} - T) - 3.05[5.73 - 0.007(M - W) - p_a] \\ - 0.42[(M - W) - 58.15] - 0.0173M(5.87 - p_a) \\ - 0.0014M(34 - T) \end{aligned} \tag{6-2}$$

where W is the active work (W/m^2), p_a (kPa) is the partial water vapor pressure and f_{cl} is the clothing area factor (1 *clo* = 0.155 m^2 K/W), expressed as:

$$f_{cl} = \begin{Bmatrix} 1.05 + 0.645\, I_{cl}, & I_{cl} > 0.078 \\ 1 + 1.29\, I_{cl}, & I_{cl} < 0.078 \end{Bmatrix} \tag{6-3}$$

The term I_{cl} is the resistance to sensible heat transfer provided by a clothing ensemble (*clo*) and assumed to be 0.5 *clo*. T_{cl} (°C) is the surface temperature of the clothing and is determined as below:

$$\begin{aligned} T_{cl} = 35.7 - 0.028(M - W) \\ - I_{cl}\{3.96 \times 10^{-8} f_{cl}\, [(T_{cl} + 273)^4 - (T_r + 273)^4] \\ + f_{cl} h_c (T_{cl} - T)\} \end{aligned} \tag{6-4}$$

where T_r (°C) is the mean radiant temperature, T (°C) is the calculated air temperature, and h_c (W/m^2 K) is the convective heat transfer coefficient between the occupant and the environment, the latter being given by the following empirical formula:

$$h_c = \begin{cases} 2.38(T_{cl} - T)^{0.25}, & for \;\; 2.38(T_{cl} - T)^{0.25} \geq 12.1\, u^{0.5} \\ 12.1\, u^{0.5} \quad , & for \;\; 2.38(T_{cl} - T)^{0.25} \leq 12.1\, u^{0.5} \end{cases} \qquad (6\text{-}5)$$

where u is the local velocity calculated by the CFD model and further details can be found in reference [107, 163].

PPD predicts the percentage of occupants that will be dissatisfied with the thermal conditions and is a function of PMV. According to ASHRAE 55, the recommended acceptable PPD range of thermal comfort is less than 10% of persons dissatisfied with an interior space, since PPD is a function of PMV, it can be defined as:

$$PPD = 100 - 95e^{[-(0.03353PMV^4 + 0.2179PMV^2)]} \qquad (6\text{-}6)$$

Equations (6-1)to (6-6)were coded in the UDF file (User-Defined-Function), linked with ANSYS FLUENT and used to calculate the values of PMV and PPD.

A validation process was performed for the PMV model before its use in the current study. The ASHRAE standard 55 thermal comfort tool [164] was used to verify the PMV model. The predicted PMV values at different points in the building were compared with the results of the ASHRAE tool, and the deviations were found not to exceed 5%. However, this model is derived from the steady-state heat transfer theory and calibrated through climatic chamber experiments. As a result, it will overestimate the subjective warmth sensations of occupants of buildings without air-conditioning, although it is a good predictor of thermal sensation in buildings with HVAC systems [165]. Therefore, Fanger and Toftum [166] have developed an extension of the PMV model for use in non-air conditioned buildings in warm climates by introducing an expectancy factor. They have estimated the expectancy factor for a non-air-conditioned building located in a region where air-conditioned buildings are common between 0.9-1. The expectancy factor used in the current study is 1.0. Moreover, for such naturally ventilated buildings, an adaptive model has been proposed [167] where the variable in this model is the average monthly outdoor temperature only without including human activity, feelings or clothing. Although the thermal sensation based on the PMV scale was applied for the hot climate in the previous study [168], the equation underestimated the thermal sensation by 12% in autumn and 22% in spring for a hot and dry climatic region [169].

6.6 Results and discussion

The numerical results of the three cases are presented and compared in terms of velocity and temperature contours, followed by predicted mean vote (PMV) and predicted percentage of dissatisfied (PPD) values. Moreover, a comparison between these cases in terms of human thermal comfort is also discussed thoroughly in the following sections to provide helpful information for the effective design of buildings. Furthermore, investigation of opening positions and outside weather conditions would give the designer valuable information in obtaining more energy-efficient designs and naturally ventilated buildings. The area of the openings in all cases was kept constant, as was the wind incidence angle of 0^o.

The thermal comfort indices predicted for metabolic rates, M, were 58 W/m^2 (seated), and 70 W/m^2 (standing). The thermal resistance due to typical clothing insulation in summer conditions was set as being equal to 0.5 clo, the relative humidity was fixed at 30% with zero external work (W). The PMV, PPD and temperature contours of a horizontal plane at a height of 0.6 m from the ground of the building were calculated for the seated case as recommended by ASHRAE 55 [13] and 1.1 m for the standing case according to the International Organization for Standardization (ISO 7730:2005) [10].

6.6.1 Impact of opening location

The impact of the locations of the window openings on thermal comfort is studied in this section. Figure 6-3 and 6-4 present the average of PMV, PPD, velocity and temperature of the rooms for Case-I, II, and III, whilst Figure 6-5 to 6-8 present the PMV and temperature contours of these cases in the seated and standing levels. The wind speed was kept constant (3 m/s) at 25^oC. As shown in Figure 6-3, Case-I and Case-II were more comfortable than Case-III in rooms B, where the average of PMV in the seated plane was higher than 0.2 of the counterpart room in Case-III, whilst the room A in Case-II was more comfortable than the counterpart rooms in others cases. The values found for PPD showed the same trends, which were 12% for room A and 9% for room B in Case-I, whilst in Case-III were 16% and 13% for rooms A and B, respectively. Over the whole seated plane, Case-III predicted slightly higher PPD than Case-I and Case-II because the average air temperature was higher than for other cases, and PPD are highly dependent on the temperature of the flow (Eq. 4 and 5). The PPD calculated for the whole plane were 9.5%, 10% and 11.5% for Case-I, II and III, respectively, the small differences among these cases leading to the conclusion that the opening positions in these cases did not have any significant effect on the values of the thermal comfort indices. The average values of temperature and PMV in rooms A and B were lower than those in other rooms in all cases. The reason for the low temperatures predicted in rooms A and B is due to the high flow velocity predicted for these rooms, where the flow drives a large amount of heat to the outside of the room, thus reducing the temperature.

As regards the standing level, the differences in PMV amongst these cases are increased noticeably when comparing the seated planes, in spite of a slight decrease of average temperature and a small increase in average velocity (Figure 6-4)). This is because of the higher assumed metabolic rate in the standing plane than the seated plane. However, the PPD predicted in Case-I was 8%, whilst for Case-II and Case-III the predictions were 11% and 10%, respectively, which is somewhat similar to the seated plane because of the high metabolic rate increasing the PMV of the rooms, since for the front rooms the PPD decreased, the thermal conditions changed to the neutral and the plane remained at the same PPD.

The thermal contour plots can provide more useful information for designers when applying natural ventilation as an example. Although the average values of the PMV in the seated plane are in the acceptance range for all rooms, the contour plots show two zones (coloured in red) inside rooms C, D and E with high PMV values (> 1.5) and two zones (coloured in red) inside rooms A and B with low PMV values (< -1.5) (Figure 6-5), which could cause discomfort for the occupants. Therefore, the occupants should avoid these zones when either sleeping or when they are seated. Regarding the standing plane, these zones are generally more comfortable, especially in the front rooms when the PMV values were around -1.2 and in room C was less than 1 except for Case-I, whilst in the rear rooms the red zones were larger than in the seated plane, again except for Case-I (Figure 6-6). Moreover, the counter plot showed that room C was more comfort in Case-III than for the other two cases in both the seated and standing levels.

Overall, the contour plots for the three cases show non-identical patterns though there are some similarities, especially in rooms D and E where high PMV zones are noticed in all cases, while in the front rooms reduced PMV zones are predicted and the location of these zones are different from case to case. In conclusion, the three horizontal opening positions have a noticeable influence on the patterns of the thermal comfort distribution, the noticeable feature among these cases is the patterns in room C for Case-III where both seated and standing planes are asymptotic and there are no discomfort zones in either plane.

Because the PMV values are highly dependent on the temperature of the flow, the pattern of the contour plots for PMV will follow the contour plot pattern for temperature. Thus, the pattern of the contour plots for temperature (Figure 6-7 and 6-8) for all three cases in the seated and standing planes are similar to the pattern plots for PMV (Figure 6-5 and 6-5). These figures showed that in rooms D and E, the temperature was higher than 30°C for the seated and standing planes in all cases; therefore, high values of PMV were predicted in these rooms (> 1.5) in the seated plane, while for the standing plane these rooms had a low PMV (≤ 1.2) because the predicted temperature was lower than that in the seated plane as well, especially in Case-I.

By comparing the PPD for the three cases for both levels, it can be concluded that the performance in Case-I was slightly better than the other two cases, whilst the contour plot for Case-III showed that the areas of the discomfort zones are smaller than for the other two cases. The reason why these positions did not show a significant variation was because they were located at the same height whilst the different levels' positions will result in a large change in the flow streamlines, and will thus change the thermal comfort considerably [35]. Therefore it is necessary to compare the results for different façade opening alternatives in an initial design stage to make better natural ventilation design decisions to improve the building's thermal comfort and energy efficiency [132].

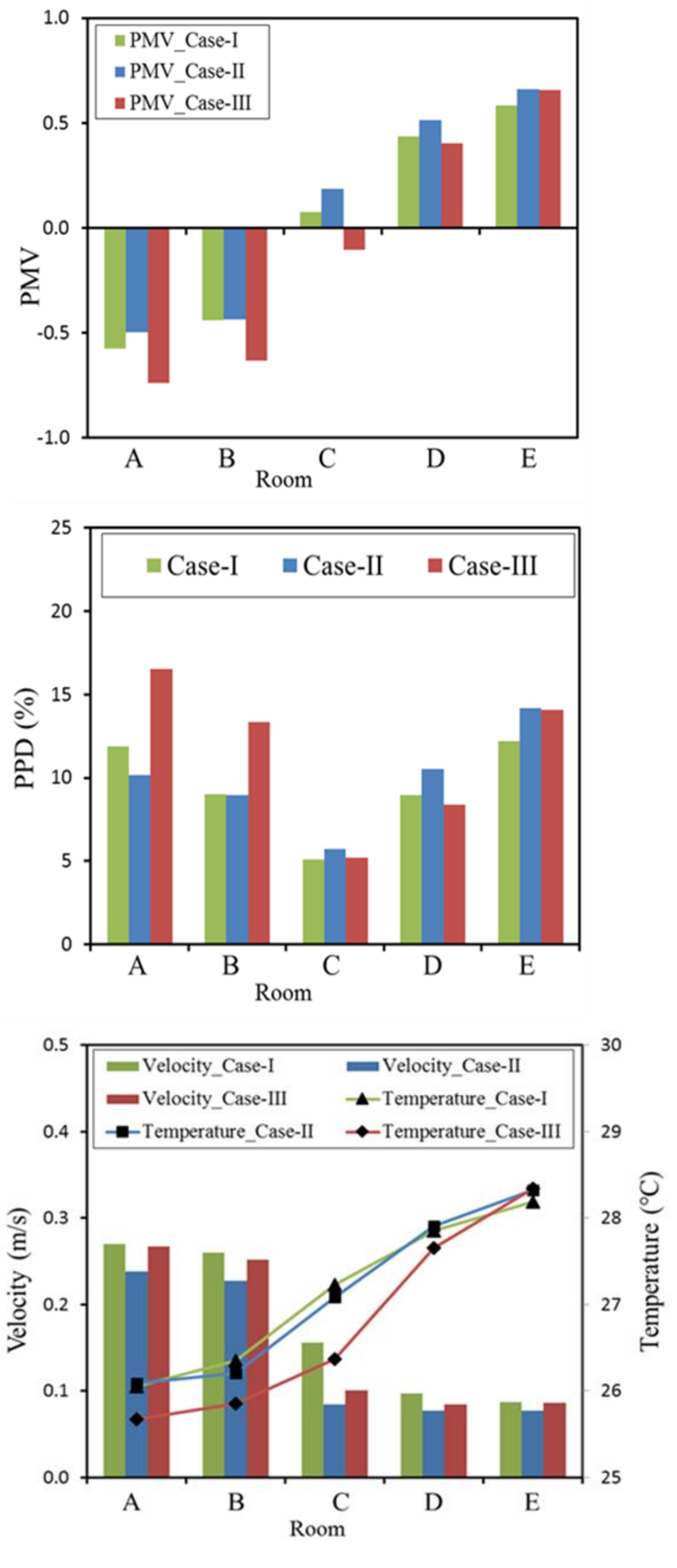

Figure 6-3: The room average PMV, PPD, velocity and temperature in the seated plane for Case-I, Case-II and Case-III.

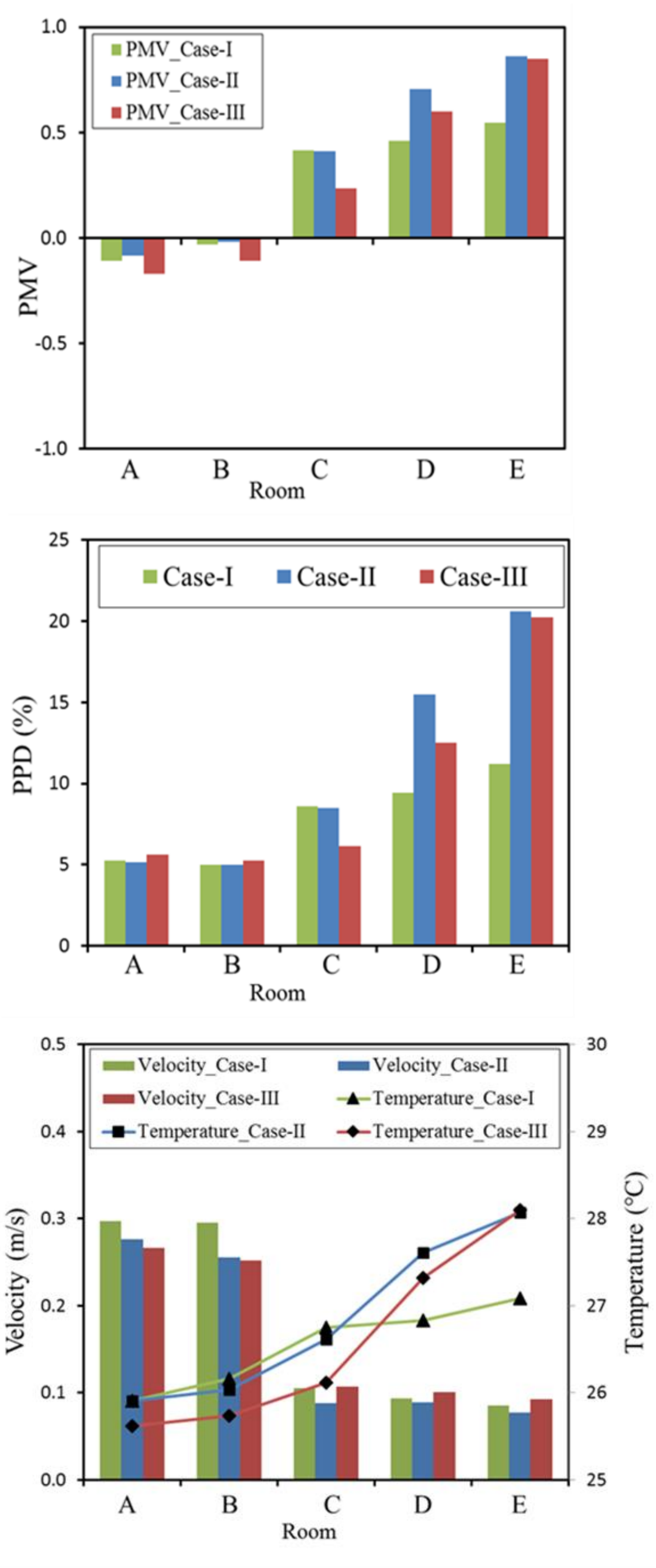

Figure 6-4: The room average PMV, PPD, velocity and temperature in the standing plane for Case-I, Case-II and Case-III.

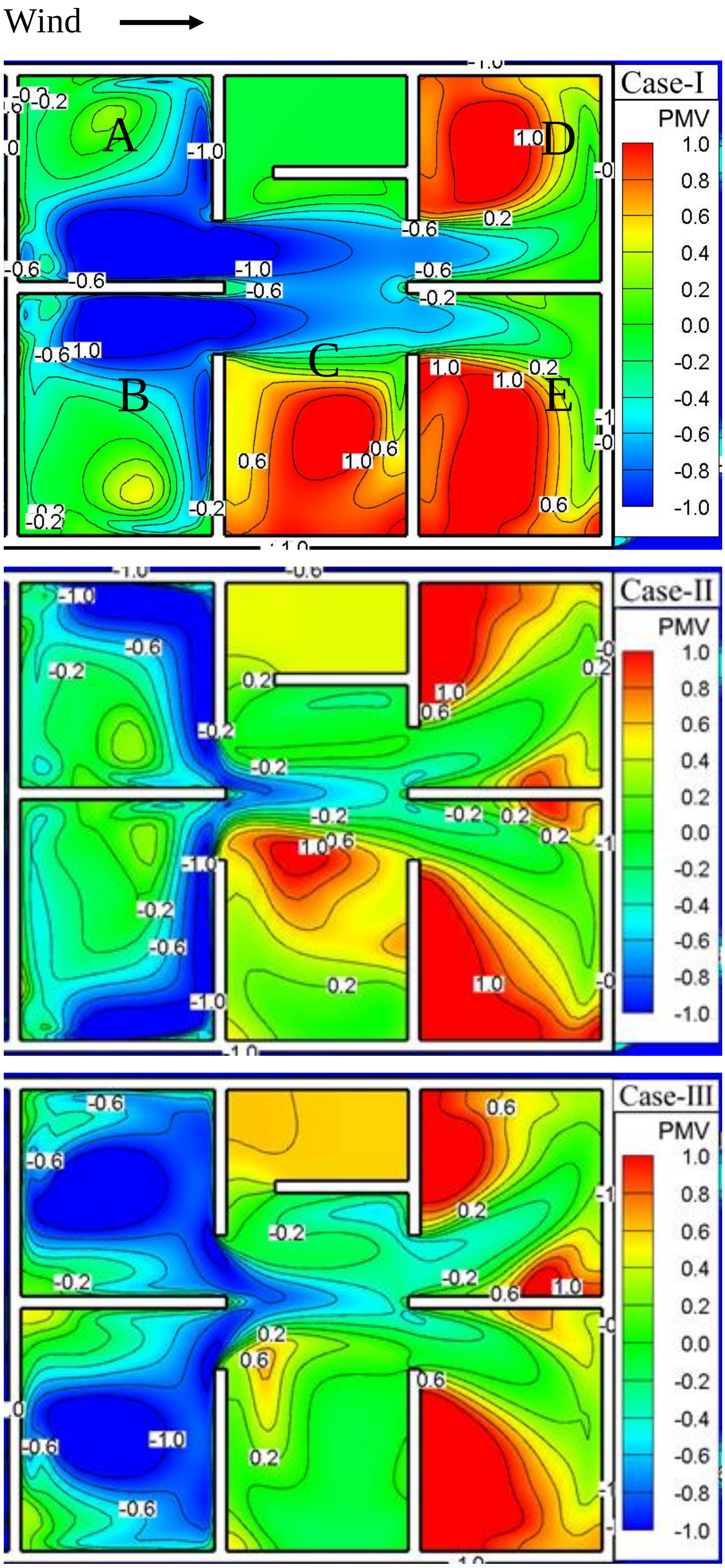

Figure 6-5: PMV contours in the horizontal plane (seated level) for Case-I, Case-II and Case-III.

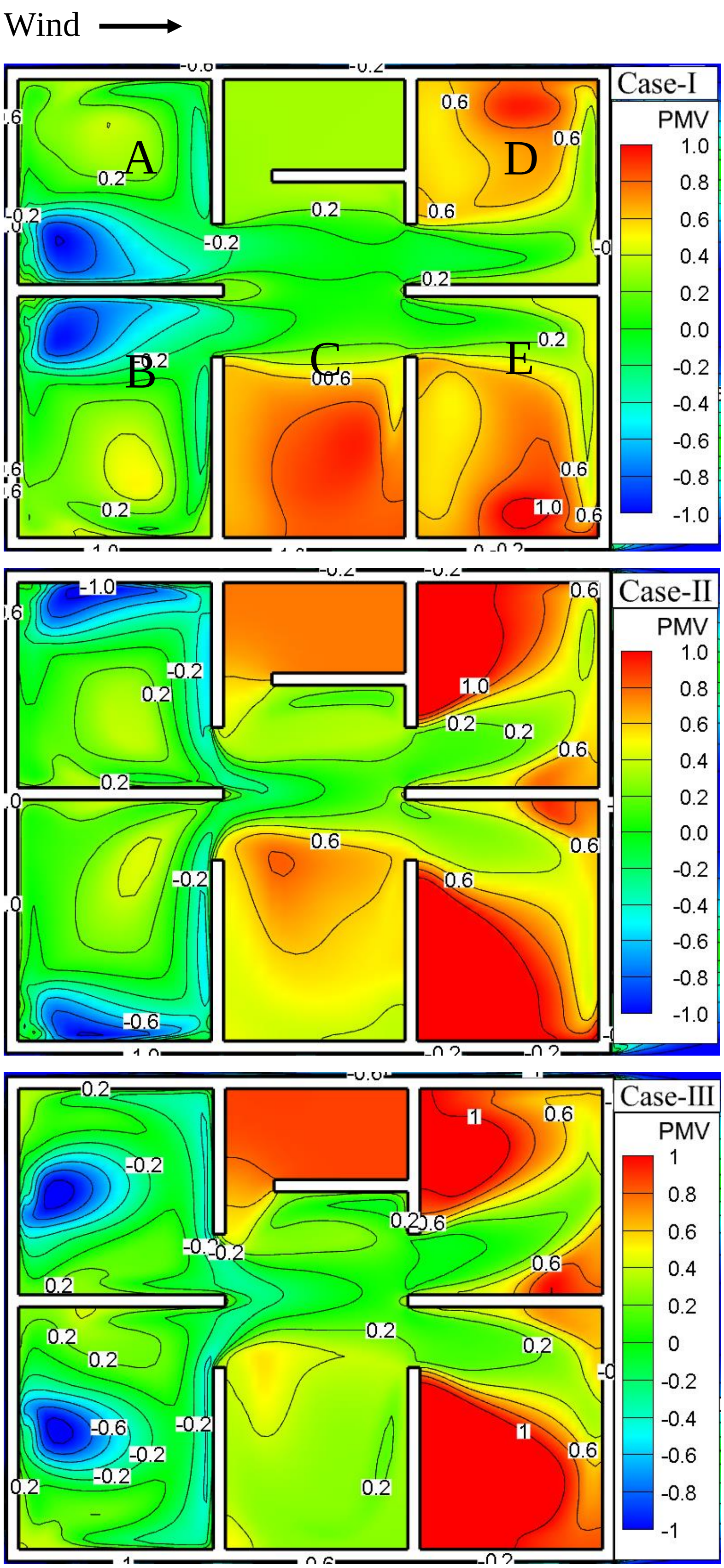

Figure 6-6: PMV contours in the horizontal plane (standing level) for Case-I, Case-II and Case-III.

.

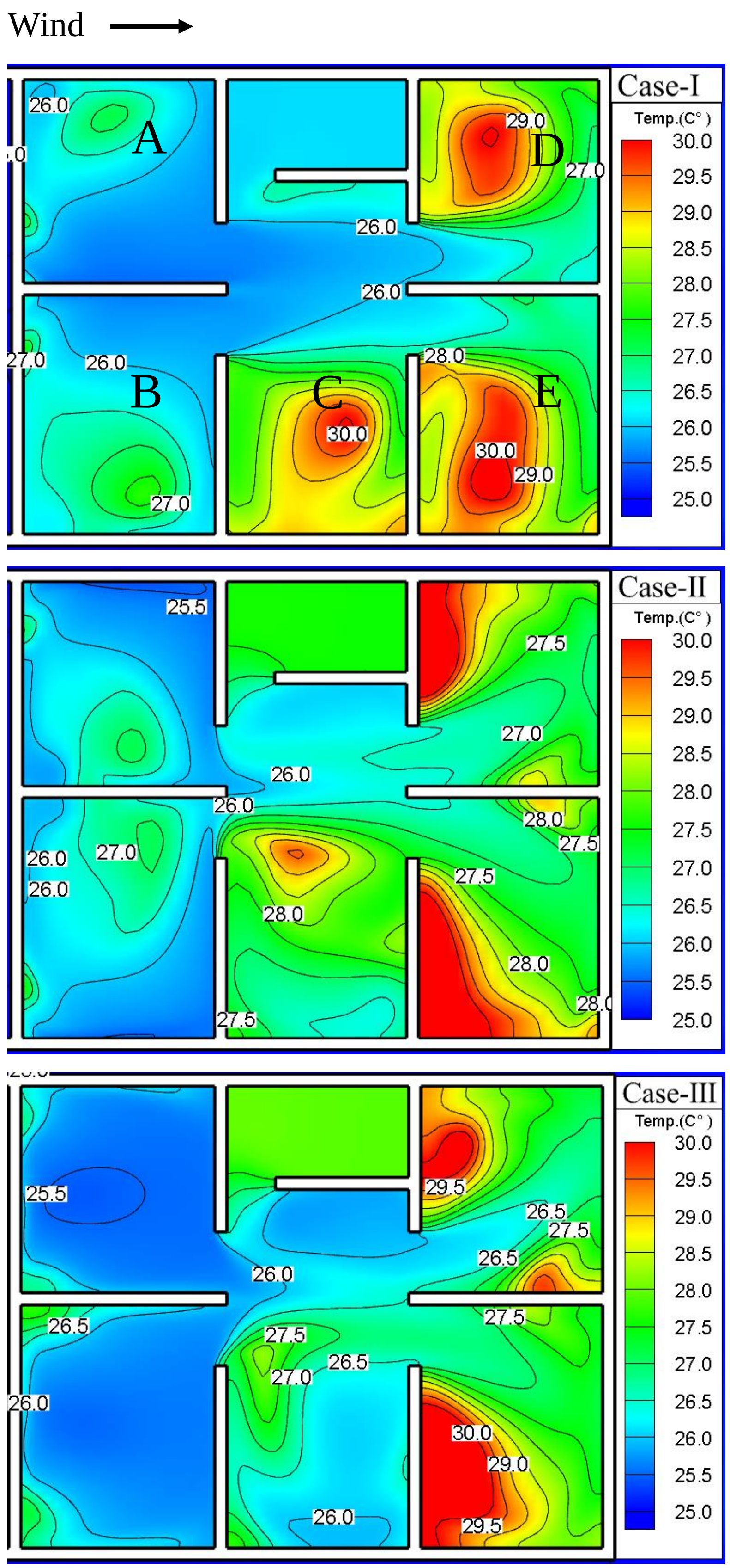

Figure 6-7: Temperature contours in the horizontal plane (seated level) for Case-I, Case-II and Case-III.

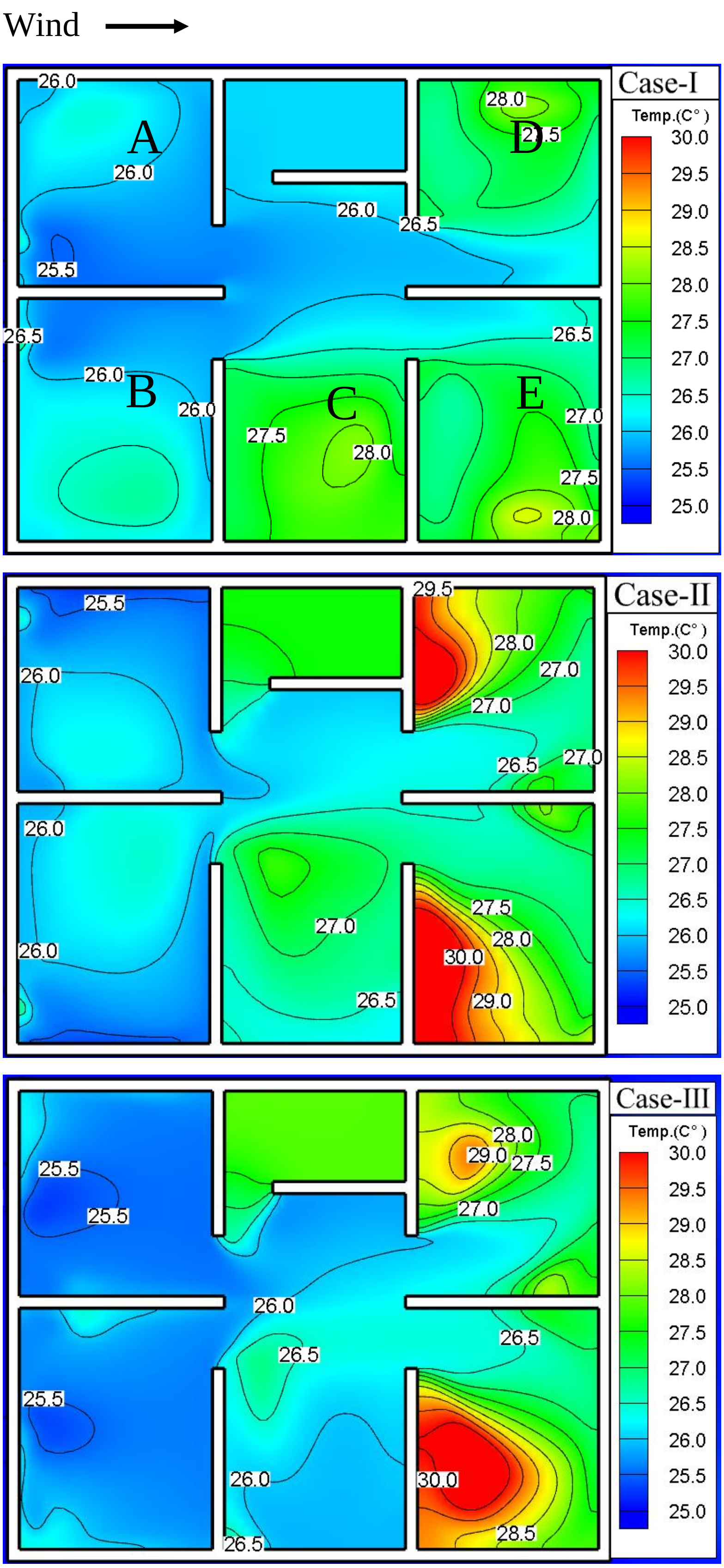

Figure 6-8: Temperature contours in the horizontal plane (standing level) for Case-I, Case-II and Case-III.

6.6.2 Impact of wind speed

The impact of outdoor wind speed on the indoor thermal comfort was studied by choosing Case-III because the opening positions in the three cases do not show significant influence on the thermal comfort indices, and the openings in Case-I and II are located near the walls and the flow may be affected by adding furniture to these rooms. Therefore, Case-III has been chosen for the remainder of the study. The reference wind speeds (U_{ref}) of 1 to 6 m/s at the building height H were used, whilst the temperature was fixed at 25°C. The numerical results are presented and compared in terms of average velocity and temperature, followed by PMV and PPD for the seated level and sanding levels. Figure 6-9 and 6-10 show the average velocities, temperatures, PMV and PPD in the seated plane 0.6 m above the floor. Under the reference velocity of 3 m/s, the seated plane was found to have an average velocity of 0.16 m/s and acceptable thermal comfort with a PPD of around 11%, whereas at a U_{ref} of 1 m/s the PPD increased to higher than 33% and the average velocity decreased to lower than 0.06 m/s, resulting in warm conditions inside the building. When U_{ref} was 6 m/s, the average velocity of the seated plane increased to 0.35 m/s, decreasing the average temperature by around 1°C and resulting in a high PPD of 22%, though the plane still had acceptable thermal comfort (-1 < PMV > +1). In addition, the wind-driven ventilation delivered a low air velocity for the rear rooms (D and E) with an average of approximately 0.1 m/s at the U_{ref} of 3 m/s and high air velocity for the front rooms (A and B) of 0.25 m/s at the same reference velocity, therefore significant differences appeared between these rooms in terms of thermal comfort. For instance, the differences between the front rooms A and B and the rear rooms D and E of PPD were 4% when U_{ref} was 3 m/s, while in the case where U_{ref} was 6 m/s this difference increased to 34%. It can also be seen that the difference in the thermal index (PPD) for the front rooms was higher than that for the rear rooms by 45% at a reference velocity of 1 m/s. This is because, at high velocity, the differences in temperature between the front and rear rooms were small and the differences in velocity were high, thus the velocity was thought (Eq. 8) to become more influential than temperature in creating these differences in values of thermal comfort indices between these rooms. At low velocity, the differences in temperatures were high between the front and rear rooms and differences in velocities were small; therefore, temperature was thought to become more influential on the thermal comfort indices, as shown in Figure 6-9 and 6-10. The small differences in of PPD at U_{ref} of 3 m/s between the front and rear rooms lead us to conclude that the building will be in a good comfortable thermal condition at reference velocities of around 3 m/s.

The thermal comfort indices, average velocity and temperature for standing activities at a height of 1.1 m were also analysed, the results of which are presented in Figure 6-11 and 6-12. The results showed the same trend as the seated level, despite the level of this plane being located nearer to the level of the opening positions than the seated plane. The average velocities for the standing plane were almost the same as the average velocity for the seated plane because both levels are distant to some extent from the opening positions' level, whilst the change in thermal comfort indices occurred because of the higher assumed metabolic rate in this plane than the seated plane. However, when the reference velocity was set to 3 m/s, the PPD for the seated and the standing planes were small, while significant differences in PMV were noted at a low U_{ref} of 1 m/s and high U_{ref} of 6 m/s. This means that at a reference velocity between 2-5 m/s the human thermal comfort zone (between the seated level and standing level) is in an acceptable thermal condition. Generally, it can be concluded that cross ventilation can provide an acceptable thermal comfortable environment for this type of building as long as the wind speed ranged between 2-5 m/s, despite there being a few locations inside the house where PMVs were still higher than the acceptable range.

The thermal contour plot can provide useful information for the designers when applying natural ventilation as an example. The PMV contours showed that the area around the two zones (coloured in red and yellow) in Figure 6-13, as discussed in the previous section, increased with decreasing wind speed. For instance, the areas of the discomfort zones in rooms D and E were small when the U_{ref} was 4 m/s, but increased and covered around half the area of the rooms when U_{ref} was 2 m/s, whereas the areas of the discomfort zones (coloured in blue) in rooms A and B increased with increasing reference velocity.

Although the average values of the PMV are in an acceptance range in rooms D and E (PMV ≈ 0.5) for the seated plane when U_{ref} was 3 m/s (Figure 6-9), the contour plot shows two zones (coloured in red) inside these rooms with high PMV values (> 1.5), as shown in Figure 6-13, which will cause discomfort for any occupants. In the standing plane (Figure 6-14), these two zones are warmer than at the seated level due to the higher metabolic rate assumed in the standing plane than the seated plane; therefore, occupants should avoid these zones when either sleeping or when seated. Overall, the figure showed that the implementation of cross ventilation in this kind of building can create a thermally comfortable indoor environment, but becomes inadequate to provide thermal comfort, especially in rooms C, D and E, when the air velocity is low (U_{ref} < 2 m/s) and in rooms A and B when the air velocity is high (U_{ref} > 5 m/s).

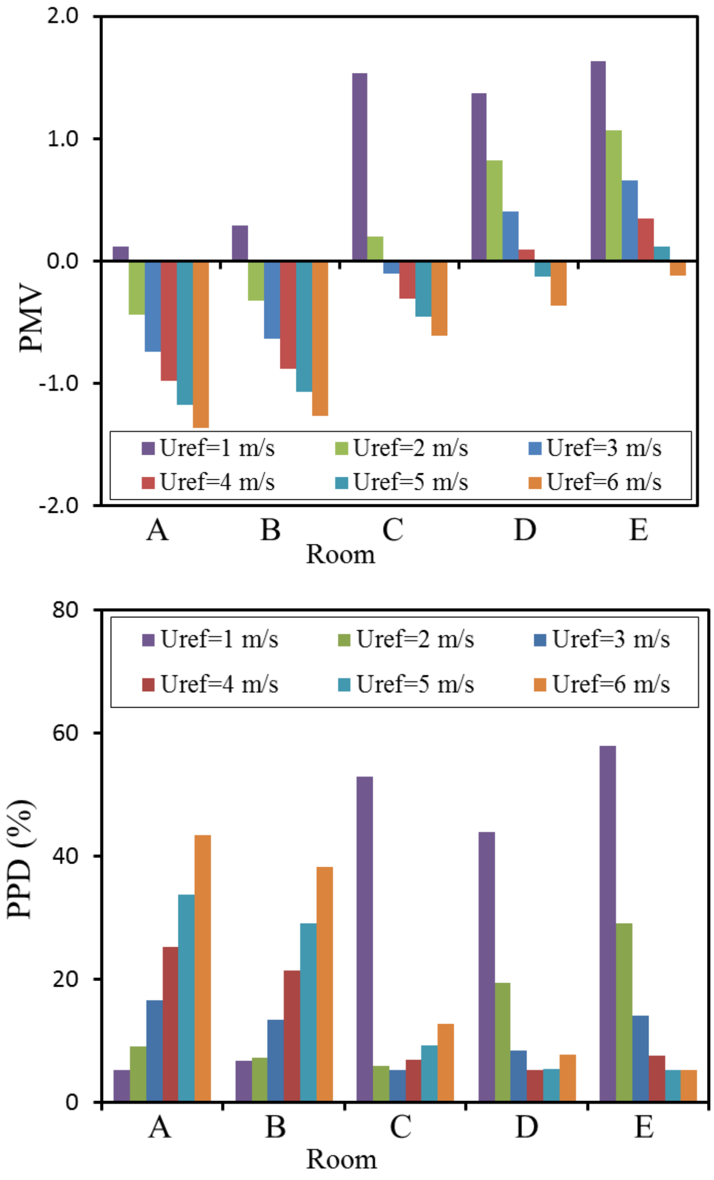

Figure 6-9: The room average PMV and PPD in the seated horizontal plane for Case-III.

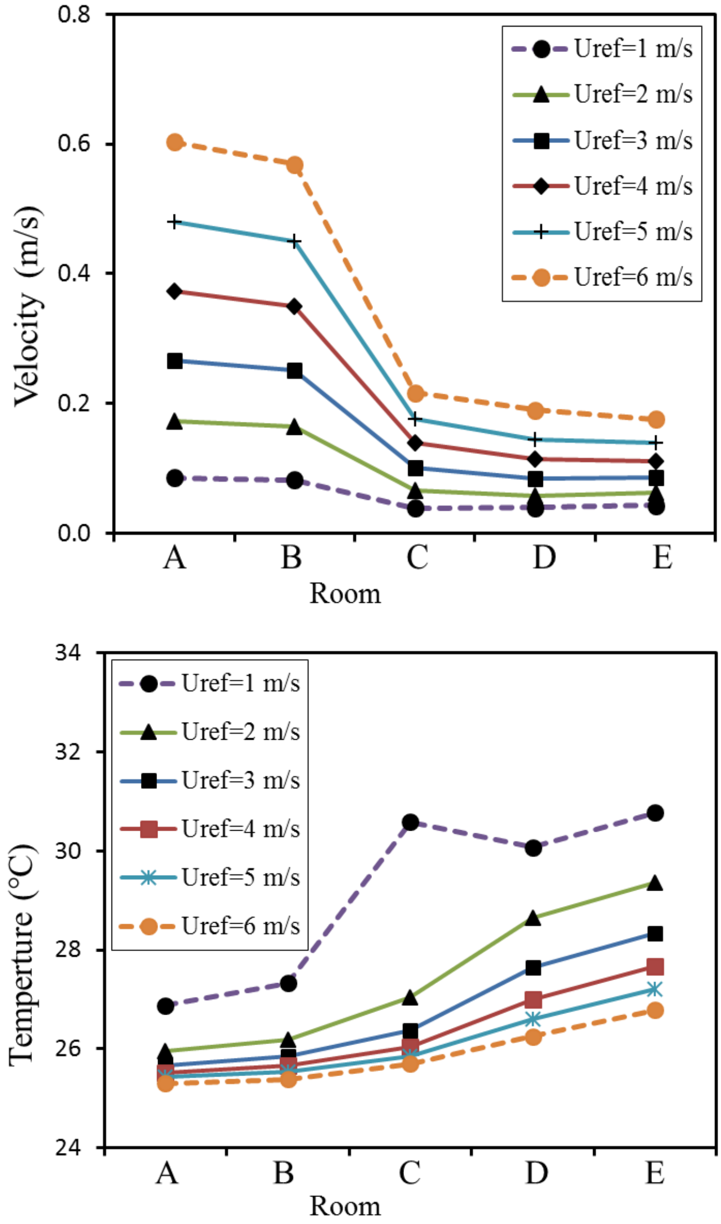

Figure 6-10: The room average velocity and temperature in the seated horizontal plane for Case-III.

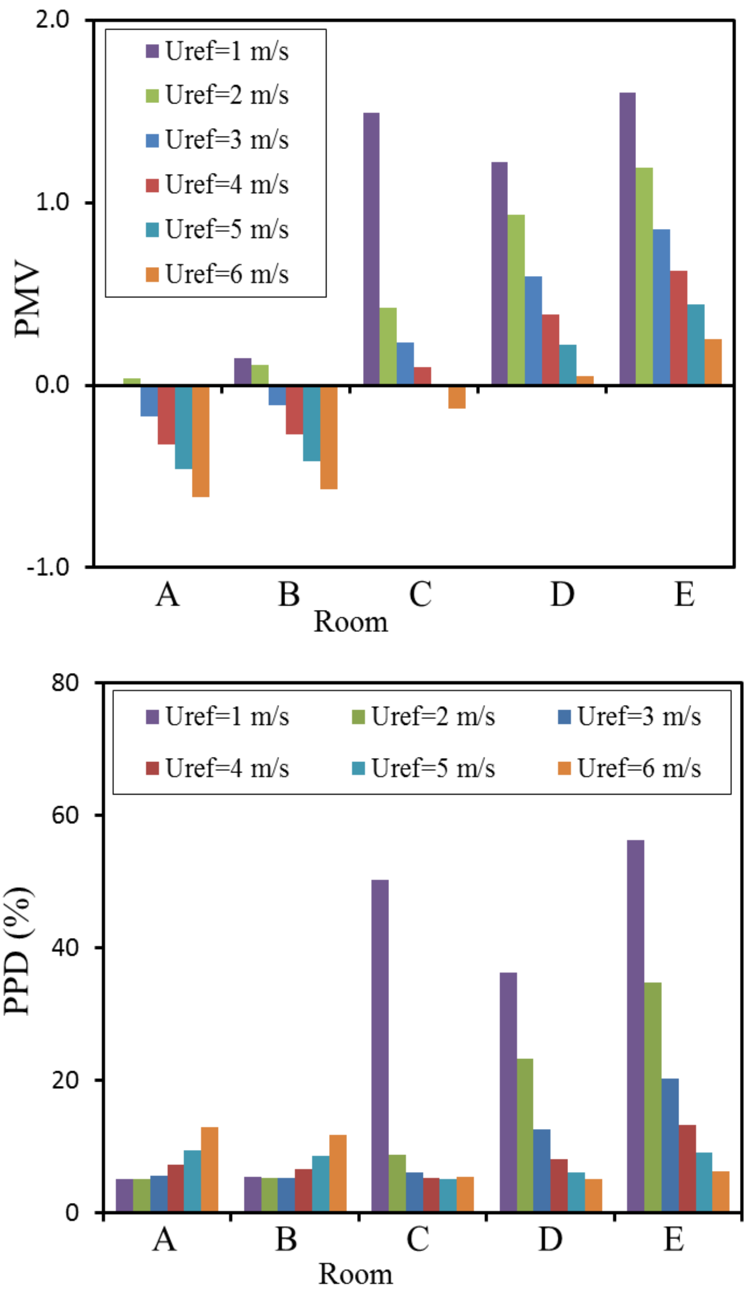

Figure 6-11: The room average PMV and PPD in the standing horizontal plane for Case-III.

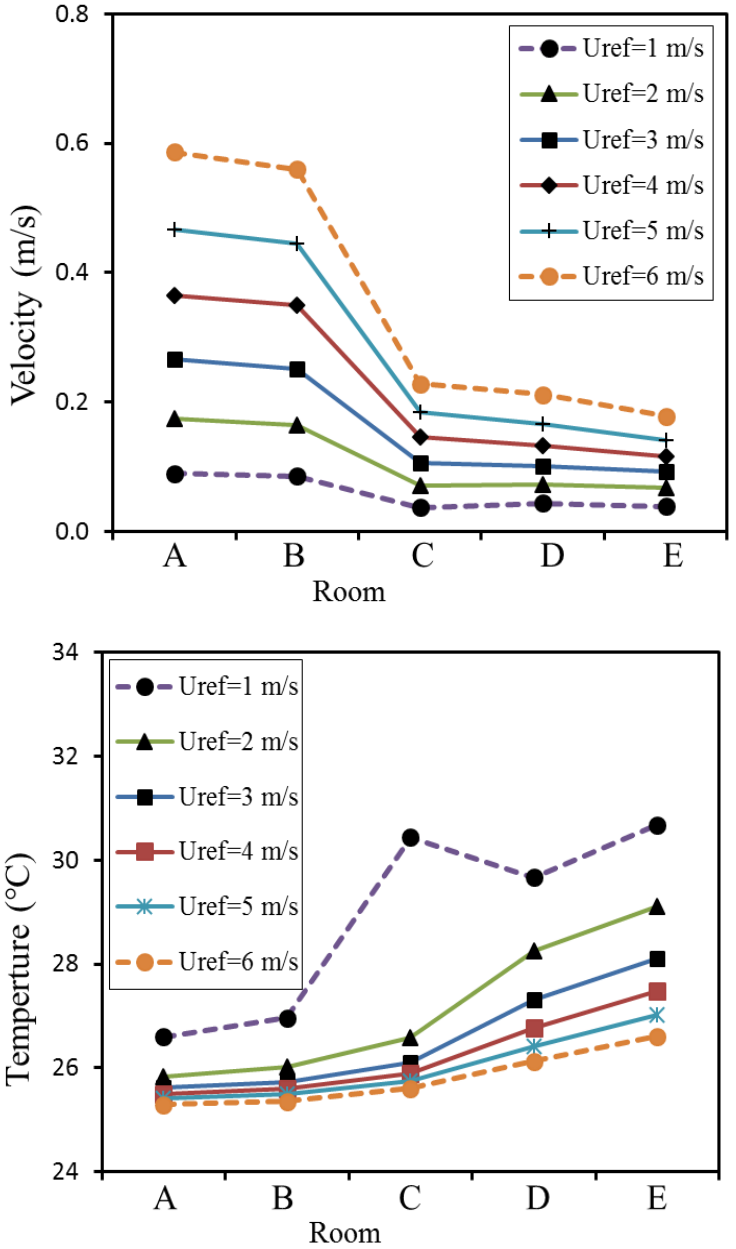

Figure 6-12: The room average velocity and temperature in the standing horizontal plane for Case-III.

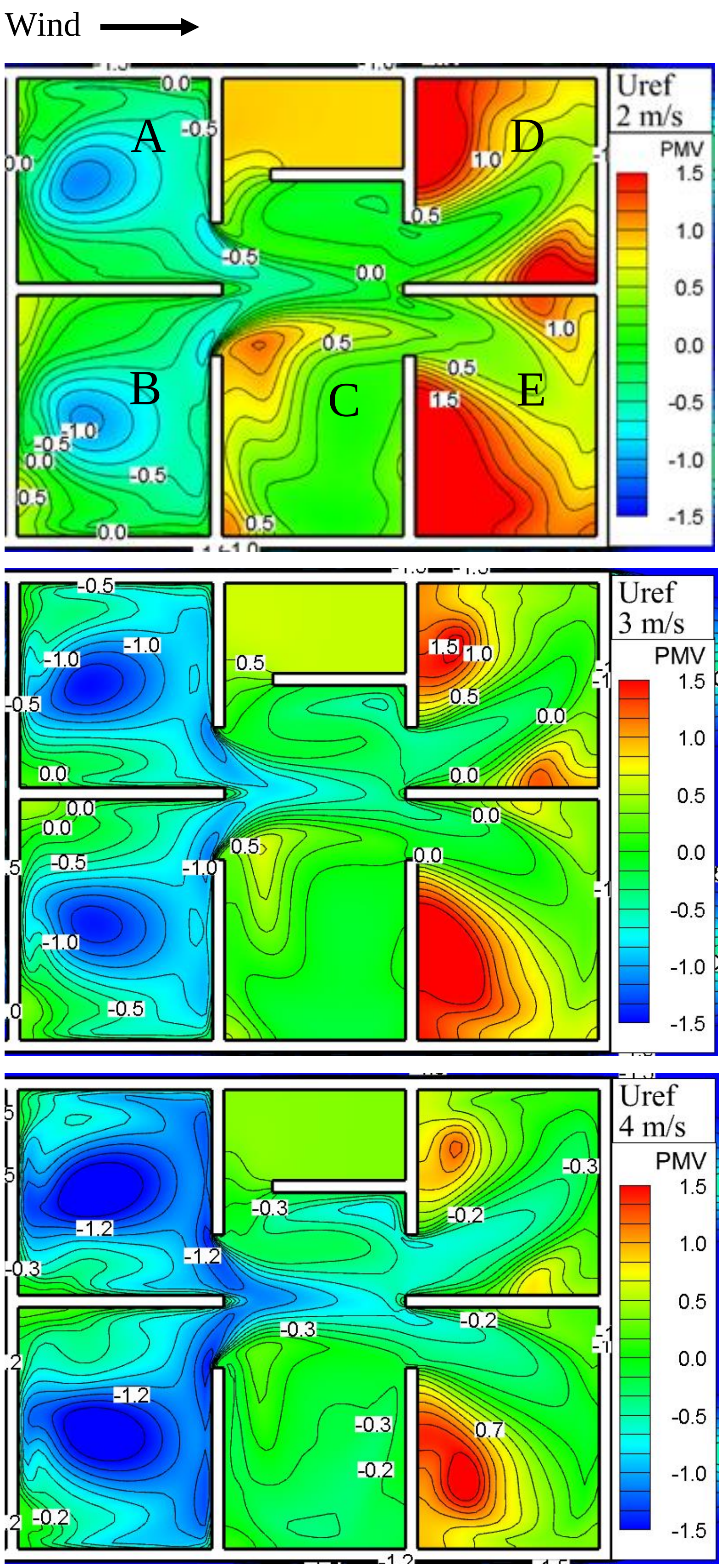

Figure 6-13: PMV contours in the horizontal plane (seated level) for Case-III at different wind velocity.

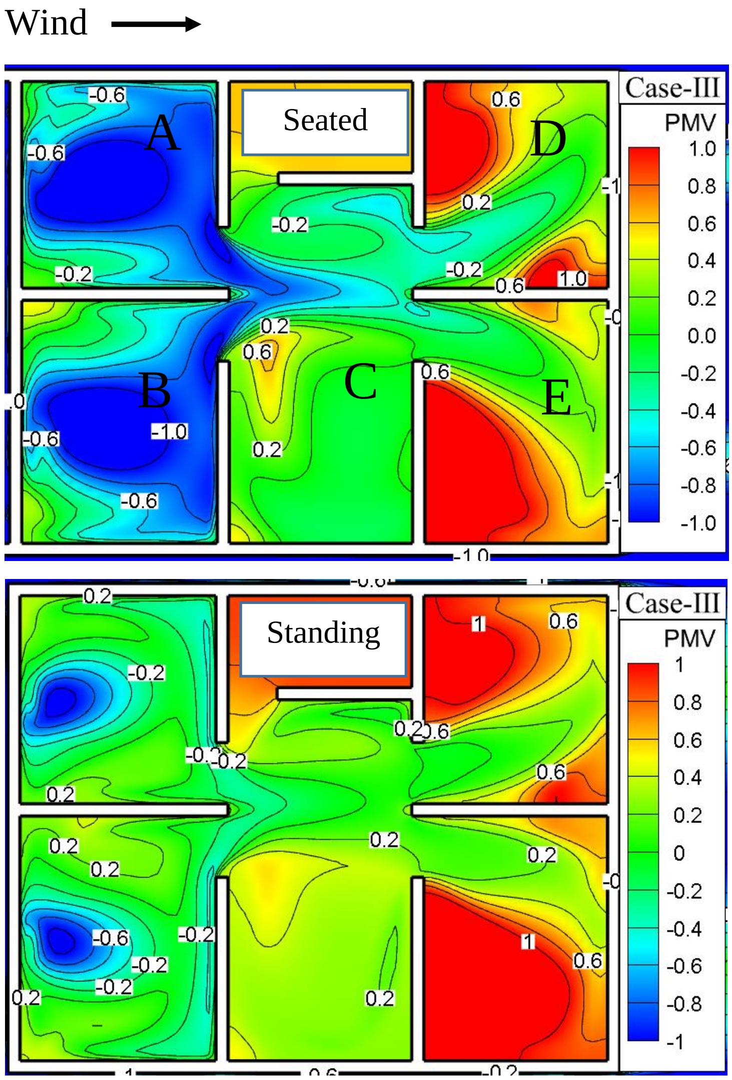

Figure 6-14: PMV contours in the horizontal plane for Case-III at U_{ref} = 3 m/s.

6.6.3 Impact of ambient temperature

The impact of ambient temperature on indoor thermal comfort is studied in this section. Case-III was chosen as a reference under a fixed wind speed of 3 m/s and with the ambient temperature changed from 20 to 29°C. Figure 6-15 and 6-16 show the average PMV and PPD in each room of the building in both the seated and standing planes. The results showed that the wind temperature that provided the best thermal comfort in the seated plane was 25°C, where all rooms were in a comfortable condition and the PPD was around 11%. The PMV values remained close to comfortable conditions when the temperature increased to 27°C or decreased to 24°C and the PPD for the rooms in the seated plane raised to 20% which is reasonably good, though a high PMV was predicted in the rear rooms as discussed previously, while the thermal conditions changed to slightly warm/cool when the outside air temperature increased to 28°C or decreased to 23°C, respectively.

The results for the standing plane showed that a range of outside wind temperatures between 22-26°C can provide an acceptable PMV of +1 to -1 inside all rooms, i.e., between slightly cool and slightly warm, while the rooms remain very comfortable when the wind temperature is at 24°C and close to neutral conditions for PMV when increased to 25°C or decreased to 23°C and the PPD for the rooms was less than 10%, implying that about 90% of the occupants would probably not find the thermal conditions uncomfortable. Overall, natural ventilation can be applied to this type of building across a range of wind temperatures between 22-28°C for the seated plane and 20-28°C for the standing plane. Thus, the conditions can be described as being between slightly cool and slightly warm.

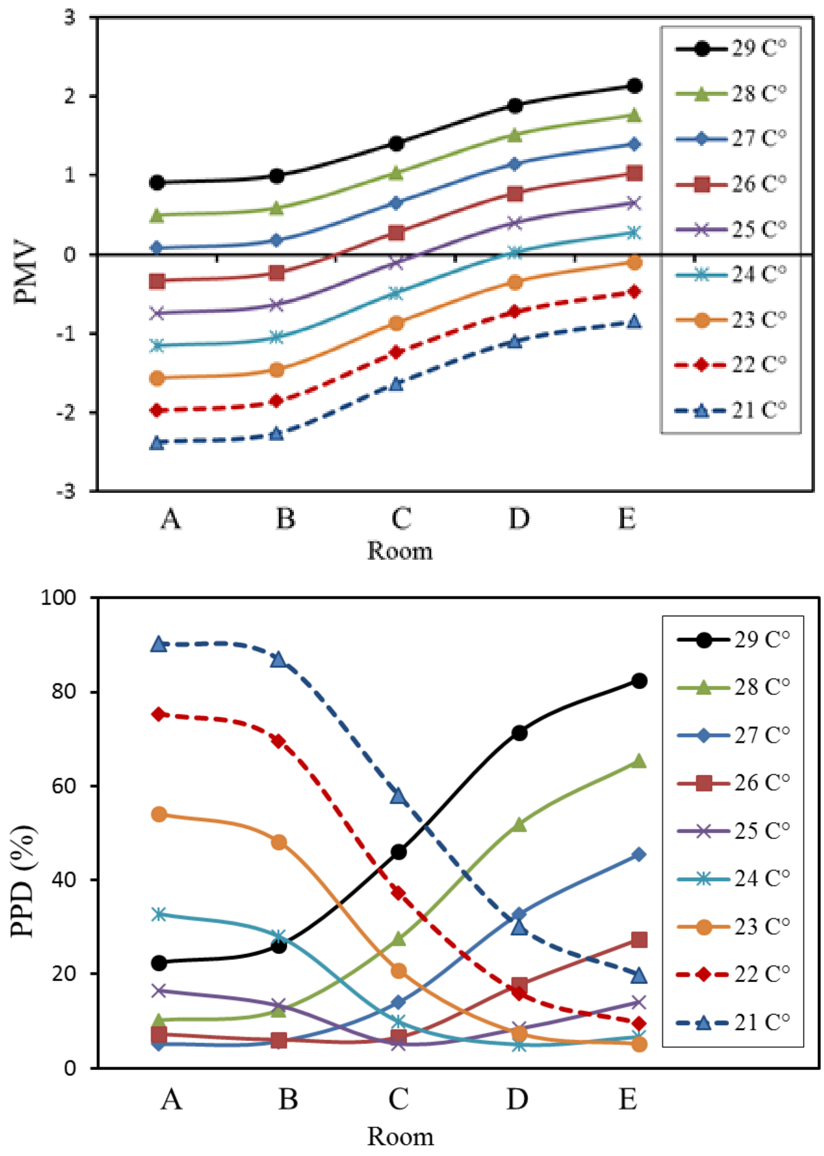

Figure 6-15: The room average PMV and PPD in the seated horizontal plane for Case-III.

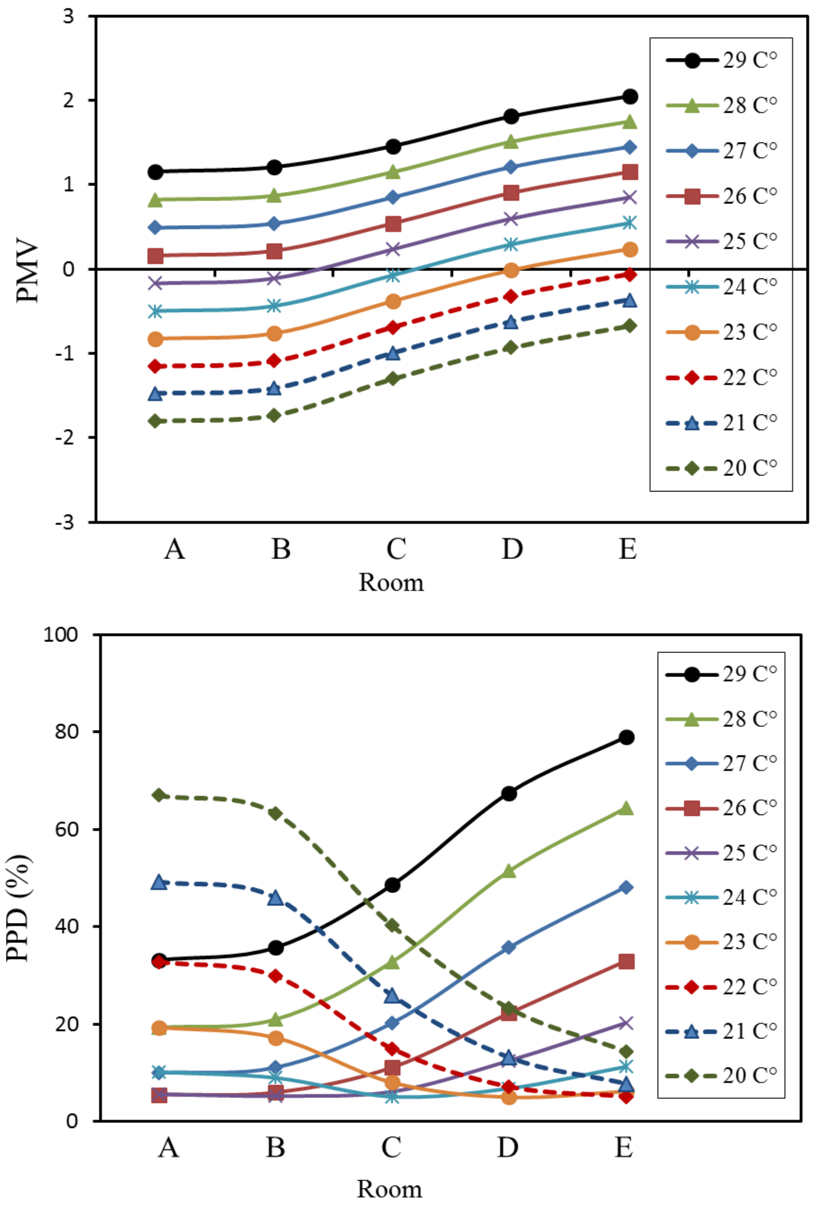

Figure 6-16: The room average PMV and PPD in the standing horizontal plane for Case-III.

6.7 Conclusion

This study has examined the changes in human thermal comfort in terms of PMV and PPD inside an average residential building in Iraq when the opening position, outdoor wind speed and wind temperature were changed via the steady RANS method. Investigating indoor thermal comfort in a multi-zone building could give designers valuable information regarding more energy-efficient designs in naturally ventilated buildings. The following conclusions were obtained:

- The study finds that the three horizontal opening positions have only a slight impact on the level of the thermal comfort indices in both the seated and the standing planes.
- The contour plots clearly show the places where it would be more comfortable for any occupants to perform their daily activities.
- The study concludes that the cross ventilation can provide acceptable thermal comfort for this type of building when the wind speeds are between 2 and 5 m/s at the temperature of 25°C, despite there being a number of locations inside the house that are still higher than the acceptable PMV range.
- The study has demonstrated that the range of wind temperature conditions under which all the rooms in the house can be maintained within an acceptable thermal comfort range for the seated levels is between 22-28 °C and for the standing planes is between 20-28 °C with an external wind speed of 3 m/s.

Chapter 7 Effect of heat loads and furniture on thermal comfort under a naturally ventilated environment

7.1 Introduction

In this chapter, more realistic situations are considered and begin with modelling furniture within the building and then modelling for heat sources (e.g., TV, oven, and refrigerator) with a natural cross-ventilation environment in the hot climate. The evaluation impact of the furniture and heat loads on the thermal comfort indices are analysed through a series of CFD simulations using the Renormalization Group RNG k-ε model. This chapter will discuss the changes in the human thermal comfort in terms of the PMV and PPD values inside the building with heat loads being applied via the RANS model. Finally, the chapter concludes with the thermal comfort evaluation of all the scenarios explored.

7.2 Case description

Case-III has two opening positions, the details of which are provided in Figure 6-1. This case did not include any furniture, whilst of course in a realistic family house, there would be many pieces of furniture and heat sources. Therefore, furniture and heat sources are modelled, the layout of the house is shown in Figure 7-1 and the dimensions of the furniture are provided in Table 7-1. Five scenarios are simulated in this study, the details of which are provided in Table 7-2. The first scenario (Case-F) included the building geometry without furniture and four human bodies, whilst the second scenario (Case-FF) included furniture only (without human bodies). The three remaining scenarios (Case-F1, F2, and F3) included one style furnished the house, as shown in Figure 7-1, with different heat loads, as provided in Table 7-2 [170]. In Case-F and Case-FF the heat load is applied as an energy source to the fluid inside the building (Watt per unit volume of fluid). In the other cases the heat loads are applied uniformly to the surfaces of the human bodies and appliances as a boundary conditions (Watt per unit area). In all scenarios, the wind speed was based on the reference at the height of the building (U_{ref}) with an angle of incidence of 0^{o}.

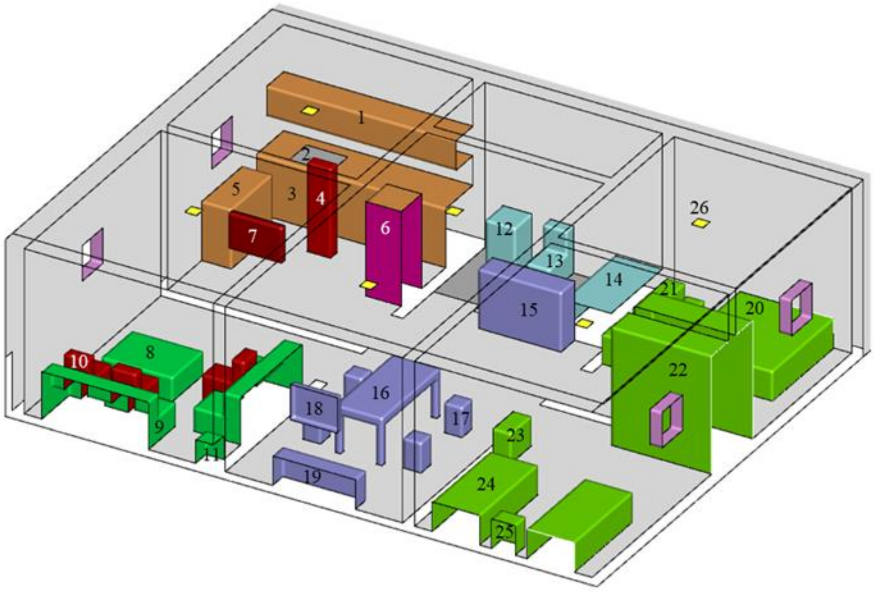

Figure 7-1: The layout of the furniture in the building.

Table 7-1: Dimensions of the furniture and the human bodies in meters.

	Size (*Length*×*Height* *Width*)		Size (*Length*×*Height* *Width*)		Size (*Length*×*Height* *Width*)
1	3.2×0.5×0.5	10	0.4×0.6×0.2 0.4×0.2×0.5 0.4×0.6×0.2	19	1.4×0.5×0.3
2	0.7×0.0×0.5	11	0.4×0.3×0.3	20	1.8×0.5×1.6
3	3.2×1.0×0.8	12	0.5×0.8×0.5	21	1.0×0.5×0.3
4	0.4×1.5×0.2	13	0.4×0.8×0.2 0.4×0.4×0.5	22	1.7×2.0×0.5
5	1.2×1.0×0.5	14	1.5×0.5×0.8	23	0.6×0.5×0.3
6	0.6×1.6×0.6	15	1.4×1.0×0.4	24	1.7×0.5×0.8
7	0.9×0.6×0.1	16	1.7×0.15×0.8 0.1×0.65×0.1	25	0.4×0.5×0.3
8	1.2×0.4×0.9	17	0.3×0.5×0.3	26	0.2×0.0×0.2
9	1.8×0.4×0.8 1.8×0.4×0.3	18	0.8×0.6×0.1		

Table 7-2: Heat loads of the study cases.

Cases	Interior load (W/m^3)	Lights (W/m^2)	Humans (W/m^2)	TV (W/m^2)	Refrigerator (W/m^2)	Oven (W/m^2)
Case-F	900	----	----	----	----	----
Case-FF	900	0.0	----	0.0	0.0	0.0
Case-F1	0.0	0.0	38.5	0.0	0.0	0.0
Case-F2	0.0	500	38.5	178	118	0.0
Case-F3	0.0	500	38.5	178	118	1142

7.3 CFD case study: setting and parameters

7.3.1 Computational domain and grid

The computational domain of all the cases (F, FF, F1, F2, and F3) had dimensions (25×5×12.6) H, as shown in Figure 7-2, and was constructed based on the guidelines of Franke et al. [22] and Tominaga et al. [153]. The building was set inside the duct and the blockage ratio was 4.2%, which was within the range recommended by the two guidelines to avoid any impact of blocking and unphysical flow acceleration. The two guidelines recommended at least 15H as the distance between the end of the building and the outflow boundary, which was sufficient to allow the flow to redevelop in the wake region whereas and 5H was considered sufficient for the distance between the beginning of the building and the inflow boundary as mentioned in the two guidelines. The numerical grid used in all cases consists of around 8×10^6 hexahedral computational cells except for Case-F, which was around 6.7×10^6 cells. A fine mesh structure was used near the walls, whereas a coarse mesh was used away from the walls in all directions, as shown in Figure 7-2. The minimum grid spacing used in each case was 0.005H in all directions to capture the laminar sub-layer. Figure 7-3 illustrates the mesh inside the building.

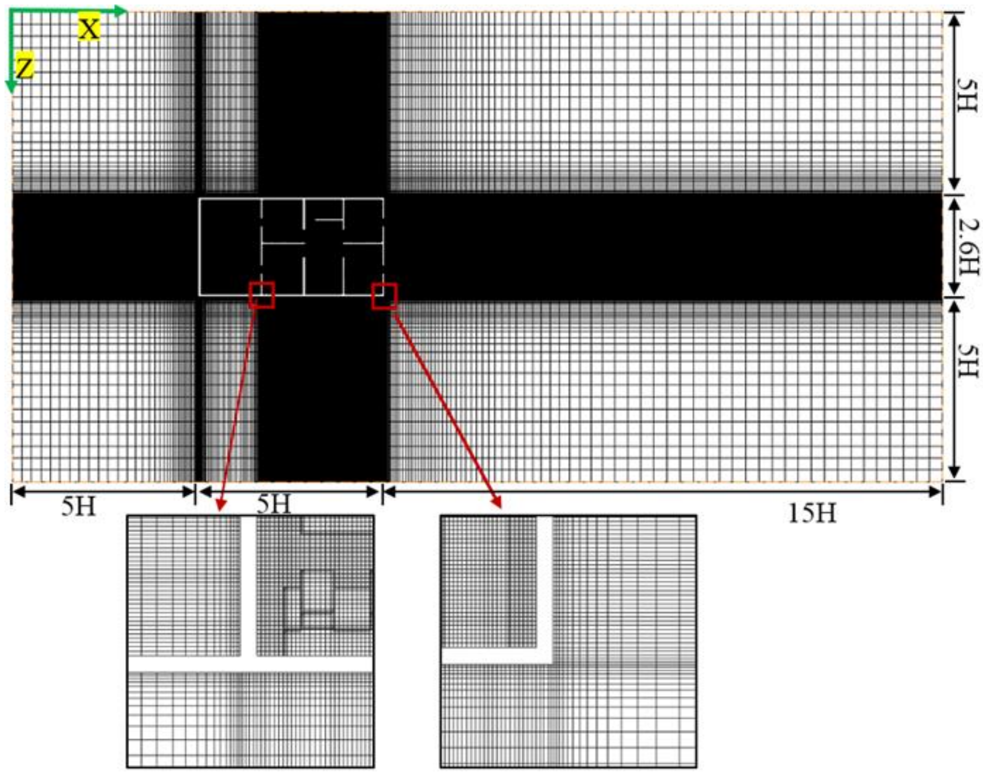

Figure 7-2: Computational domain and the mesh layout of the grid (Top view).

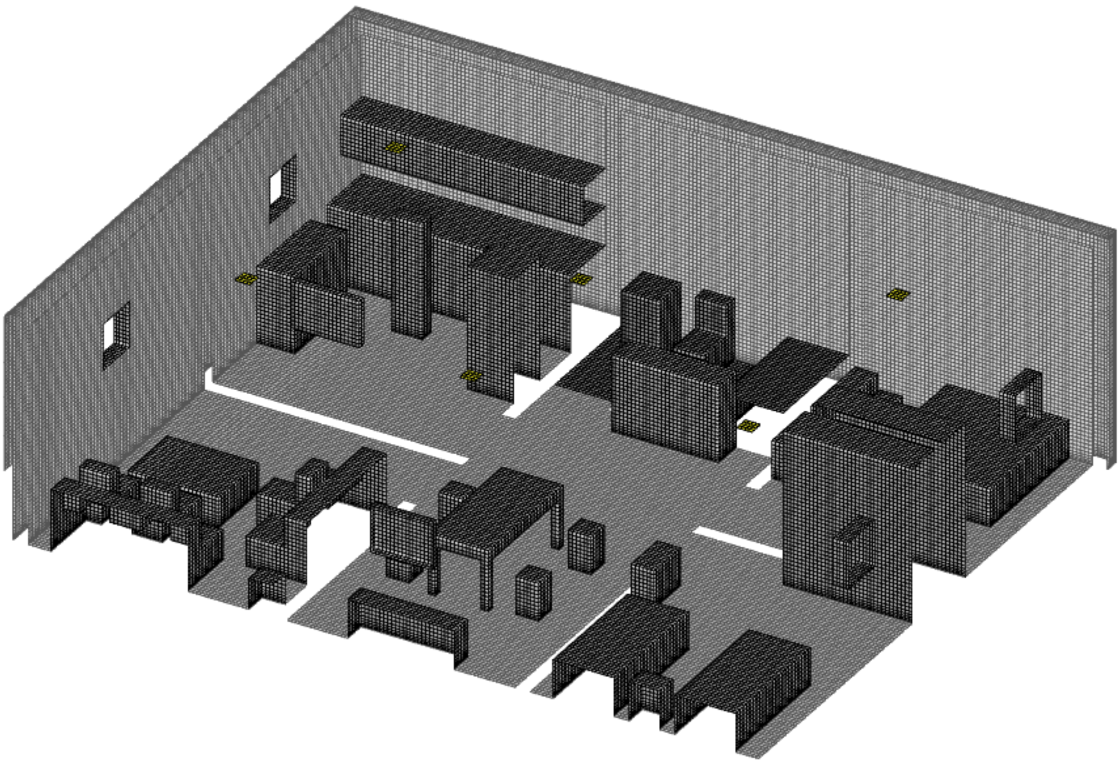

Figure 7-3: The mesh layout of the building with furniture.

7.3.2 Boundary conditions and solver settings

The vertical profiles of the mean wind velocity, turbulent kinetic energy and turbulent dissipation rate are imposed at the inlet of the domain (Eqs 4-3, 4-4 and 4-5) as described in chapter 4. The ground of the domain was modelled as having no-slip boundaries, whilst a slip boundary with zero shear (symmetry boundary conditions) was applied to the two sides and the top of the domain. The outflow boundary condition was specified at the end of the domain [149]. The surfaces of the house were modelled as no-slip boundaries and assumed to be under adiabatic conditions. The family house analysed was comprised of several electrical appliances and the number of occupants of an average family; their generated heat values are provided in Table 7-2 according to the reveal case. This generated heat was uniformly applied to the surface of the appliances and occupants as a boundary condition. A uniform temperature of 25°C was specified at the inlet of the duct as a boundary condition.

7.4 Results and discussion

The impact of heat loads and the presence of the furniture on the thermal comfort of an average family house in a hot climate are exemplified and subsequently discussed in this section via five scenarios (cases). The numerical results of all cases are presented and compared in terms of average velocity, temperature, PMV and PPD of two commonly used levels in assessing thermal comfort in residential buildings in order to provide helpful information for the effective design of buildings [171]. Furthermore, the contour plots of velocity, temperature and PMV are presented and discussed in detail. Investigating the impacts of heat loads and the presence of furniture on the human thermal comfort would give the designer valuable information in terms of obtaining more energy-efficient designs and naturally ventilated buildings, particularly in hot climates where natural ventilation is frequently used. The area of the openings in all cases was held constant, as was the wind incidence angle of 0º and the wind speed (3 m/s at 25ºC). The thermal comfort indices predicted for metabolic rates, M, were 58 W/m^2 (seated level), and 70 W/m^2 (standing level). The relative humidity (RH) was fixed at 30% with zero external work (W). The two commonly used levels were used in the current study; the seated level at a height of 0.6 m from the ground of the building [13] and the standing level at a height of 1.1 m from the ground of the building [10].

7.4.1 The effect of furniture on the thermal comfort

The effect of the furniture within the building is considered in this section. Two cases are compared; Case-F, without furniture and Case-FF, with furniture, at U_{ref} f 3 m/s and temperature of 25°C. The average velocity, temperature and thermal comfort indices are compared and discussed in detail at both common levels; seated and standing (Figure 7-4 and 7-5). The contour plots of the velocity and temperature at the seated plane, and PMV distribution of the seated and standing planes are presented in Figure 7-6 and 7-7.

The results showed that the impact of the current arrangement of the furniture (Figure 7-1) on the thermal comfort indices was actually small at both the standing and the seated levels. At the seated level, the presence of the furniture slightly increased the average velocity along the plane and this impact does not result in any noticeable change in temperature or thermal comfort indices. Since the velocity increased in the front rooms (A and B) whilst decreased in the rest of the rooms.

Regarding the seated level, the greatest increases in PPD was in room A and B, where an increase of 3% was observed, whilst other rooms saw a constant of PPD. The figure illustrating the thermal comfort indices (Figure 7-4) showed that there were small differences between the two cases as a result of adding furniture to the building. The same trend was observed for the standing level, where the average velocity of the front rooms increased slightly but less than the seated level and did not result in any noticeable change in PMV or PPD due to the standing level higher than the seated level, and thus less affected by the volume of the furniture. Overall, no significant differences between the empty building (Case-F) and the furniture building (Case-FF) were observed in the comparison of the thermal comfort indices (PMV and PPD).

The contour plots for the velocity, temperature and PMV did not show remarkable differences in distributing of these variables at the standing level because most of the volume of the furniture itself was located at levels lower than the specified level, so clearly one would not expect any particularly significant impact on the streamlines of the flow. However, the seated level contours showed some differences between the two cases especially, in rooms C, D and E where the low-velocity zones (coloured blue) increased behind the internal walls and increasing the area of high-temperature zone but generally did not result in any significant change in temperature and PMV contours. It can be concluded that the presence of the furniture in this arrangement needs not be included in any engineering calculations during the design of the natural cross-ventilation system for this type of the building. Whereas for the pattern of the flow, temperature and thermal comfort distribution should be considered and choosing a proper place to avoid changing the direction of the flow.

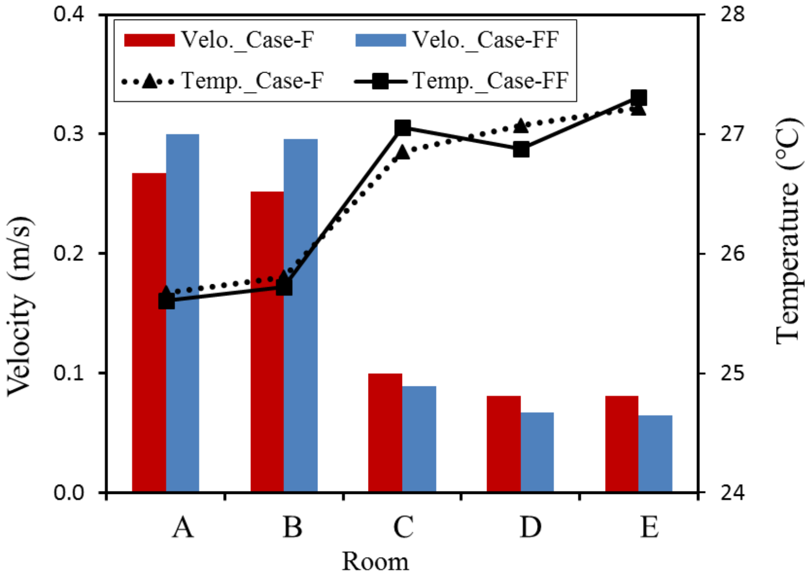

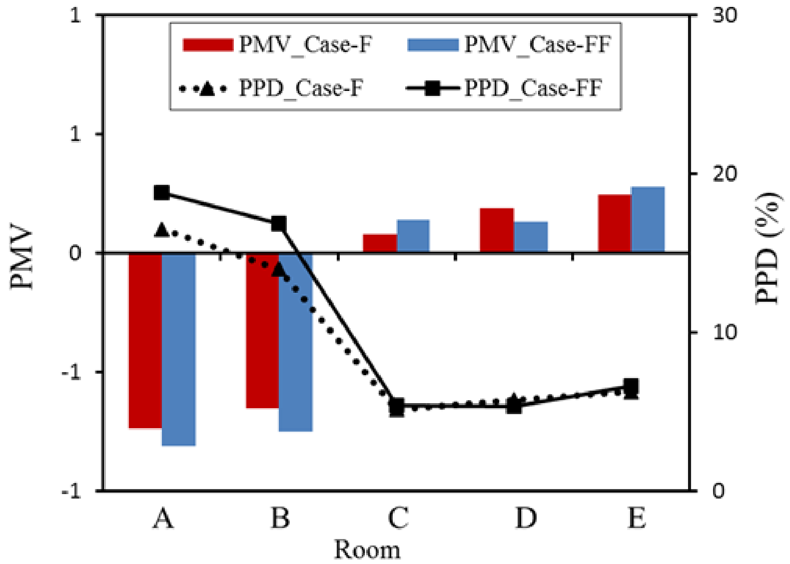

Figure 7-4: The room average velocity, temperature, PMV and PPD in the seated plane for Case-F and Case-FF.

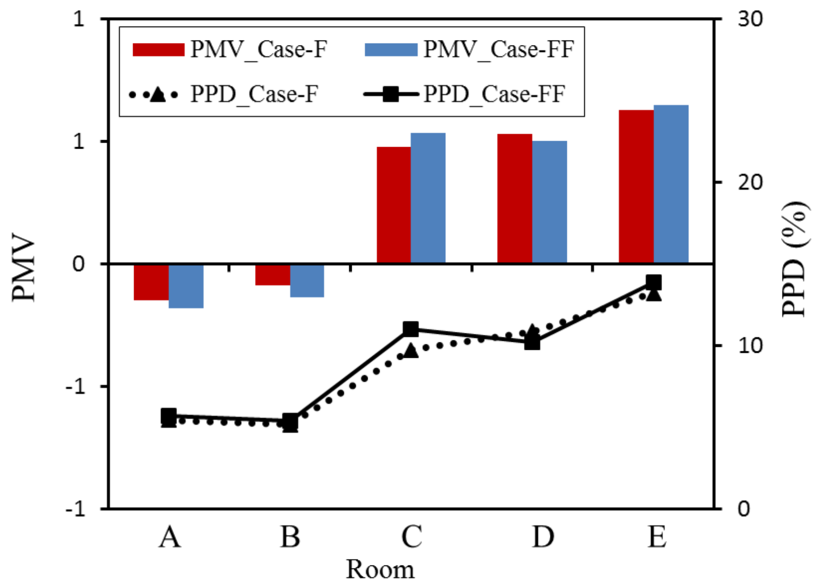

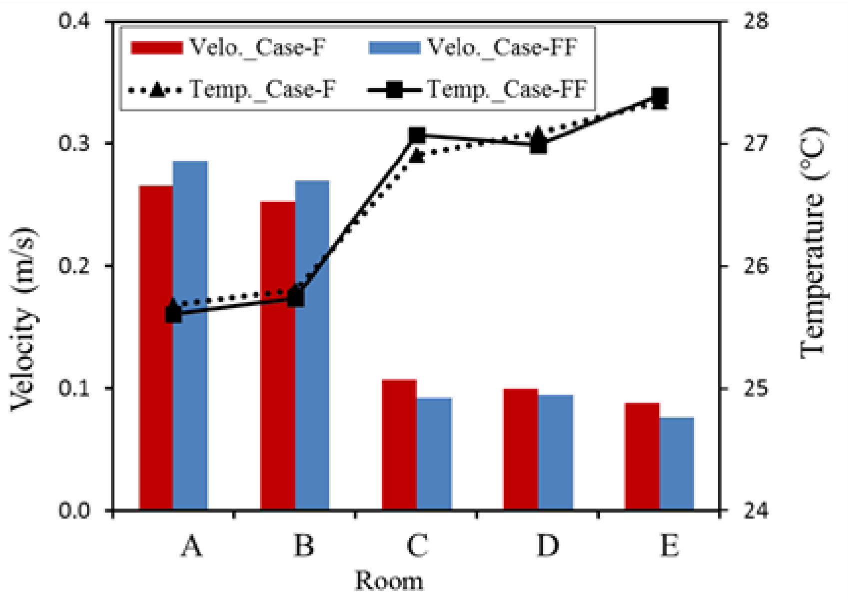

Figure7-5: The room average velocity, temperature, PMV and PPD in the standing plane for Case-F and Case-FF.

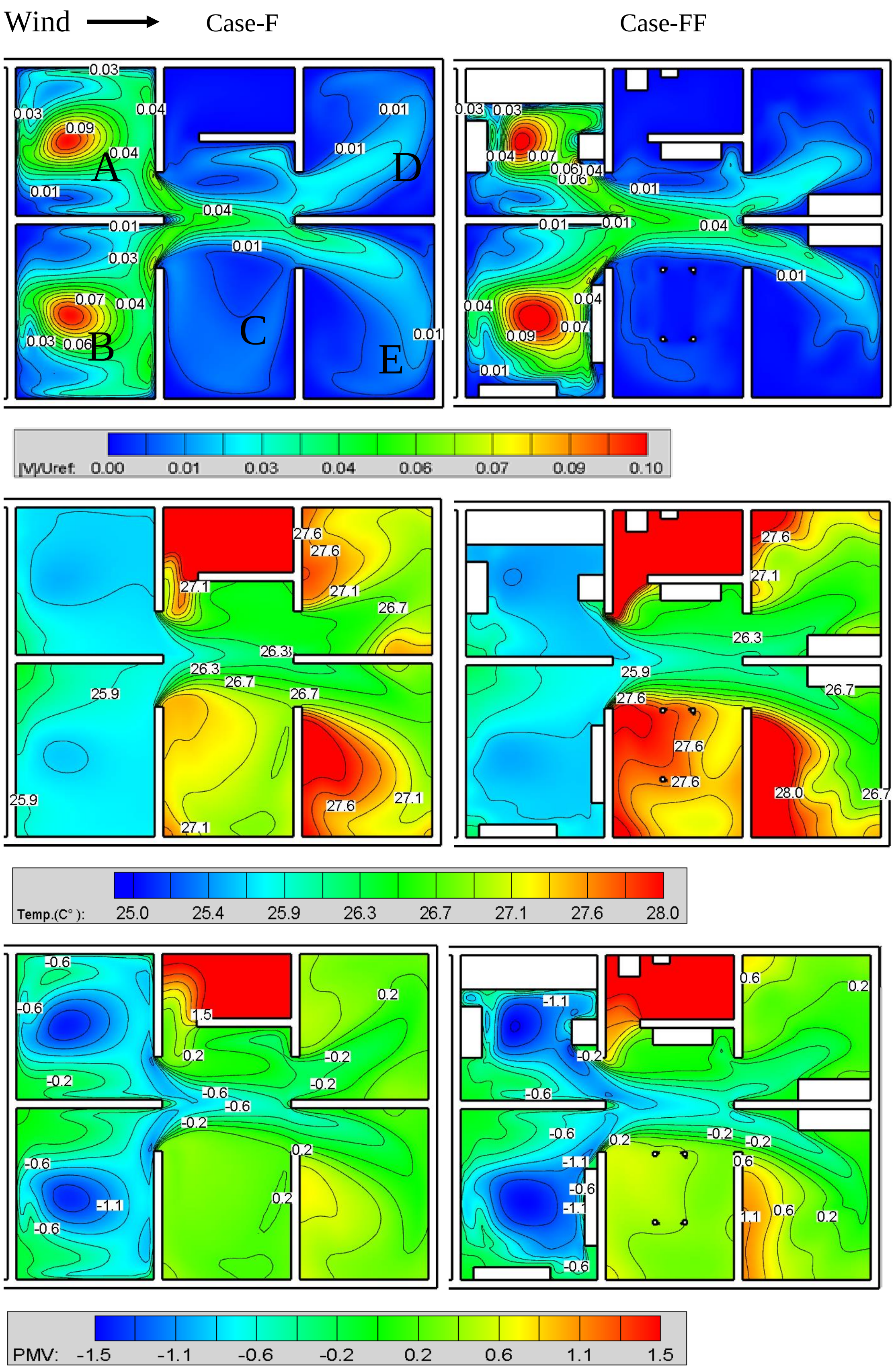

Figure 7-6: Contours of dimensionless velocity magnitude ($|V|/U_{ref}$), temperature and PMV in the seated plane.

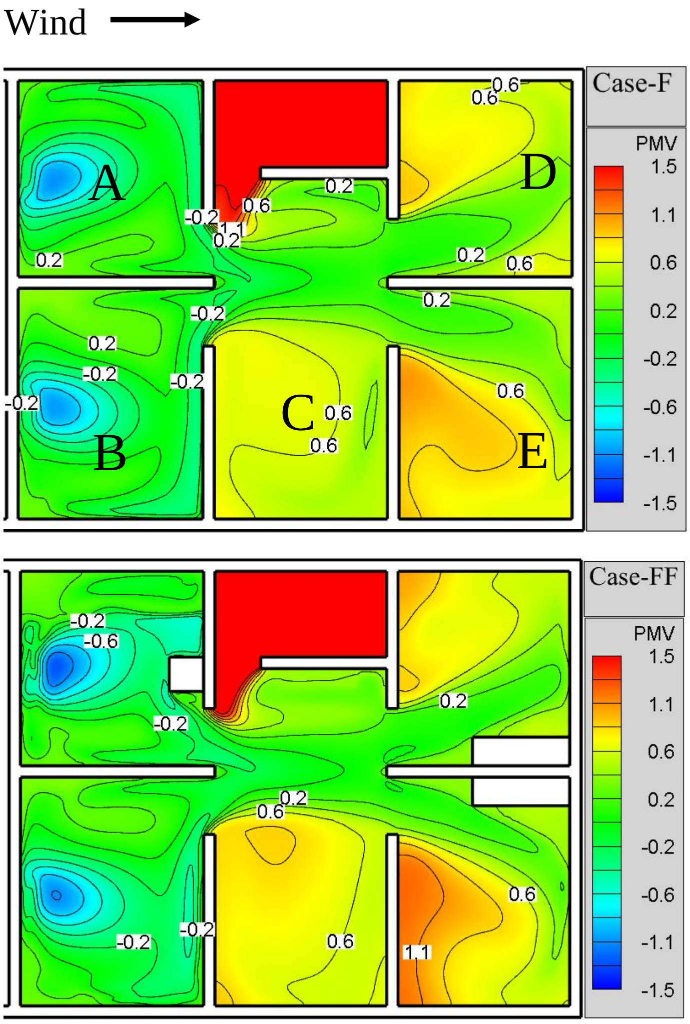

Figure 7-7: PMV contours in the standing plane for Case-F and Case-FF.

7.4.2 The Effect of heat loads on the thermal comfort

The impact of the heat loads on the thermal comfort of the building is studied in this section. Various heat loads are modelled to analyse their impacts on the temperature distribution and the thermal comfort indices in the building. Three cases are modelled with different heat loads, and the amount of the heat loads of these cases are provided in Table 7-2. The heat sources from the human bodies are kept constant for the three cases at 38 W/m^2. The furnished house with heat loads from appliances of a daily life Case-F2 under a range of wind temperature 20-30°C has been examined to obtain the active temperature for the rest of the study. As shown in Figure 7-8, the results showed that at wind temperature of 26°C the seated plane would be in a neutral thermal comfort and PPD was around 5% whilst for the standing plane, the neutral thermal condition was at temperature of 25°C, therefore the temperature 25.5 °C has been selected as an average of both levels of the rest of the study.

The average temperature, PMV and PPD of all rooms of the building are presented and compared in Figure 7-9 and Figure 7-10 in terms of the seated and the standing levels. In addition, temperature contours and distribution of PMV at the seated and the standing planes are provided in Figure 7-11 and Figure 7-12.

7.4.2.1 **Case-F1 versus Case-F2**

As shown in Figure 7-9 and Figure 7-10, the average temperatures in the seated and the standing planes were increased for all rooms (Case-F2) by around 0.5°C when adding heat loads to the building (Case-F1). Therefore, the PMV in both planes are slightly increased, and especially so in the seated plane where the thermal comfort approached to the neutral condition with PPD around 7%. The increase in PMV in both planes was around 0.2 only, therefore, it can be concluded that the electrical appliances typical to daily life (TV, lights, and refrigerator) have only a small effect on the thermal comfort indices due to their use of only small amounts of energy compared to other appliances such as ovens or cookers. Regarding the contour plots in Figure 7-11 and Figure 7-12 and, the temperature contour for Case-F1 and Case-F2 are different, where higher temperatures at the standing level were noticed in front of the TV and on both sides of the refrigerator due to heat dissipation. The seated level, however, showed lower influence for heat dissipation from the TV because the TV level was above the seated plane. The ambient air enters the building, is heated, moves directly to the leeward rooms through room C and dissipates its heat within these rooms. Thus, the PMV thermal comfort index increases in these rooms.

7.4.2.2 **Case-F1 versus Case-F3**

In Case-F3, an additional heat source (oven) was added to the other heat sources within the building for Case-2 to predict the change in the temperature and the thermal indices of the rooms when all these loads are present at the same time (Table 7-2). The average temperature of Case-F3 saw an increase of around 1.1°C in the seated plane and 1.4°C in the standing plane, as shown in Figure 7-9 and Figure 7-10. The greatest increase in temperature was at the standing level and was 3.5°C, as seen in room A, increasing the PMV and PPD to around 1.0 and 26%, respectively, whereas the smallest increase occurred in room B and was around 0.4°C because the room location is parallel to room A and it is not affected by the latter's flow. The results of the simulation predicted that the PMV would change markedly along both levels when the additional heat source (oven) was operated at the same time as the other appliances, at 0.5 for the standing level and 0.4 for the seated plane.

7.4.2.3 **Case-F2 versus Case-F3**

To determine the impact of the heat dissipated from the oven on the thermal comfort indices and the temperature distribution of the building, additional heat loads (1142 W/m^2) were added to Case-F2 (Table 7-2). By adding a new heat source to the building in room A (Case-F3), more heat was dissipated from the oven in this room and resulting in an increase in temperature, especially in the standing plane, of around 3^{o}C (Figure 7-9 and Figure 7-10). The seated plane in this room, however, was less influenced by adding the heat source, due to this plane being located at lower the heat source level, such that the majority of the heat dissipated upwards towards the standing plane. As discussed in the previous section, the results of the Case-F3 model showed that the presence of the heat source in room A did not change the thermal comfort level of room B. Regarding room D, although the flow circulated inside room C, results showed that the heat dissipated from room A had more influence on room D than room E, and the heat exiting room B had more influence on room E than room D because the rooms A and D were located on one side of the building and the rooms B and E on the other.

The temperature contours in Figure 7-13 and Figure 7-14 showed high temperature distribution in room A in both planes (Case-F2) because of the additional heat source (oven) in this room. Furthermore, the temperature distribution at the standing level is higher than for the seated level because the heat source (oven) was located near the standing plane, and thus most of the heat dissipated upwards into the standing level. Due to higher velocity magnitude in the incoming jet of the airflow inside rooms A, and B, low-temperature zones were formed inside these regions, resulting in a decrease in PMV as shown in Figure 7-13 and Figure 7-14.The horizontal locations of these zones were smaller and nearer to the openings in the standing plane than the seated plane. The PMV values at the centres of these rooms were lower than -1.0 in the standing and seated planes and were thus expected to be thermally uncomfortable zones when the outside temperature is lower than 25°C.

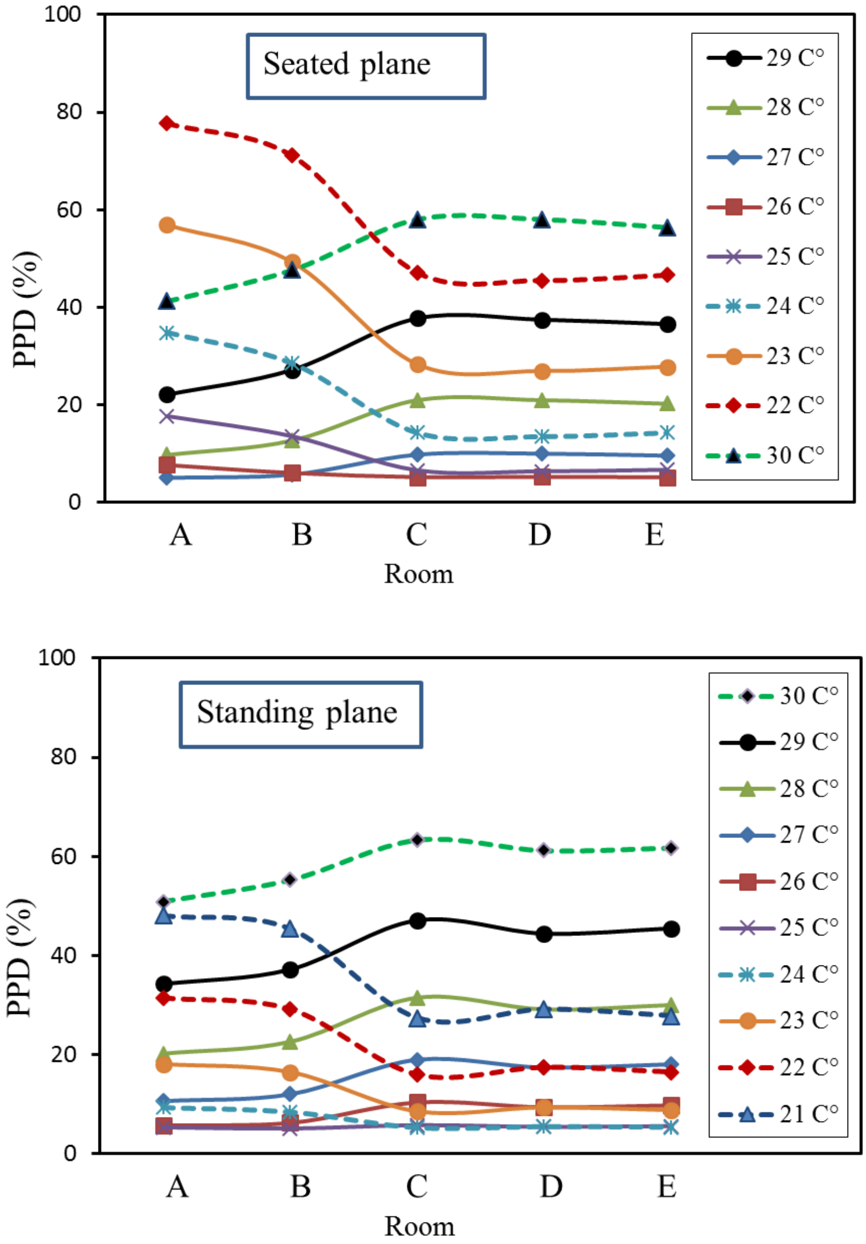

Figure 7-8: The room average PPD in the seated and the standing planes for Case-F2 at different wind temperature.

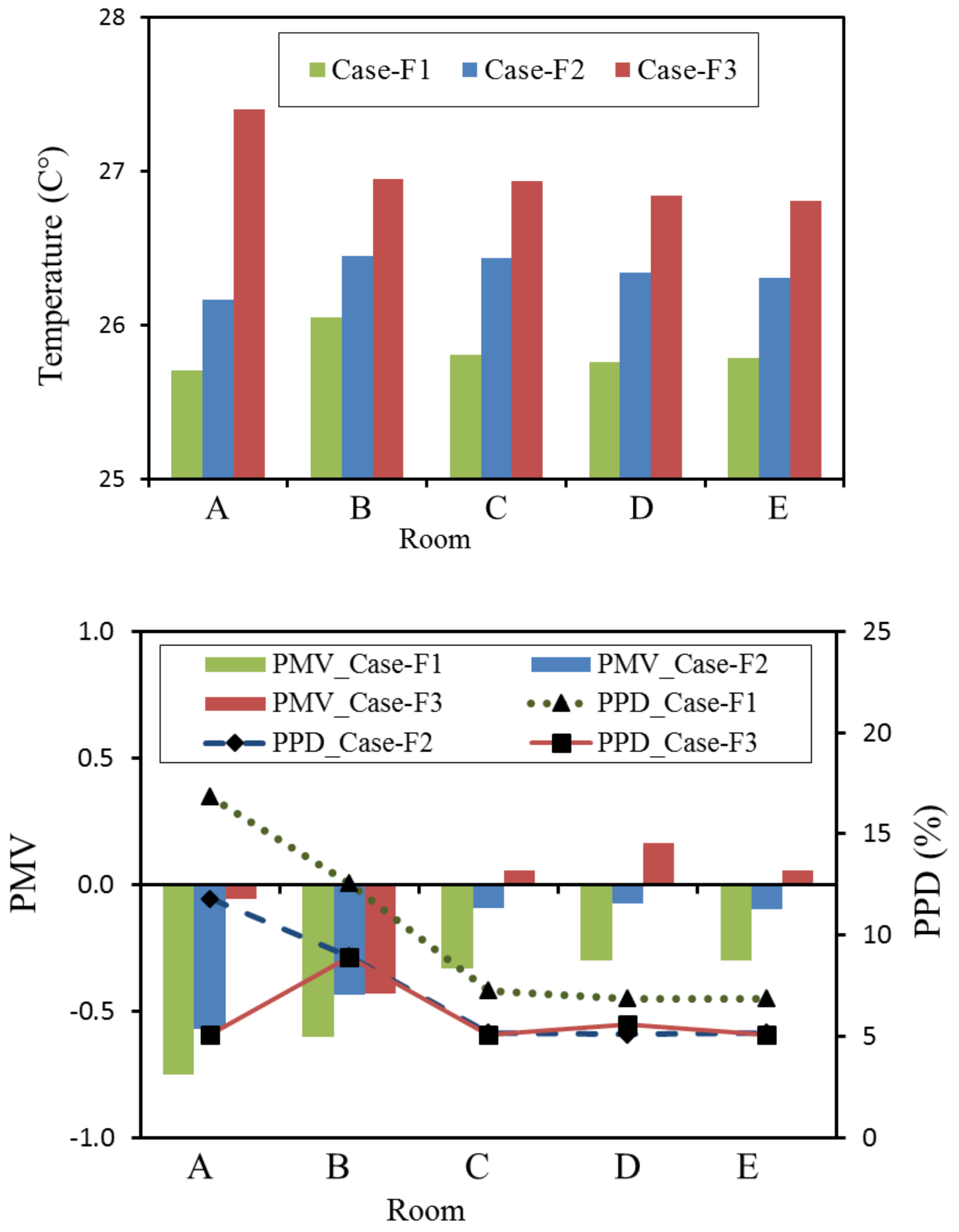

Figure 7-9: The room average temperature, PMV and PPD in the seated plane for Case-F1, Case-F2 and Case-F3.

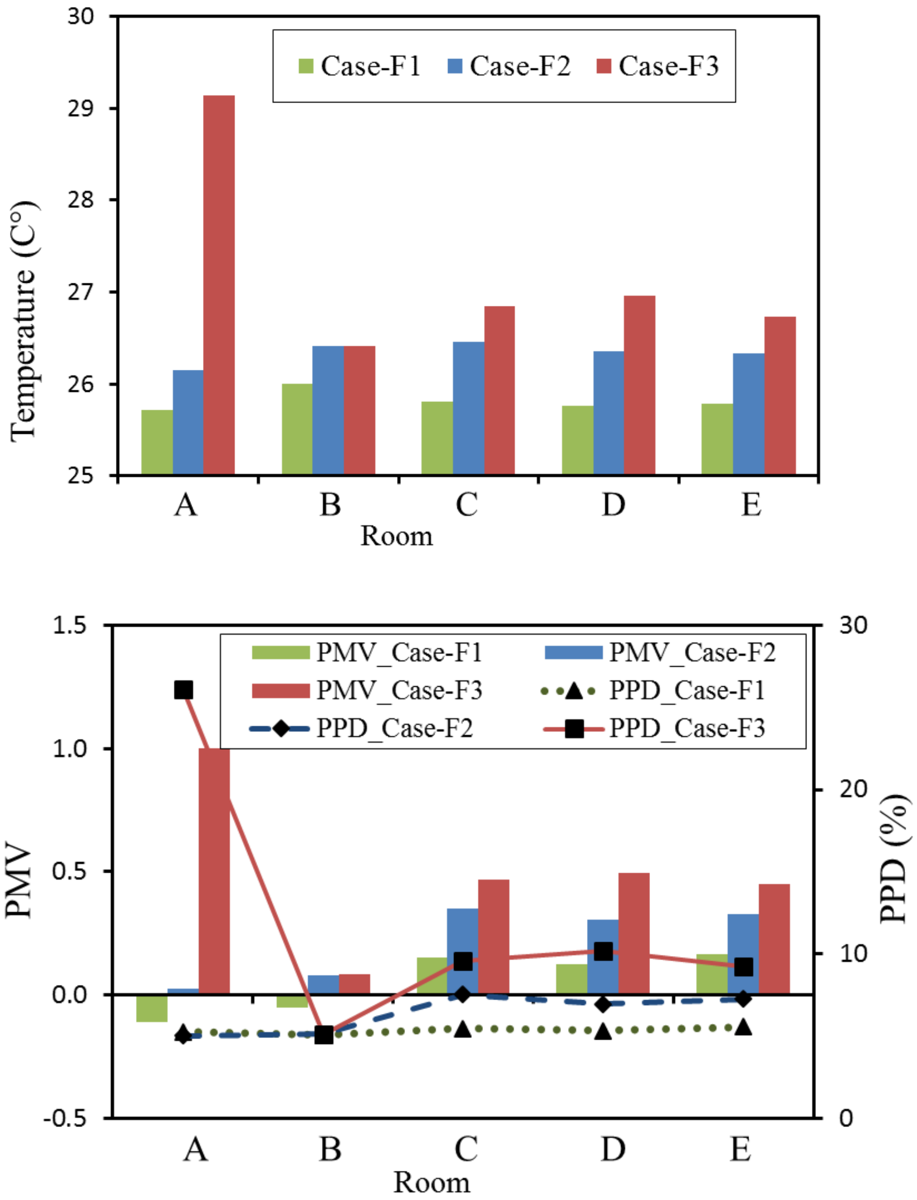

Figure 7-10: The room average temperature, PMV and PPD in the standing plane for Case-F1, Case-F2 and Case-F3.

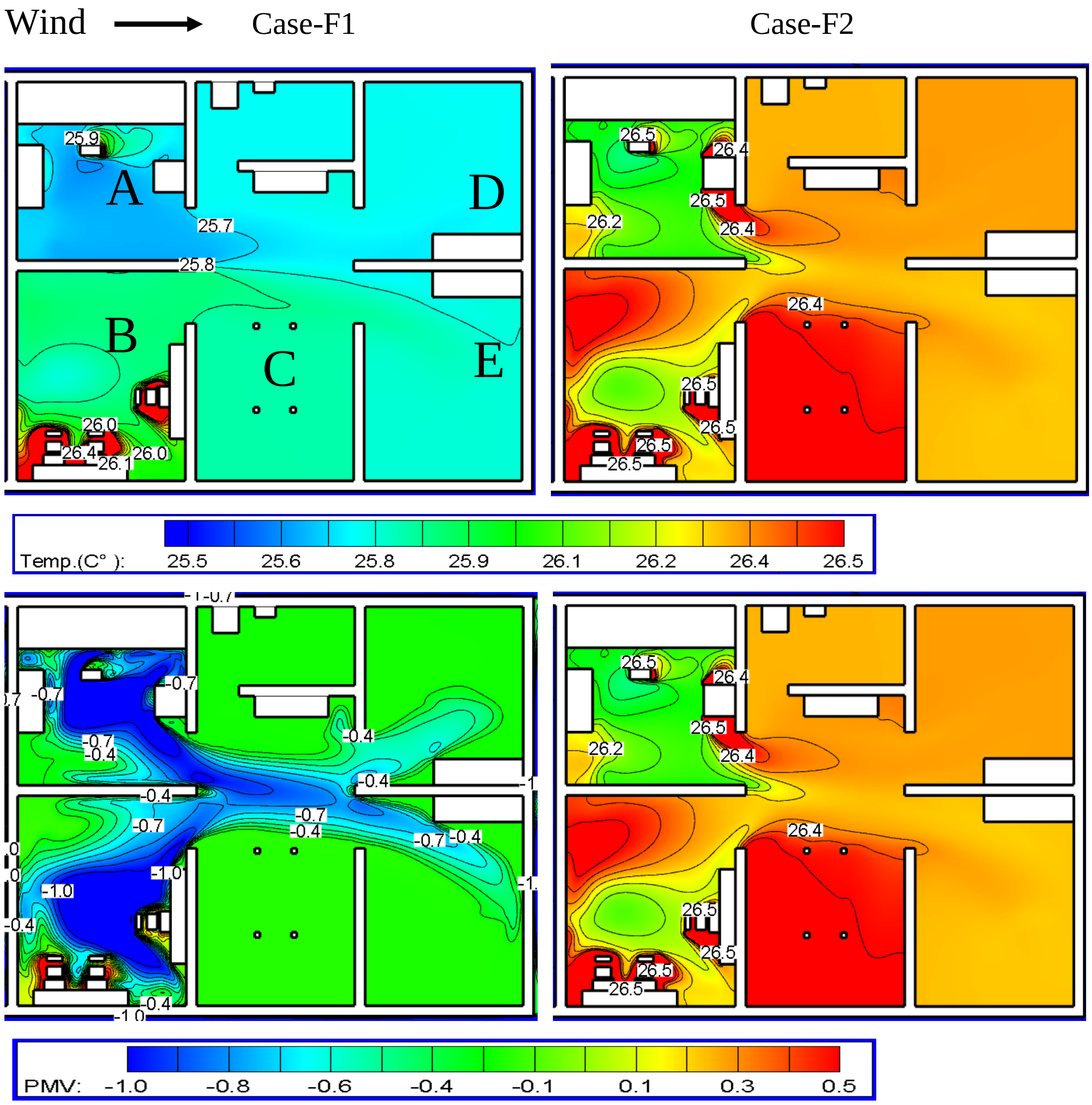

Figure 7-11: Temperature and PMV contours in the seated plane for Case-F1 and Case-F2.

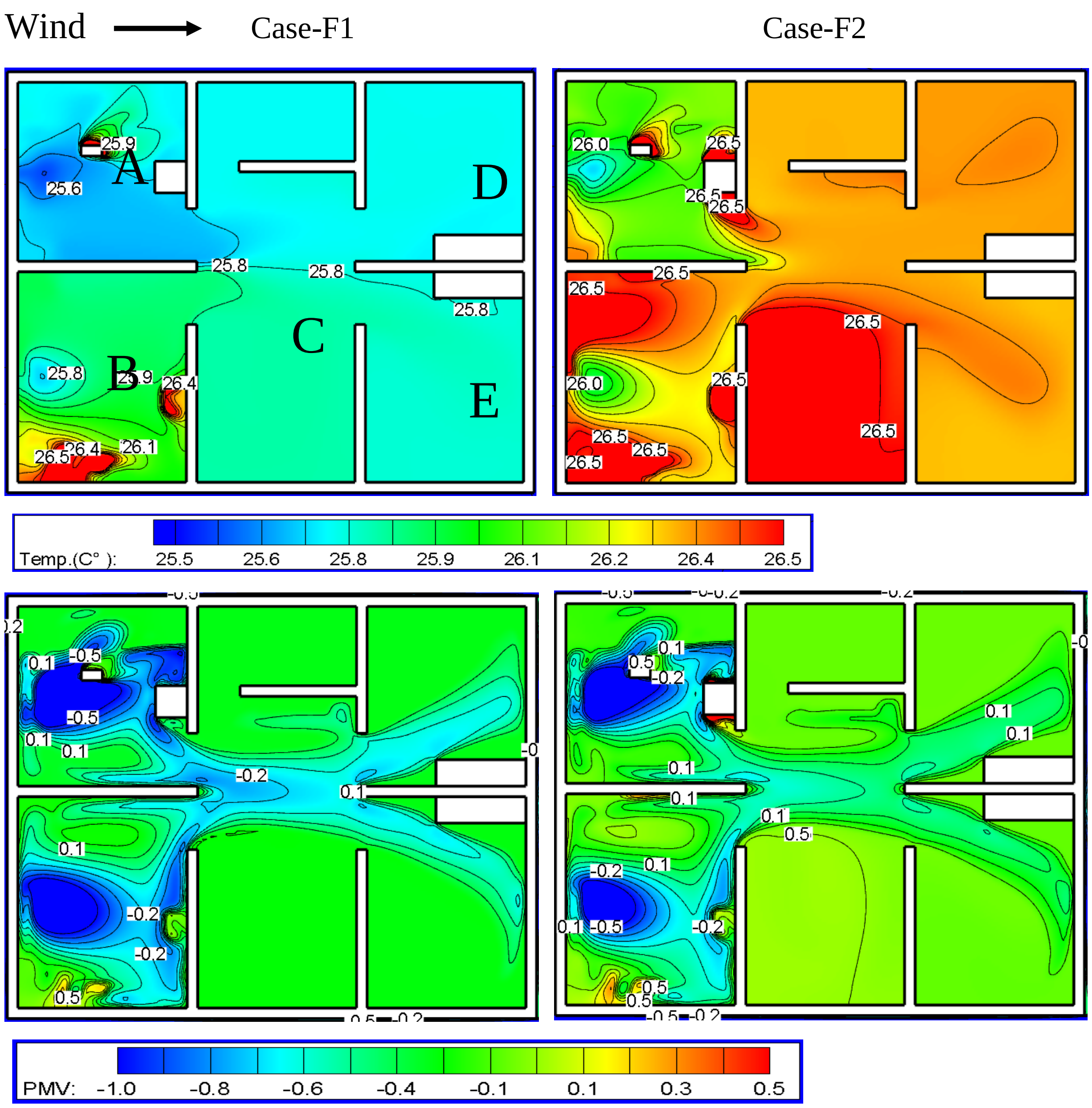

Figure 7-12: Temperature and PMV contours in the standing plane for Case-F1 and Case-F2.

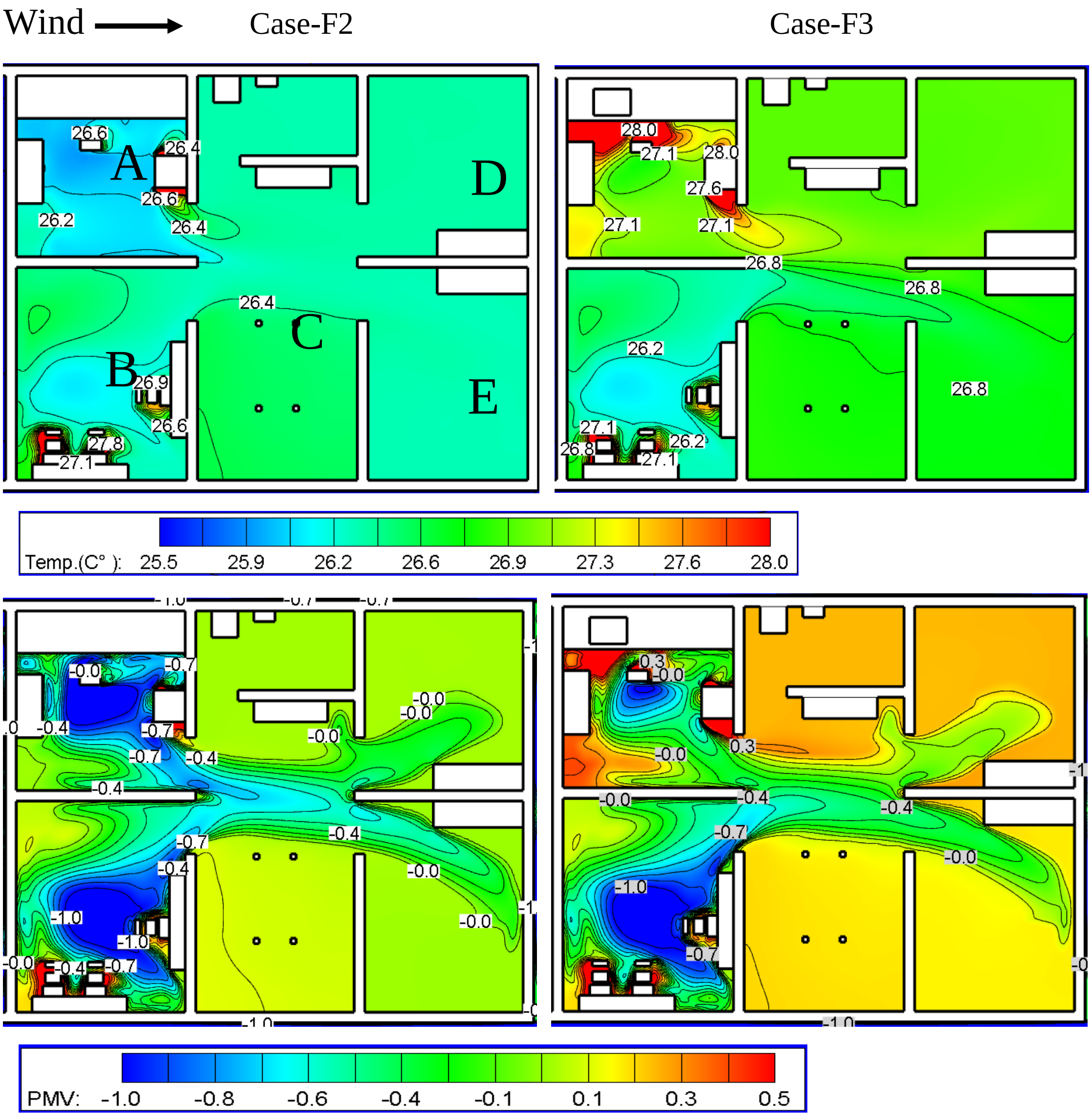

Figure 7-13: Temperature and PMV contours in the seated plane for Case-F2 and Case-F3.

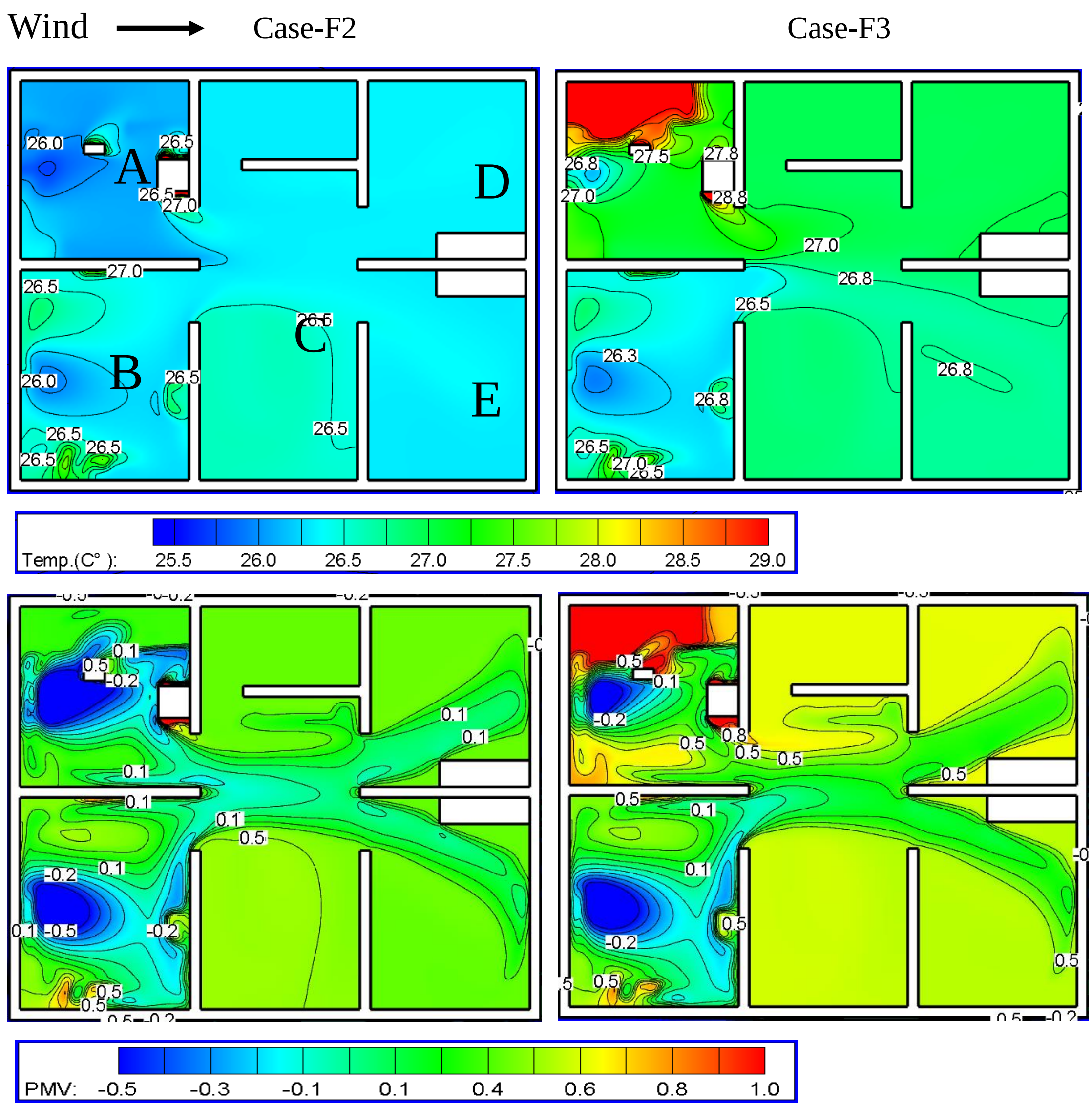

Figure 7-14: Temperature and PMV contours in the stand plane for Case-F2 and Case-F3.

7.4.2.4 **Seated level versus standing level**

The comparison between the seated level and the standing level for Case-F2 are presented in terms of the average velocity, temperature, PMV and PPD (Figure 7-15). Furthermore, contour plots for the velocity, temperature and PMV are presented in Figure 7-16. The differences in the averages velocity between the seated and standing levels were small for all rooms and were not a result of the difference in temperature. The noticed difference was in room A around 5% and resulting in a very small change in temperature. Although the differences in temperature between the two planes for all rooms were effectively non-existent because of the small differences in the average velocities; the PMV and PPD at the standing level were higher than for the seated level by 0.4-0.5 because of the higher assumed the metabolic rate in the standing plane than the seated plane. Generally, the PMV averages in the seated and standing planes for all rooms were found to be near to neutral conditions and the PPD for the rooms was around 6%, implying that about 94% of the occupants would probably not find the thermal conditions uncomfortable.

Although no obvious difference between the standing level and the seating level in terms of the velocity and temperature, the PMV plots showed clear differences between the two levels because of the higher assumed the metabolic rate in the standing plane than the seated plane as mentioned previously.

Regarding rooms A and B, the differences between the levels were clear, and at the standing level the discomfort zones (coloured blue) were small whilst at the seated level were large and cover most of the plane space. Therefore, it can be concluded that the room thermally is more comfort for the standing activity than the seated and room A can suitable for the kitchen whilst room B needs improvement to achieve desirable conditions for occupants if it was chosen for sitting. The improvement in room A can be done by adding louvre to the window to change the direction of the flow towards the door of the room. Moreover, the contour plots showed that the heat dissipated from the sources of the front rooms towards the other rooms, increasing the temperature and PMV of these rooms noticeably and the standing plane showed more affected by the dissipation heat.

In general, it can be concluded that the PMV plot is an appropriate way to illustrate the heat dissipation from the heat sources, find its path distribution and find comfortable or uncomfortable areas inside the rooms of the building. The contour plot showed the places where it would be more comfortable for any occupants to perform their daily activities.

To achieve the desired level of human thermal comfort, it will be necessary to control the influence of the wind, e.g. through an appropriate arrangement of ventilation openings.

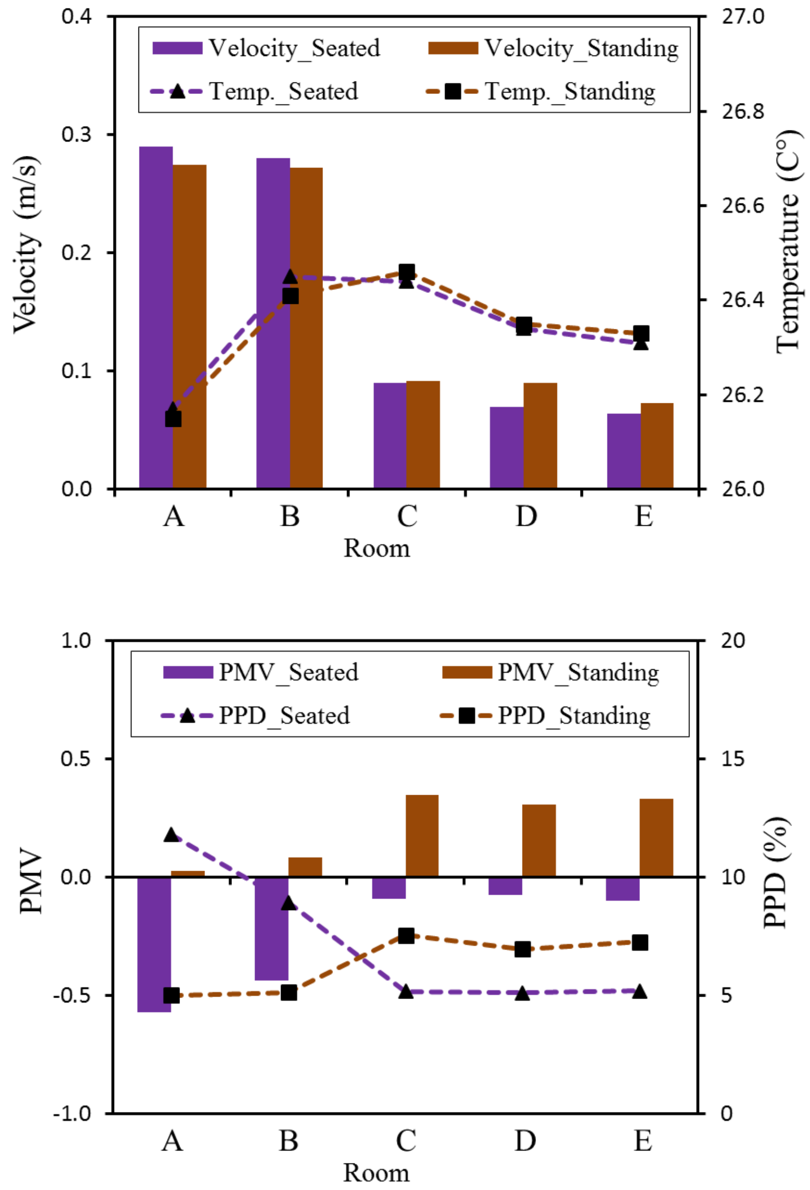

Figure 7-15: The room average velocity, temperature, PMV and PPD in the seated and the standing planes.

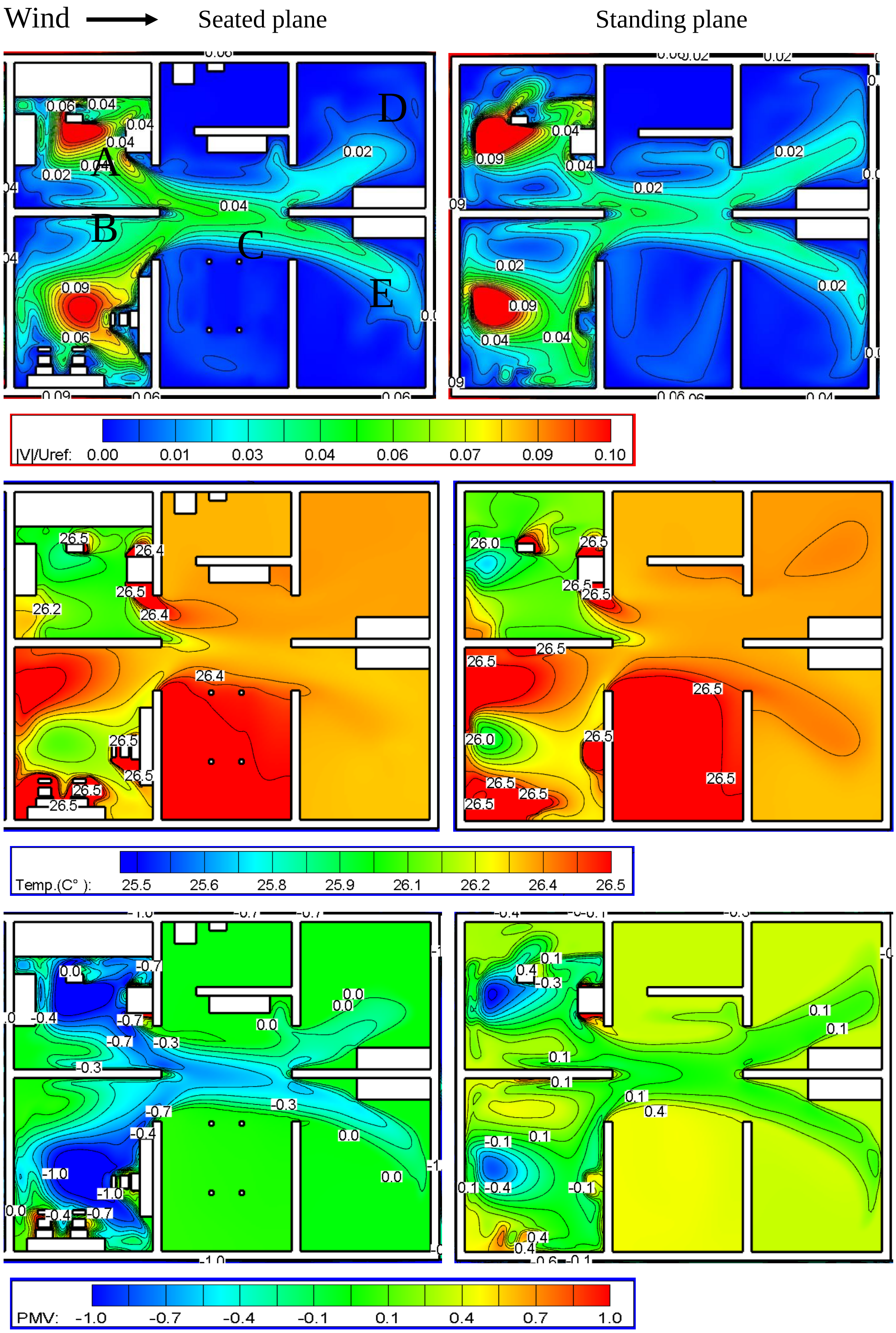

Figure 7-16: Contours of dimensionless velocity magnitude ($|V|/U_{ref}$), temperature and PMV in the seated plane and the standing plane.

7.5 Conclusion

This study has examined the changes in the human thermal comfort in terms of the PMV and PPD values inside an average residential building in Iraq with heat loads being applied via the RANS model. In summary, the following conclusions were reached:

- No significant differences between the empty building (Case-F) and the furniture-filled building (Case-FF) have been noted when comparing the air velocity, temperature and indoor thermal comfort indices (PMV and PPD).
- The study has demonstrated that common electrical appliances used in daily life (TV, lights, and refrigerator) have very little effect on the human thermal comfort indices due to them using only small amounts of energy compared with other appliances such as ovens or cookers.
- In the current study, PMV is found increasing markedly at the seated and standing levels by around 0.4 and 0.5, respectively, when an additional heat source (e.g. oven) was used with the other appliances.
- The PMV averages in the seated and standing planes for all rooms were found to be near to neutral conditions at wind speed 3 m/s and temperature 25°C, and the PPD for the rooms was around 6%, implying that about 94% of the occupants would probably not find the thermal conditions uncomfortable.
- The study has also shown that the PMV contour plot is an appropriate way to show the heat being dissipated from the various heat sources, to find its path distribution and to find the comfortable or uncomfortable areas inside each room of the building.

Chapter 8 Conclusion and Future Work

8.1 Conclusion

This research has focused on the potential to use natural cross-ventilation during the spring and autumn seasons in an average family house to provide an acceptable thermal comfort by using CFD analyses. By predicting the thermal comfort of the natural cross-ventilation implemented in the building, valuable guidance for future refurbishment projects could be identified. Moreover, if natural ventilation delivers the occupants' thermal comfort expectations, there is a potential to carry out this on a large-scale for a significant energy consumption reduction. The limitations of this study and suggestions for future works are also presented in this chapter after providing the main conclusions of all objectives of the study.

8.1.1 Impact of windward inlet opening positions on fluctuation characteristics of wind-driven natural cross-ventilation

Natural cross-ventilation in a small-scale building exposed to outdoor conditions was investigated numerically using CFD analysis. Openings were shown to be an important design factor in terms of its effect on the airstream pattern inside a building. The numerical approach used in such studies gives the architect the best view of the natural mechanisms of ventilation in a building by providing further insight into the induced flow-field inside and around it, with information that would not otherwise be produced by experimental methods. The study concluded that the rate of fluctuations of the flow rate through the inlet openings depends on the position of the openings. In Case-II, where the openings were near the side wall, this rate was 33%, whereas in Case-I was around 22% when the openings were in the middle of the front wall. The flow rates of openings located near the centre of the building were steadier and higher than the flow rates of openings located near the sides of the building. In agreement with earlier studies [35], the indoor air flow pattern changes when the positions of the inlet openings are changed, which also changes the direction of circulation inside a room from clockwise to anticlockwise or from horizontal to vertical circulation.

8.1.2 Impact of an external boundary wall on indoor flow field and natural cross-ventilation

The study has examined the impact of an external boundary wall on the indoor ventilation performance of the building using the CFD analysis. The analysis of the three proposed cases included the average mean velocity, streamline distribution, and turbulent kinetic energy on the working plane of the CFD models exposed to the turbulent streams. The study confirmed, in agreement with previous studies, that the type and placement of the external elements can affect indoor air flow rates and patterns. The boundary wall caused a reduction in the ventilation rate by around 48% in Case-EF and 67% in Case-EFH compared with the basic case without the wall. On the other hand, adding the boundary wall to the building can provide uniform distribution of the indoor mean velocity, and subsequently enhancing the indoor environment for occupants in terms of indoor airflow velocity. Finally, increasing the height of boundary wall by around 20% did not produce noticeable improvement in the indoor mean velocity distribution.

8.1.3 Thermal comfort evaluation under a naturally ventilated environment

This study has also investigated the changes in human thermal comfort in terms of PMV and PPD inside an average family house in Iraq when the opening position, outdoor wind speed and wind temperature were changed via the steady RANS method. Investigating indoor thermal comfort in a multi-zone building could give designers valuable information regarding more energy-efficient designs in naturally ventilated buildings. The study finds that the three horizontal opening positions have only a slight impact on the level of the thermal comfort indices in both the seated and the standing planes. The study concludes that the cross ventilation can provide acceptable thermal comfort for this type of building when the wind speeds are between 2 and 5 m/s at the temperature of 25°C, despite there being a number of locations inside the house that are still higher than the acceptable PMV range. Moreover, the range of wind temperature conditions under which all the rooms in the house can be maintained within an acceptable thermal comfort range for the seated levels is between 22-28 °C and for the standing planes is between 20-28 °C with an external wind speed of 3 m/s.

8.1.4 Effect of heat loads and furniture on thermal comfort under a naturally ventilated environment

The study has examined the changes in the human thermal comfort in terms of the PMV and PPD values inside an average family house in Iraq with furniture and heat loads and being applied via the RANS model and the following conclusions were obtained: No significant differences between the empty building (Case-F) and the furniture-filled building (Case-FF) have been noted when comparing the air velocity, temperature and indoor thermal comfort indices (PMV and PPD).The study has demonstrated that common electrical appliances used in daily life (TV, lights, and refrigerator) have a very little effect on the human thermal comfort indices due to them using only small amounts of energy compared with other appliances such as ovens or cookers. Whereas the PMV is found increasing markedly at the seated and standing levels by around 0.4 and 0.5, respectively, when an additional heat source (e.g. oven) was used with the other appliances. In addition, the PMV averages in the seated and standing planes for all rooms were found to be near to neutral conditions at wind speed 3 m/s and temperature 25°C, and the PPD for the rooms was around 6%, implying that about 94% of the occupants would probably not find the thermal conditions uncomfortable. Lastly, the study has also shown that the PMV contour plot is an appropriate way to show the heat being dissipated from the various heat sources, to find its path distribution and to find the comfortable or uncomfortable areas inside each room of the building.

8.2 Future work

The main goal of this study on wind-driven cross ventilation is to evaluate the thermal comfort indices of an average family house in a hot climate in Iraq. Although different parameters have been tested and analysed in the study such as horizontal opening position, wind speed and temperature, head loads, and furniture, it is important to note a number of limitations in this work, which should be considered in any future research:

- An isolated building was used in this study, so future work should focus on buildings surrounded by other buildings, and areas of greenery. Inside the building, only one configuration was used for all cases.
- The study neglected the wind direction, which plays an important role on the air change rate of a building, and further the wind direction was normal to the front ($\theta = 0°$) of the building; so different wind angles should be used in further research, especially $\theta = 30°, 90°$ and $45°$.
- A simplistic outer form of the building was used whilst other configurations, such as shape and height of the roof, length and shape of the eaves or overhang, were ignored.
- The simulations in this study were performed for a building with adiabatic walls, whilst future work should focus on non-adiabatic walls to study the effect of heat transfer through the walls of the building.
- It should be noted that the results of this study are based on the simulation data predicted by the CFD package and for more improvement the results can be validated with measurements from the building.
- The solar radiation through the window is not included in the CFD model, which might affect the simulations of indoor air temperature to some extent and further study is required to quantify this effect.
- Further study during other seasons is needed in order to obtain a complete set of recommendations for the thermal comfort during the whole year.

Appendices

Appendix 1 Publication List

Journal Papers

- Hawendi S, Gao S. Impact of an external boundary wall on indoor flow field and natural cross-ventilation in an isolated family house using numerical simulations. Journal of Building Engineering. 2017; 10:109-23.
- Hawendi S, Gao S. Impact of windward inlet-opening positions on fluctuation characteristics of wind-driven natural cross ventilation in an isolated house using LES. International Journal of Ventilation. 2017:1-27.
- Hawendi S, Gao S. Thermal comfort evaluation of an isolated family house under a naturally ventilated environment in a hot climate. “Under review”
- Hawendi S, Gao S. Effect of heat loads and furniture on the thermal comfort of an isolated family house under a naturally ventilated environment. “Under review”

Conference Papers

- Hawendi S, Gao S. Investigation of Opening Positions on the Natural Ventilation in a Low-Rise Building by CFD Analysis. Proceedings of the 3rd International Conference on Fluid Flow, Heat and Mass Transfer (FFHMT'16, Paper No151). Ottawa, Canada 2016.
- Hawendi S, Gao S. Numerical investigation of thermal comfort in an isolated family house under natural cross-ventilation. Energy and Sustainability VII. 2017; 224:159.

References

[1] Spentzou E. Refurbishment of apartment buildings in the Mediterranean Region for natural ventilation: implications for building design: © Eftychia Spentzou; 2015.

[2] Santamouris M, Asimakopoulos D. Passive cooling of buildings: James & James London;; 1996.

[3] Databook BE. US Department of Energy and annual energy review 2007. DOE/EIA-0384 (2007). Energy Information Administration, US Department of Energy; 2008.

[4] da Graça GC, Linden P. Ten questions about natural ventilation of non-domestic buildings. Building and Environment. 2016;107:263-73.

[5] Larsen TS, Heiselberg P. Single-sided natural ventilation driven by wind pressure and temperature difference. Energy and Buildings. 2008;40:1031-40.

[6] Amos-Abanyie S, Koranteng C, Apeatse K. AN EVALUATION OF THE EFFECTS OF EXTERNAL LANDSCAPING ELEMENTS ON INDOOR AIRFLOW RATE AND PATTERNS USING COMPUTATIONAL FLUID DYNAMICS. European Scientific Journal. 2014;10.

[7] Chu C-R, Chiang B-F. Wind-driven cross ventilation in long buildings. Building and Environment. 2014;80:150-8.

[8] Larsen TS. Natural ventilation driven by wind and temperature difference: Aalborg Universitet, Denmark.; 2006.

[9] KAMORU SA. EFFECT OF BUILDING DESIGN FOR NATURAL VENTILATION ON THE COMFORT OF BUILDING OCCUPANTS IN SOUTH–WESTERN NIGERIA: THE POLYTECHNIC IBADAN, NIGERIA; 2010.

[10] ISO P. 7730 Ergonomics of the thermal environment. Analytical determination and interpretation of thermal comfort using calculation of the PMV and PPD indices and local thermal comfort criteria. 2005; London:British Standards Institution, p.10.

[11] Al-Awainati N, Fahkroo MI, Musharavati F, Pokharel S, Gabbar HA. Evaluation of thermal comfort and cooling performance of residential buildings in arid climates. Smart Energy Grid Engineering (SEGE), 2013 IEEE International Conference on: IEEE; 2013. p. 1-6.

[12] Asfour OS. EFFECT OF BUILDING PLAN FORM ON HUMAN THERMAL COMFORT IN NATURALLY VENTILATED OPEN-PLAN ENCLOSURES LOCATED IN HOT CLIMATES. Journal of Green Building. 2017;12:112-29.

[13] ASHRAE AS. Standard 55-2013. Thermal Environmental Conditions for Human Occupancy. 2013.

[14] Allocca C, Chen Q, Glicksman LR. Design analysis of single-sided natural ventilation. Energy and buildings. 2003;35:785-95.

[15] Coleman HW, Stern F. Uncertainties and CFD code validation. Journal of Fluids Engineering. 1997;119:795-803.

[16] Casey M, Wintergerste T. Quality and Trust in Industrial CFD: Best Practice Guidelines, ERCOFTAC. 2000.

[17] Alexander D, Jenkins H, Jones P. A comparison of wind tunnel and CFD methods applied to natural ventilation design. Proceedings of Building Simulation1997. p. 321-6.

[18] Mora L, Gadgil A, Wurtz E. Comparing zonal and CFD model predictions of isothermal indoor airflows to experimental data. Indoor air. 2003;13:77-85.

[19] Hawendi S, Gao S. Impact of windward inlet-opening positions on fluctuation characteristics of wind-driven natural cross ventilation in an isolated house using LES. International Journal of Ventilation. 2017:1-27.

[20] Kim D. The Application of CFD to Building analysis and Design: A Combined Approach of An Immersive Case Study and Wind Tunnel Testing: Virginia Tech; 2014.

[21] Stavrakakis G, Zervas P, Sarimveis H, Markatos N. Optimization of window-openings design for thermal comfort in naturally ventilated buildings. Applied Mathematical Modelling. 2012;36:193-211.

[22] Franke J, Hellsten A, Schlunzen KH, Carissimo B. The COST 732 Best Practice Guideline for CFD simulation of flows in the urban environment: a summary. International Journal of Environment and Pollution. 2011;44:419-27.

[23] FLUENT User's Guide, November 2013.

[24] Najmaddin PM, Whelan MJ, Balzter H. Application of Satellite-Based Precipitation Estimates to Rainfall-Runoff Modelling in a Data-Scarce Semi-Arid Catchment. Climate. 2017;5:32.

[25] Rasul A, Balzter H, Smith C. Diurnal and seasonal variation of surface urban cool and heat islands in the semi-arid city of Erbil, Iraq. Climate. 2016;4:42.

[26] Peel MC, Finlayson BL, McMahon TA. Updated world map of the Köppen-Geiger climate classification. Hydrology and earth system sciences discussions. 2007;4:439-73.

[27] Hawendi S, Gao S. Investigation of Opening Positions on the Natural Ventilation in a Low-Rise Building by CFD Analysis. Proceedings of the 3rd International Conference on Fluid Flow, Heat and Mass Transfer (FFHMT'16, Paper No151). Ottawa, Canada 2016.

[28] Kato S, Murakami S, Mochida A, Akabayashi S-i, Tominaga Y. Velocity-pressure field of cross ventilation with open windows analyzed by wind tunnel and numerical simulation. Journal of Wind Engineering and Industrial Aerodynamics. 1992;44:2575-86.

[29] Ernest D, Bauman F, Arens E. The effects of external wind pressure distributions on wind-induced air motion inside buildings. Journal of Wind Engineering and Industrial Aerodynamics. 1992;44:2539-50.

[30] Kindangen J, Krauss G, Depecker P. Effects of roof shapes on wind-induced air motion inside buildings. Building and Environment. 1997;32:1-11.

[31] Elmualim AA, Awbi HB. Wind tunnel and CFD investigation of the performance of "Windcatcher" ventilation systems. International Journal of ventilation. 2002;1:53-64.

[32] Evola G, Popov V. Computational analysis of wind driven natural ventilation in buildings. Energy and buildings. 2006;38:491-501.

[33] Tominaga Y, Blocken B. Wind tunnel analysis of flow and dispersion in cross-ventilated isolated buildings: impact of opening positions. Journal of Wind Engineering and Industrial Aerodynamics. 2016;155:74-88.

[34] Ohba M, Goto T, Kurabuchi T, Endo T, Akamine Y. Experimental study on predicting wind-driven cross-ventilation flow rates and discharge coefficients based on the local dynamic similarity model. International Journal of Ventilation. 2006;5:105-14.

[35] Karava P, Stathopoulos T, Athienitis A. Airflow assessment in cross-ventilated buildings with operable façade elements. Building and Environment. 2011;46:266-79.

[36] Straw M, Baker C, Robertson A. Experimental measurements and computations of the wind-induced ventilation of a cubic structure. Journal of Wind Engineering and Industrial Aerodynamics. 2000;88:213-30.

[37] Yang T. CFD and field testing of a naturally ventilated full-scale building: University of Nottingham, The United Kingdom; 2004.

[38] Stavrakakis G, Koukou M, Vrachopoulos MG, Markatos N. Natural cross-ventilation in buildings: Building-scale experiments, numerical simulation and thermal comfort evaluation. Energy and Buildings. 2008;40:1666-81.

[39] Ramponi R, Blocken B. CFD simulation of cross-ventilation flow for different isolated building configurations: validation with wind tunnel measurements and analysis of physical and numerical diffusion effects. Journal of Wind Engineering and Industrial Aerodynamics. 2012;104:408-18.

[40] Perén J, van Hooff T, Leite B, Blocken B. Impact of eaves on cross-ventilation of a generic isolated leeward sawtooth roof building: Windward eaves, leeward eaves and eaves inclination. Building and Environment. 2015;92:578-90.

[41] Perén JI, van Hooff T, Leite B, Blocken B. CFD simulation of wind-driven upward cross ventilation and its enhancement in long buildings: Impact of single-span versus double-span leeward sawtooth roof and opening ratio. Building and Environment. 2016;96:142-56.

[42] Perén J, Van Hooff T, Leite B, Blocken B. CFD analysis of cross-ventilation of a generic isolated building with asymmetric opening positions: impact of roof angle and opening location. Building and Environment. 2015;85:263-76.

[43] Derakhshan S, Shaker A. Numerical study of the cross-ventilation of an isolated building with different opening aspect ratios and locations for various wind directions. International Journal of Ventilation. 2017;16:42-60.

[44] Kurabuchi T, Ohba M, Endo T, Akamine Y, Nakayama F. Local dynamic similarity model of cross-ventilation part 1-theoretical framework. International Journal of Ventilation. 2004;2:371-82.

[45] Ohba M, Kurabuchi T, Tomoyuki E, Akamine Y, Kamata M, Kurahashi A. Local Dynamic Similarity Model of Cross-Ventilation Part 2-Application of Local Dynamic Similarity Model. International Journal of Ventilation. 2004;2:383-94.

[46] Jiang Y, Chen Q. Study of natural ventilation in buildings by large eddy simulation. Journal of Wind engineering and industrial aerodynamics. 2001;89:1155-78.

[47] Jiang Y, Chen Q. Effect of fluctuating wind direction on cross natural ventilation in buildings from large eddy simulation. Building and Environment. 2002;37:379-86.

[48] Jiang Y, Alexander D, Jenkins H, Arthur R, Chen Q. Natural ventilation in buildings: measurement in a wind tunnel and numerical simulation with large-eddy simulation. Journal of Wind Engineering and Industrial Aerodynamics. 2003;91:331-53.

[49] Hu C-H, Ohba M, Yoshie R. CFD modelling of unsteady cross ventilation flows using LES. Journal of Wind Engineering and Industrial Aerodynamics. 2008;96:1692-706.

[50] Lund TS, Wu X, Squires KD. Generation of turbulent inflow data for spatially-developing boundary layer simulations. Journal of Computational Physics. 1998;140:233-58.

[51] Chu C-R, Chiang B-F. Wind-driven cross ventilation with internal obstacles. Energy and Buildings. 2013;67:201-9.

[52] Tuan L, Razak AA, Zaki S, Mohammad A, Hassan M. Large eddy simulation of natural ventilation for idealized terrace houses due to the effect of setback distance. IOP Conference Series: Materials Science and Engineering. Selangor, Malaysia: IOP Publishing; 2015. p. 012009.

[53] van Hooff T, Blocken B, Tominaga Y. On the accuracy of CFD simulations of cross-ventilation flows for a generic isolated building: comparison of RANS, LES and experiments. Building and Environment. 2017;114:148-65.

[54] Murakami S. Wind tunnel test on velocity-pressure field of cross-ventilation with open windows. ASHRAE transactions. 1991;97:525-38.

[55] Li Y, Delsante A. Natural ventilation induced by combined wind and thermal forces. Building and Environment. 2001;36:59-71.

[56] Jiang Y, Su M, Chen Q. Using large eddy simulation to study airflows in and around buildings. ASHRAE Transactions. 2003;109:517-26.

[57] Heiselberg P, Li Y, Andersen A, Bjerre M, Chen Z. Experimental and CFD evidence of multiple solutions in a naturally ventilated building. Indoor Air. 2004;14:43-54.

[58] Karava P, Stathopoulos T, Athienitis A. Wind driven flow through openings–a review of discharge coefficients. International journal of ventilation. 2004;3:255-66.

[59] Sawachi T, Ken-ichi N, Kiyota N, Seto H, Nishizawa S, Ishikawa Y. Wind pressure and air flow in a full-scale building model under cross ventilation. International Journal of Ventilation. 2004;2:343-57.

[60] Etheridge D. Natural ventilation through large openings-measurements at model scale and envelope flow theory. International journal of ventilation. 2004;2:325-42.

[61] Wright NG, Hargreaves DM. Unsteady CFD simulations for natural ventilation. International Journal of Ventilation. 2006;5:13-20.

[62] Kotani H, Yamanaka T. Flow visualization and inflow direction measurement at a cross-ventilated large opening. International Journal of Ventilation. 2006;5:79-87.

[63] Livermore SR, Woods AW. Natural ventilation of a building with heating at multiple levels. Building and Environment. 2007;42:1417-30.

[64] Karava P, Stathopoulos T, Athienitis AK. Wind-induced natural ventilation analysis. Solar Energy. 2007;81:20-30.

[65] Fitzgerald SD, Woods AW. The influence of stacks on flow patterns and stratification associated with natural ventilation. Building and Environment. 2008;43:1719-33.

[66] Horan JM, Finn DP. Sensitivity of air change rates in a naturally ventilated atrium space subject to variations in external wind speed and direction. Energy and Buildings. 2008;40:1577-85.

[67] Visagavel K, Srinivasan P. Analysis of single side ventilated and cross ventilated rooms by varying the width of the window opening using CFD. Solar Energy. 2009;83:2-5.

[68] Meroney RN. CFD prediction of airflow in buildings for natural ventilation. Proceedings of the Eleventh Americas Conference on Wind Engineering, Puerto Rico2009.

[69] Chu CR, Chiu Y-H, Wang Y-W. An experimental study of wind-driven cross ventilation in partitioned buildings. Energy and Buildings. 2010;42:667-73.

[70] Bu Z, Kato S, Takahashi T. Wind tunnel experiments on wind-induced natural ventilation rate in residential basements with areaway space. Building and Environment. 2010;45:2263-72.

[71] Nikas K-S, Nikolopoulos N, Nikolopoulos A. Numerical study of a naturally cross-ventilated building. Energy and Buildings. 2010;42:422-34.

[72] Kurabuchi T, Ohba M, Nonaka T. Domain decomposition technique applied to the evaluation of cross-ventilation performance of opening positions of a building. International Journal of Ventilation. 2009;8:207-17.

[73] Ji L, Tan H, Kato S, Bu Z, Takahashi T. Wind tunnel investigation on influence of fluctuating wind direction on cross natural ventilation. Building and Environment. 2011;46:2490-9.

[74] Bangalee M, Lin S, Miau J. Wind driven natural ventilation through multiple windows of a building: A computational approach. Energy and Buildings. 2012;45:317-25.

[75] Karava P, Stathopoulos T. Wind-induced internal pressures in buildings with large façade openings. Journal of Engineering Mechanics. 2011;138:358-70.

[76] Lo LJ, Novoselac A. Effect of indoor buoyancy flow on wind-driven cross ventilation. Building Simulation: Springer; 2013. p. 69-79.

[77] Martins NR, da Graça GC. Validation of numerical simulation tools for wind-driven natural ventilation design. Building Simulation: Springer; 2016. p. 75-87.

[78] Tong Z, Chen Y, Malkawi A, Adamkiewicz G, Spengler JD. Quantifying the impact of traffic-related air pollution on the indoor air quality of a naturally ventilated building. Environment international. 2016;89:138-46.

[79] Castillo J, Huelsz G. A methodology to evaluate the indoor natural ventilation in hot climates: Heat Balance Index. Building and Environment. 2017;114:366-73.

[80] Montazeri H, Azizian R. Experimental study on natural ventilation performance of one-sided wind catcher. Building and Environment. 2008;43:2193-202.

[81] Montazeri H. Experimental and numerical study on natural ventilation performance of various multi-opening wind catchers. Building and Environment. 2011;46:370-8.

[82] Montazeri H, Montazeri F, Azizian R, Mostafavi S. Two-sided wind catcher performance evaluation using experimental, numerical and analytical modeling. Renewable Energy. 2010;35:1424-35.

[83] Ghadiri MH, Lukman N, Ibrahim N, Mohamed MF. Computational analysis of wind-driven natural ventilation in a two sided rectangular wind catcher. International Journal of Ventilation. 2013;12:51-62.

[84] Aydin YC, Mirzaei PA. Wind-driven ventilation improvement with plan typology alteration: A CFD case study of traditional Turkish architecture. Building Simulation: Springer; 2017. p. 239-54.

[85] Montazeri H, Montazeri F. CFD simulation of cross-ventilation in buildings using rooftop wind-catchers: impact of outlet openings. Renewable Energy. 2017.

[86] Blocken B, van Hooff T, Aanen L, Bronsema B. Computational analysis of the performance of a venturi-shaped roof for natural ventilation: venturi-effect versus wind-blocking effect. Computers & Fluids. 2011;48:202-13.

[87] van Hooff T, Blocken B, Aanen L, Bronsema B. Numerical analysis of the performance of a venturi-shaped roof for natural ventilation: influence of building width. Journal of Wind Engineering and Industrial Aerodynamics. 2012;104:419-27.

[88] Kobayashi T, Chikamoto T, Osada K. Evaluation of ventilation performance of monitor roof in residential area based on simplified estimation and CFD analysis. Building and Environment. 2013;63:20-30.

[89] Mak C, Niu J, Lee C, Chan K. A numerical simulation of wing walls using computational fluid dynamics. Energy and Buildings. 2007;39:995-1002.

[90] Prajongsan P, Sharples S. Enhancing natural ventilation, thermal comfort and energy savings in high-rise residential buildings in Bangkok through the use of ventilation shafts. Building and Environment. 2012;50:104-13.

[91] Yang A-S, Wen C-Y, Juan Y-H, Su Y-M, Wu J-H. Using the central ventilation shaft design within public buildings for natural aeration enhancement. Applied thermal engineering. 2014;70:219-30.

[92] Mukhtar A, Ng KC, Yusoff MZ. Optimal Design of Opening Ventilation Shaft by Kriging Metamodel Assisted Multi-objective Genetic Algorithm. International Journal of Modeling and Optimization. 2017;7:92.

[93] Ai Z, Mak C, Niu J, Li Z, Zhou Q. The effect of balconies on ventilation performance of low-rise buildings. Indoor and Built Environment. 2011;20:649-60.

[94] Ai Z, Mak C, Niu J, Li Z. The assessment of the performance of balconies using computational fluid dynamics. Building Services Engineering Research and Technology. 2011;32:229-43.

[95] Montazeri H, Blocken B. CFD simulation of wind-induced pressure coefficients on buildings with and without balconies: validation and sensitivity analysis. Building and Environment. 2013;60:137-49.

[96] Mohamed MF, King S, Behnia M, Prasad D. The effects of balconies on the natural ventilation performance of cross-ventilated high-rise buildings. Journal of Green Building. 2014;9:145-60.

[97] Kindangen JI. Window and roof configurations for comfort ventilation. Building Research & Information. 1997;25:218-25.

[98] Wiren B. Effects of surrounding buildings on wind pressure distributions and ventilative heat losses for a single-family house. Journal of Wind Engineering and Industrial Aerodynamics. 1983;15:15-26.

[99] Lam KP, Kim SH, Satwiko P, Jennings J, Cole J. Assessment of the effects of environmental factors on air flow in and around buildings. 23rd International Conference on Passive and Low Energy Architecture, Geneva, Switzerland2006. p. 6-8.

[100] Tong Z, Chen Y, Malkawi A. Defining the Influence Region in neighborhood-scale CFD simulations for natural ventilation design. Applied Energy. 2016;182:625-33.

[101] Bauman F, Ernest D, Arens EA. The effects of surrounding buildings on wind pressure distributions and natural ventilation in long building rows. Ashrae Transactions. 1988;94.

[102] A. Krishan KJ, M. Rajgopalon, and P. Yewari. Shelter of form: the "process of design" in question, Proceedings of the Climatically Responsive Energy Efficient Architecture. Proceedings of the Climatically Responsive Energy Efficient Architecture. New Delhi1995.

[103] Ikeguchi A, Zhang G, Okushima L, Bennetsen J. Windward windbreak effects on airflow in and around a scale model of a naturally ventilated pig barn. Transactions of the ASAE. 2003;46:789.

[104] Aynsley R. Natural ventilation in passive design. Environment Design Guide. 2014:1.

[105] Gromke C, Buccolieri R, Di Sabatino S, Ruck B. Dispersion study in a street canyon with tree planting by means of wind tunnel and numerical investigations–evaluation of CFD data with experimental data. Atmospheric Environment. 2008;42:8640-50.

[106] Buccolieri R, Gromke C, Di Sabatino S, Ruck B. Aerodynamic effects of trees on pollutant concentration in street canyons. Science of the Total Environment. 2009;407:5247-56.

[107] Horikiri K, Yao Y, Yao J. Numerical optimisation of thermal comfort improvement for indoor environment with occupants and furniture. Energy and Buildings. 2015;88:303-15.

[108] Pourshaghaghy A, Omidvari M. Examination of thermal comfort in a hospital using PMV–PPD model. Applied ergonomics. 2012;43:1089-95.

[109] Alfano FRdA, Ianniello E, Palella BI. PMV–PPD and acceptability in naturally ventilated schools. Building and Environment. 2013;67:129-37.

[110] Barbhuiya S, Barbhuiya S. Thermal comfort and energy consumption in a UK educational building. Building and Environment. 2013;68:1-11.

[111] Alahmer A, Abdelhamid M, Omar M. Design for thermal sensation and comfort states in vehicles cabins. Applied Thermal Engineering. 2012;36:126-40.

[112] Li F, Liu J, Pei J, Lin C-H, Chen Q. Experimental study of gaseous and particulate contaminants distribution in an aircraft cabin. Atmospheric environment. 2014;85:223-33.

[113] Bos MA, Love JA. A field study of thermal comfort with underfloor air distribution. Building and Environment. 2013;69:233-40.

[114] Park SH, Chung WJ, Yeo MS, Kim KW. Evaluation of the thermal performance of a Thermally Activated Building System (TABS) according to the thermal load in a residential building. Energy and Buildings. 2014;73:69-82.

[115] Ahmed AQ, Gao S, Kareem AK. Energy saving and indoor thermal comfort evaluation using a novel local exhaust ventilation system for office rooms. Applied Thermal Engineering. 2017;110:821-34.

[116] Ahmed AQ, Gao S, Kareem AK. A numerical study on the effects of exhaust locations on energy consumption and thermal environment in an office room served by displacement ventilation. Energy Conversion and Management. 2016;117:74-85.

[117] Hens HS. Thermal comfort in office buildings: two case studies commented. Building and Environment. 2009;44:1399-408.

[118] Jang M, Koh C, Moon I. Review of thermal comfort design based on PMV/PPD in cabins of Korean maritime patrol vessels. Building and Environment. 2007;42:55-61.

[119] ASHRAE A. Standard 55-2004. Thermal environmental conditions for human occupancy. 2004;744.

[120] Gagge AP. An effective temperature scale based on a simple model of human physiological regulatory response. Ashrae Trans. 1971;77:247-62.

[121] Fanger PO. Thermal comfort. Analysis and applications in environmental engineering. Thermal comfort Analysis and applications in environmental engineering. 1970.

[122] Gagge AP, Fobelets A, Berglund L. A standard predictive index of human response to the thermal environment. ASHRAE Trans;(United States). 1986;92.

[123] Honjo T. Thermal comfort in outdoor environment. Global environmental research. 2009;13:43-7.

[124] Hunt G, Linden P. Steady-state flows in an enclosure ventilated by buoyancy forces assisted by wind. Journal of Fluid Mechanics. 2001;426:355-86.

[125] Cook M, Ji Y, Hunt G. CFD modelling of natural ventilation: combined wind and buoyancy forces. International Journal of Ventilation. 2003;1:169-79.

[126] Hassan M, Guirguis N, Shaalan M, El-Shazly K. Investigation of effects of window combinations on ventilation characteristics for thermal comfort in buildings. Desalination. 2007;209:251-60.

[127] Milne M, Kohut T. Eliminating air conditioners in new southern california housing. Proceeding of ASES2010.

[128] Walker C, Tan G, Glicksman L. Reduced-scale building model and numerical investigations to buoyancy-driven natural ventilation. Energy and Buildings. 2011;43:2404-13.

[129] Stavridou AD, Prinos PE. Natural ventilation of buildings due to buoyancy assisted by wind: Investigating cross ventilation with computational and laboratory simulation. Building and Environment. 2013;66:104-19.

[130] Koranteng C, Essel C, Nkrumah J. Passive Analysis of the Effect of Window Size and Position on Indoor Comfort for Residential Rooms in Kumasi, Ghana. International Journal on Architecture Science. 2015;2.

[131] Prakash D, Ravikumar P. Analysis of thermal comfort and indoor air flow characteristics for a residential building room under generalized window opening position at the adjacent walls. International Journal of Sustainable Built Environment. 2015;4:42-57.

[132] Mora-Pérez M, Guillen-Guillamón I, López-Patiño G, López-Jiménez PA. Natural Ventilation Building Design Approach in Mediterranean Regions—A Case Study at the Valencian Coastal Regional Scale (Spain). Sustainability. 2016;8:855.

[133] Spentzou E, Cook MJ, Emmitt S. Natural ventilation strategies for indoor thermal comfort in Mediterranean apartments. Building Simulation: Springer; 2017. p. 1-17.

[134] Lei Z, Liu C, Wang L, Li N. Effect of natural ventilation on indoor air quality and thermal comfort in dormitory during winter. Building and Environment. 2017;125:240-7.

[135] Baglivo C, Congedo PM, Di Cataldo M, Coluccia LD, D'Agostino D. Envelope Design Optimization by Thermal Modelling of a Building in a Warm Climate. Energies. 2017;10:1808.

[136] Miño-Rodríguez I, Naranjo-Mendoza C, Korolija I. Thermal Assessment of Low-Cost Rural Housing—A Case Study in the Ecuadorian Andes. Buildings. 2016;6:36.

[137] Ai Z, Mak C. Analysis of fluctuating characteristics of wind-induced airflow through a single opening using LES modeling and the tracer gas technique. Building and Environment. 2014;80:249-58.

[138] Niu J, Tang Y, Mak C. The application of Computational Fluid Dynamics to the assessment of green features in buildings: Part 2: Communal sky gardens. Architectural Science Review. 2005;48:337-44.

[139] Chen Q. Ventilation performance prediction for buildings: A method overview and recent applications. Building and environment. 2009;44:848-58.

[140] Versteeg HK, Malalasekera W. An introduction to computational fluid dynamics: the finite volume method: Pearson Education; 2007.

[141] Liu J, Srebric J, Yu N. Numerical simulation of convective heat transfer coefficients at the external surfaces of building arrays immersed in a turbulent boundary layer. International Journal of Heat and Mass Transfer. 2013;61:209-25.

[142] Kader B. Temperature and concentration profiles in fully turbulent boundary layers. International journal of heat and mass transfer. 1981;24:1541-4.

[143] Gousseau P, Blocken B, Stathopoulos T, Van Heijst G. CFD simulation of near-field pollutant dispersion on a high-resolution grid: a case study by LES and RANS for a building group in downtown Montreal. Atmospheric Environment. 2011;45:428-38.

[144] Porté-Agel F, Pahlow M, Meneveau C, Parlange MB. Atmospheric stability effect on subgrid-scale physics for large-eddy simulation. Advances in Water Resources. 2001;24:1085-102.

[145] Germano M, Piomelli U, Moin P, Cabot WH. A dynamic subgrid-scale eddy viscosity model. Physics of Fluids A: Fluid Dynamics. 1991;3:1760-5.

[146] Kim W-W, Menon S, Kim W-W, Menon S. Application of the localized dynamic subgrid-scale model to turbulent wall-bounded flows. 35th aerospace sciences meeting and exhibit. American Institute of Aeronautics and Astronautics, Reno, USA.1997. p. 210.

[147] Perén J, Van Hooff T, Ramponi R, Blocken B, Leite B. Impact of roof geometry of an isolated leeward sawtooth roof building on cross-ventilation: Straight, concave, hybrid or convex? Journal of Wind Engineering and Industrial Aerodynamics. 2015;145:102-14.

[148] Ohba M, Irie K, Kurabuchi T. Study on airflow characteristics inside and outside a cross-ventilation model, and ventilation flow rates using wind tunnel experiments. Journal of Wind Engineering and Industrial Aerodynamics. 2001;89:1513-24.

[149] Hawendi S, Gao S. Impact of an external boundary wall on indoor flow field and natural cross-ventilation in an isolated family house using numerical simulations. Journal of Building Engineering. 2017;10:109-23.

[150] Gousseau P, Blocken B, Stathopoulos T, van Heijst GF. Near-field pollutant dispersion in an actual urban area: analysis of the mass transport mechanism by high-resolution Large Eddy Simulations. Computers & Fluids. 2015;114:151-62.

[151] Piscia D, Montero JI, Baeza E, Bailey BJ. A CFD greenhouse night-time condensation model. Biosystems Engineering. 2012;111:141-54.

[152] Cheung JO, Liu C-H. CFD simulations of natural ventilation behaviour in high-rise buildings in regular and staggered arrangements at various spacings. Energy and Buildings. 2011;43:1149-58.

[153] Tominaga Y, Mochida A, Yoshie R, Kataoka H, Nozu T, Yoshikawa M et al. AIJ guidelines for practical applications of CFD to pedestrian wind environment around buildings. Journal of wind engineering and industrial aerodynamics. 2008;96:1749-61.

[154] Celik I, Cehreli Z, Yavuz I. Index of resolution quality for large eddy simulations. Journal of fluids engineering. 2005;127:949-58.

[155] Cant S. SB Pope, Turbulent Flows, Cambridge University Press, Cambridge, UK, 2000, 771 pp. Elsevier; 2001.

[156] Richards P, Hoxey R. Appropriate boundary conditions for computational wind engineering models using the k-ϵ turbulence model. Journal of wind engineering and industrial aerodynamics. 1993;46:145-53.

[157] Park D. The Application of the Solar Chimney for Ventilating Buildings: Virginia Tech, Blacksburg, USA; 2016.

[158] Bu Z, Kato S. Wind-induced ventilation performances and airflow characteristics in an areaway-attached basement with a single-sided opening. Building and Environment. 2011;46:911-21.

[159] Hawendi S, Gao S. Impact of an external boundary wall on indoor flow field and natural cross-ventilation in an isolated family house using numerical simulations. Journal of Building Engineering. 2017;10:109-23.

[160] Wang H, Chen Q. A new empirical model for predicting single-sided, wind-driven natural ventilation in buildings. Energy and Buildings. 2012;54:386-94.

[161] World Weather Online, Kirkuk weather forecast. https://www.worldweatheronline.com/kirkuk-weather/at-tamim/iq.aspx; 2017.

[162] Park D, Battaglia F. Effect of heat loads and ambient conditions on thermal comfort for single-sided ventilation. Building Simulation: Springer; 2015. p. 167-78.

[163] Abiodun OE. Examination of thermal comfort in a naturally ventilated hostel using PMV-PPD model and field survey. American Journal of Engineering Research. 2014;3 (8):63.

[164] Tyler H, Stefano, S, Alberto, P, Dustin, M, Kyle, S. CBE Thermal Comfort Tool. Center for the Built Environment, University of California Berkeley 2013 http://cbe.berkeley.edu/comforttool/.

[165] Brager GS, De Dear RJ. Thermal adaptation in the built environment: a literature review. Energy and buildings. 1998;27:83-96.

[166] Fanger PO, Toftum J. Extension of the PMV model to non-air-conditioned buildings in warm climates. Energy and buildings. 2002;34:533-6.

[167] De Dear RJ, Brager GS, Reardon J, Nicol F. Developing an adaptive model of thermal comfort and preference/discussion. ASHRAE transactions. 1998;104:145.

[168] Berkovic S, Yezioro A, Bitan A. Study of thermal comfort in courtyards in a hot arid climate. Solar Energy. 2012;86:1173-86.

[169] Farghal A, Wagner A. Studying the adaptive comfort model a case study in a hot dry climate, Cairo, Egypt. Proceedings of Conference, Adapting to Change: New Thinking on Comfort2010. p. 9-11.

[170] "Estimating Appliance and Home Electronic Energy Use." Energy.gov. accessed November 1, 2017. http://energy.gov/energysaver/articles/estimating-appliance-and-home-electronic-energyuse. 2014.

[171] Prianto E, Depecker P. Optimization of architectural design elements in tropical humid region with thermal comfort approach. Energy and buildings. 2003;35:273-80.